

# **Renormalization Group Approaches to Low-Dimensional Systems**

## **Scrutinization of the Spin-Functional RG for the 2D XXZ Model**

**&**

## **Real-Time RG Study of a Generic 2-Level Quantum Dot in the Coulomb Blockade Regime in Nonequilibrium**

Von der Fakultät für Mathematik, Informatik und Naturwissenschaften  
der RWTH Aachen University zur Erlangung des akademischen Grades  
eines Doktors der Naturwissenschaften genehmigte Dissertation

vorgelegt von

**Stefan Göttel, M.Sc.**

aus Bochum

**Berichter:**                      **Universitätsprofessor Dr. phil. Herbert Schoeller**  
   **Assistenzprofessor Dr. rer. nat. Dirk Schuricht**

**Tag der mündlichen Prüfung:**                      **22. Mai 2015**

Diese Dissertation ist auf den Internetseiten der Hochschulbibliothek online verfügbar.

**Contact Information:**

**Stefan Göttel**

**Institut für Theorie der Statistischen Physik  
Physikzentrum, RWTH Aachen  
Otto-Blumenthal Straße  
52074 Aachen**

**phone: +49 241 8027032**

**email: goettel (at) physik.rwth-aachen.de**

**Berichter:                   Universitätsprofessor Dr. phil. Herbert Schoeller  
                                  Assistenzprofessor Dr. rer. nat. Dirk Schuricht \***

\* Utrecht University

# List of Acronyms

<b>1PI</b>	one particle irreducible
<b>BKT</b>	Berezinskii-Kosterlitz-Thouless
<b>DM</b>	Dzyaloshinskii-Moriya
<b>FRG</b>	functional renormalization group
<b>PMS</b>	poor man's scaling
<b>PT</b>	perturbation theory
<b>QD</b>	quantum dot
<b>QMC</b>	quantum Monte Carlo
<b>RG</b>	renormalization group
<b>RPA</b>	random phase approximation
<b>RTRG</b>	real time renormalization group
<b>SVD</b>	singular value decomposition



# Contents

<b>List of Acronyms</b>	<b>iii</b>
<b>Introduction</b>	<b>1</b>
<b>1 Short Summary</b>	<b>3</b>
<b>2 Introduction</b>	<b>5</b>
<b>Scrutinization of the Spin-FRG for the 2D XXZ Model</b>	<b>9</b>
<b>3 Motivation</b>	<b>11</b>
<b>4 Model: The 2D XXZ Model</b>	<b>13</b>
4.1 The 2D XXZ Model on a Square Lattice . . . . .	13
4.2 Fermionization of the XXZ Model . . . . .	14
<b>5 Method: The Spin-FRG</b>	<b>17</b>
5.1 General Renormalization Group Idea . . . . .	17
5.2 Functional Renormalization Group Formalism . . . . .	18
5.3 Flow Equations . . . . .	19
5.4 Truncation Schemes . . . . .	21
5.5 Extension to Spin Systems . . . . .	23
5.6 Physical Observable: The Susceptibility . . . . .	25
5.7 Other Methods . . . . .	27

<b>6</b>	<b>Results</b>	<b>29</b>
6.1	Susceptibility . . . . .	29
6.2	Finite Size and Frequency Discretization Effects . . . . .	31
6.3	Critical Scale and Temperature . . . . .	31
6.4	Auxiliary Fermion Self-Energy . . . . .	34
<b>7</b>	<b>Conclusion</b>	<b>37</b>
<b>RTRG Study of a QD in the Coulomb Blockade Regime</b>		<b>41</b>
<b>8</b>	<b>Motivation</b>	<b>43</b>
<b>9</b>	<b>Model: The Quantum Dot</b>	<b>47</b>
9.1	Generic Z-Level Quantum Dot Model . . . . .	47
9.2	Effective 2-Level QD with Fixed Particle Number $N=1$ . . . . .	57
<b>10</b>	<b>Method: Real-Time Renormalization Group</b>	<b>65</b>
10.1	Dot Density Matrix in Liouville Space . . . . .	66
10.2	Wick's Theorem . . . . .	68
10.3	Current . . . . .	73
10.4	Different RG Schemes . . . . .	74
10.5	Derivation of Flow Equations in the E-Flow Scheme . . . . .	76
10.6	Frequency Integrals . . . . .	78
10.7	RG-Equations for Slowly Varying Parts . . . . .	80
10.8	Weak Coupling Expansion . . . . .	83
10.9	Summary of the RTRG . . . . .	86
10.10	Poor Man's Scaling . . . . .	86
<b>11</b>	<b>Comparison between RTRG and PMS</b>	<b>89</b>
11.1	Splitting of the Vertex Functions . . . . .	89
11.2	Analytic Evaluation of the Differential Equations . . . . .	92

---

<b>12</b>	<b>Results</b>	<b>97</b>
12.1	Singular Value Decomposition . . . . .	97
12.2	Determination of the Effective Magnetic Field . . . . .	101
12.3	Magnetization and Current for the Generic Case . . . . .	102
12.4	Solution for Two Reservoirs in the Scaling Limit . . . . .	110
12.5	Problems for more than 2 Dot-Levels . . . . .	116
<b>13</b>	<b>Conclusion and Outlook</b>	<b>119</b>
13.1	Conclusion . . . . .	119
13.2	Outlook . . . . .	120
<b>Appendix</b>		<b>123</b>
<b>A</b>	<b>Flow Equations for the Vertices of the Spin-FRG</b>	<b>I</b>
<b>B</b>	<b>Liouville Algebra and Useful Relations</b>	<b>V</b>
B.1	Superoperator Basis for the 2-Level Quantum Dot . . . . .	V
B.2	Superoperator Algebra . . . . .	VI
B.3	Spectral Decomposition of the Bare Liouvillian . . . . .	VII
B.4	Useful Relations . . . . .	VIII
<b>Supplements</b>		<b>IX</b>
<b>Bibliography</b>		<b>XXI</b>
<b>List of Publications</b>		<b>XXIII</b>
<b>Curriculum Vitae</b>		<b>XXV</b>





# Introduction



# Chapter 1

## Short Summary

**English** In this thesis, we study two recently developed methods to tackle low-dimensional correlated quantum systems.

In the first part, we benchmark the extension of the functional renormalization group to spin-systems. We apply it to the two-dimensional XXZ model and reproduce the prediction for the phase transition from planar to axial ordering at the isotropic point. The interpretation of the critical scale (where the flow of the susceptibility diverges) as the critical temperature of the system can be questioned, since it yields only good results in the Ising limit. Especially near the isotropic point, this interpretation becomes unsatisfactory as the Mermin-Wagner theorem is violated. We discuss several problems of the method and conclude that it should only be used to explore phase diagrams.

In the second part, we extend previous works to two-level quantum dots in the Coulomb blockade regime with special hopping matrices in nonequilibrium, e.g., the Kondo model, to the generic form, including ferromagnetic leads, spin-orbit interactions etc. The dot and the transport observables are determined completely by the hybridization matrix, leading to one of our major results that all these models can be mapped to the Anderson impurity model with ferromagnetic leads. We investigate this model with a well-controlled real-time renormalization group approach and justify the results of a poor man's scaling analysis. By using a singular value decomposition of the tunneling matrix we can rotate the model to the anisotropic Kondo model in the high-energy regime to solve the flow equations analytically. With this, we calculate the stationary dot magnetization and the current. The minimum of the magnetization is found to be an ellipsoid as function of the magnetic field, where the stretching factor determines the distance to the scaling limit. Afterwards, we consider the special case of two external reservoirs and the system being in the scaling limit and discuss the golden-rule as well as the quantum-interference regime in detail. We can give a recipe how to extract the effective model parameters by measuring the current through the dot. Finally, the case of more than two dot-levels is discussed, where our approach becomes inapplicable.

**Deutsch** In dieser Arbeit diskutieren wir zwei kürzlich entwickelte Methoden zur Betrachtung niedrig-dimensionaler Systeme.

Im ersten Teil überprüfen wir die Erweiterung der funktionalen Renormierungsgruppe auf Spinsysteme. Hierzu wenden wir sie auf das zweidimensionale XXZ Modell an und können so die Vorhersage des Phasenübergangs von planarer zu axialer Ordnung am isotropen Punkt reproduzieren. Die Interpretation der kritischen Skala, bei der der Fluss der Suszeptibilität divergiert, als kritische Temperatur des Systems liefert jedoch nur gute Resultate im Ising-Limes. Vor allem in der Nähe des isotropen Punktes wird sie sehr problematisch, da das Mermin-Wagner-Theorem verletzt wird. Wir diskutieren mögliche Probleme und schlussfolgern, dass die Methode nur zum Untersuchen von Phasenübergängen verwendet werden sollte.

Im zweiten Teil betrachten wir zwei-Level Quantenpunkte im Coulomb-Blockade Bereich im Nichtgleichgewicht. Ein Beispiel hierfür ist das Kondo-Modell. Wir erweitern frühere Arbeiten mit speziellen Hüpfmatrixstrukturen auf den generischen Fall, welcher z.B. ferromagnetische Reservoirs und eine Spin-Orbit Wechselwirkung beinhaltet. Die lokalen Quantenpunkt- und die Transportobservablen sind durch die Hybridisierungsmatrix bestimmt, was auf eines unserer Hauptresultate führt, dass alle diese Modelle auf das Störstellen-Anderson-Modell mit ferromagnetischen Reservoirs abgebildet werden können. Dieses untersuchen wir mit einem kontrollierten Echtzeit-Renormierungsgruppen-Ansatz und verifizieren so die Resultate einer Poor Man's Scaling Untersuchung. Durch die Verwendung einer Singulärwertzerlegung der Tunnelmatrix kann das Modell im Hochenergie-Sektor auf das anisotrope Kondo-Modell abgebildet werden, wodurch die Flussgleichungen analytisch gelöst werden können. Hiermit berechnen wir die Magnetisierung des Quantenpunkts und den Strom. Das Minimum der Magnetisierung ist gegeben durch ein Ellipsoid als Funktion des Magnetfelds, wobei der Streckungsfaktor mit der Distanz zum Skalenlimes zusammenhängt. Danach betrachten wir den Spezialfall von zwei externen Reservoirs, wobei sich das System im Skalenlimes befindet, und diskutieren sowohl den Goldene-Regel Bereich als auch den Quanten-Interferenz Bereich detailliert. Hier ist es uns möglich, eine Vorschrift anzugeben, wie man aus verschiedenen Strommessungen die effektiven Modellparameter bestimmen kann. Abschließend betrachten wir den Fall von mehr als zwei Leveln im Quantenpunkt und zeigen, dass das bisherige Vorgehen so nicht mehr möglich ist.

## Chapter 2

# Introduction

Low-dimensional correlated quantum systems show a wide range of fascinating physical phenomena. On the one hand, the experimental progress in fabricating and controlling those systems increased significantly in the last decades, on the other hand, the theorists are challenged to extend existing or invent new methods to explain those phenomena.

A ground breaking advancement in the field of condensed matter in recent years was the experimental control of **ultra-cold atoms**, advanced a Nobel prize in 2012. In those, extraordinarily controllable quantum systems were realized by cooling atoms in a magnetic or optical trap down to very low temperatures [Kin06, Blo08]. With this setup, model Hamiltonians, which were already treated by theorists for decades like the quantum-spin Heisenberg model [Hei28, Bet31], become realizable in real physical systems nearly without any external disturbances [Dua03, Kuk03]. Additionally, also more advanced Hamiltonians can be prepared, such that the development of new methods becomes more and more important.

These quantum-spin Heisenberg-type models gained renewed interest in the 80's after the discovery of high- $T_c$  superconductivity [Bed86, Chu87], as the two-dimensional *CuO*-planes, which are an integral compound of all cuprate superconductors, could be well described by a nearest-neighbor spin-1/2 Heisenberg model. Furthermore, frustration effects due to competing spin interactions or special lattice geometries are of particular interest. By tuning them, the systems can be driven to different phases, exhibiting quantum-phase transitions [Sac99]. Therefore, understanding these spin-systems is extremely interesting, however up to now all existing methods to tackle these systems have their individual drawbacks.

Beside the experimental advances in ultra-cold atoms, **quantum computing**, i.e., using some quantum-mechanical properties to store and manipulate information, gains more attention. For quantum computers qubits are the analog to conventional bits.

There is hope that computers build on the concepts of quantum mechanics could overcome the speed limitations of conventional computers, especially in the fields of integer factorization used, e.g., in cryptography, searching unsorted databases as well as simulating physical properties of quantum many-body Hamiltonians in polynomial instead of exponential time. However, up to now experiments are only able to handle a small number of qubits, as the preparation, manipulation and read-out of qubits is rather challenging. Thus, a working quantum computer outperforming conventional ones remains a long-term goal. Additionally, also theoretical challenges have to be solved. The qubits can be modeled by quantum dots, which is our main motivation to study them. These quantum dot models consist usually of a quasi-zero dimensional system coupled to external reservoirs. Interesting physics can arise due to strong correlations within the system like the Coulomb blockade or Kondo screening [GG98a, vdW00]. Although these strong correlations render quantum dots difficult to treat, these effects could lead to an unexpected behavior of the system, which need to be understood and might be exploited in quantum processing. Therefore, many studies of quantum dots were done in the past years concerning mostly equilibrium situations, while the non-equilibrium setup is still a newly emerging field of research and only been tackled for special cases, e.g., the Kondo model.

**Goals of this Thesis** The aim of this thesis is two-fold. In the first part, we focus on methodical development. As previously mentioned, quantum spin systems are of huge relevance to explain various physical phenomena, they are among other things needed to understand the high- $T_c$  superconductivity. Due to frustration and strong correlations, the adequate treatment of spin systems remain complicated such that until now all existing approaches suffer from different drawbacks (an exception being one-dimensional systems). In this thesis, we will perform a quantitative and qualitative test of the recently developed extension to the functional renormalization group put forward by Reuther and Wölfle [Reu10] to study its strengths and weaknesses. Providing a positive result, this extension would be a powerful tool as it is rather flexible in treating different lattice geometries and dimensions without the problem of too large numerical effort, sign problems (such as quantum Monte Carlo) etc.

Afterwards, we turn towards the real-time renormalization group method and apply it to a quantum dot coupled to an arbitrary number of reservoirs in the weak-coupling regime. Up to now, this has mostly been done for various forms of the Kondo model, which we will introduce later. In this thesis, we extend these studies and do no longer constrain the form of the reservoir-dot coupling. We will calculate nonequilibrium stationary quantities which are rather important to understand and control quantum

dots in detail.

**Outline of this Thesis** This thesis is organized as follows:

The first part begins with the resummation of the strengths and drawbacks of different methods which are used to tackle strongly correlated systems. Afterwards, we introduce the XXZ model, which will be used as the test model for the spin functional renormalization group. The functional renormalization group is outlined in chapter 5, where we will at first explain its traditional form and then its extension for spin systems. Thereafter, we present the results of this method for the susceptibility and the critical temperature of the XXZ model and compare those to other methods. This part will be concluded in chapter 7, where we will also discuss possible drawbacks of the functional renormalization group.

The next part starts with an introduction to the Kondo model and a short overview, why renormalization group methods are useful to tackle it (chapter 8). Then, we start from the generic quantum dot model and present a simplified version which is valid in the Coulomb blockade regime. In chapter 10 we describe the real-time renormalization group, where we focus on the E-Flow scheme. For this, we use a weak-coupling expansion and compare analytically those results to a poor man's scaling approach. Finally, we present the results of the real-time renormalization group calculations for the generic quantum dot model and finish this theses with a summary of this part and a brief outlook of future research avenues in this field.





# Scrutinization of the Spin-Functional RG for the 2D XXZ Model

In this part of the thesis, we compare the results of the spin-functional renormalization group for the susceptibility and the critical temperature of the XXZ Model on a two-dimensional square lattice with other methods for qualitative and quantitative benchmark. We specify the model and explain the functional renormalization group and its extension to spin systems in detail. Thereafter, we present and compare the results of various methods and draw a conclusion about the implications of our study for the spin-functional renormalization group as well as outline possible problems.

This part is based on Ref. [Gö12].



## Chapter 3

# Motivation

We discussed in the introduction of this thesis (Chapter 2) the strong interest in the understanding of low-dimensional systems and the introduction of new methods to tackle those. A large class of renormalization group (RG) based methods were developed in the last decades and they became a widely used tool for strongly correlated electron systems [S679, Sha94, Met98, Met12].

In this part of the thesis, we will focus on the functional renormalization group (FRG) where one aims at describing the flow of the vertex functions. Within the FRG framework one is able to treat energy scales successively from high to low and thus to monitor the flow to certain fixed points of the model. For fermionic systems one needs to truncate the flow in powers of fermionic fields, thus one needs a small expansion parameter usually. Hence, the FRG is often used only as a qualitative tool to differentiate low-energy behaviors, so to explore phase diagrams. Nevertheless, also quantitative results like the exponents in Luttinger liquids could be reproduced by the FRG and coincide with exact solutions to leading order [And04, Sch05].

At first glance, quantum spin systems like the XXZ model introduced later are not in the scope of a FRG approach as the Hamiltonian does not contain a weak coupling parameter, in which one could expand the RG flow, and more importantly, Wicks theorem is not applicable to spin systems due to the non-trivial commutation relation of spin operators. On the other hand, direct numerical methods are the most common approaches to those strong coupling systems but usually suffer from finite size effects and sign problems for frustrated systems. Analytical or field theoretical approaches are more involved, as one has to deal with the constraint of a fixed total spin per lattice site. Additionally, competing orders and strong quantum fluctuations in those systems [Mis05, Bal10] render their description a formidable challenge for theoretical methods, such as the FRG. Provided its applicability the FRG could thus prove to be a powerful tool to tackle

those systems. In a series of papers the standard FRG was extended to spin systems by a mapping of the spin-system to a fermionic one and a qualitative agreement to benchmark results were achieved [Reu10, Reu11b, Reu11c, Reu11d, Reu11e, Sin12]. The strength of the FRG would be its flexibility in treating different lattice geometries and dimensions without increasing the numerical effort drastically, e.g., large, frustrated spin systems could be described without sign problems. Hence, it is important to benchmark the spin-FRG approach also quantitatively with other methods.

# Chapter 4

## Model: The 2D XXZ Model

As already explained in the motivation we want to compare the results of the spin-FRG, which will be explained in detail later, to those of other methods, e.g., quantum Monte Carlo (QMC) calculations. Quantitative tests of the spin-FRG for one-dimensional models have already been discussed in Refs. [Gö11, Sä11], where predictions for the ground state energy, the spin-spin correlation function and the susceptibility of various one-dimensional spin-models calculated within the spin-FRG were compared to Bethe-Ansatz solutions. It was shown that neither the calculated ground-state energies nor the spin-spin correlation functions agreed with each other. Although quantitative checks in one dimension failed, we want to test the method for two-dimensional systems as the underlying physics is completely different. Furthermore, if the quantitative comparison fails again, we will check if at least qualitative predictions like phase transitions are possible. We will use the units  $\hbar = e = k_B = 1$ .

### 4.1 The 2D XXZ Model on a Square Lattice

We consider the spin-1/2 XXZ model with antiferromagnetic nearest-neighbor exchange interaction  $J$ . The Hamiltonian of this model is given by

$$H = J \sum_{\langle ij \rangle} \left( S_i^x S_j^x + S_i^y S_j^y + \Delta S_i^z S_j^z \right), \quad (4.1.1)$$

where  $\vec{S}_i$  is the spin-1/2 operator acting on lattice site  $i$  of a two-dimensional square lattice with periodic boundary conditions. The anisotropy parameter  $\Delta$  is restricted to  $\Delta \geq 0$  in our discussion. The ground state properties and the finite temperature phase diagram are well known, cf., e.g., Ref. [Far04], so the results produced by the spin-FRG can be tested.

At the isotropic point,  $\Delta = 1$ , the Hamiltonian has a continuous  $SU(2)$  symmetry, such that the antiferromagnetic order of the ground state is constrained to zero temperature due to the Mermin-Wagner theorem [Mer66], i.e.,  $T_c = 0$ . For  $\Delta > 1$ , called the easy-axis region, this continuous symmetry is no longer given and the Mermin-Wagner theorem is no longer applicable. From the Onsager solution [Ons44] in the Ising limit,  $\Delta \rightarrow \infty$ , it is known that a Néel-ordered ground state along the z-axis occurs, which emerges already below a finite transition temperature  $T_c \approx 2.269\Delta J/4$  and originates from a breaking of a discrete  $Z_2$  symmetry of the Hamiltonian. As the Ising limit and the isotropic point are continuously connected by a variation of  $\Delta$ , we also expect a finite critical temperature  $T_c > 0$  for all values  $\Delta > 1$ , which we will calculate by a QMC analysis. The ground-state in the easy-plane region,  $\Delta < 1$ , exhibits long-range transverse antiferromagnetic ordering within the  $xy$ -plane at zero temperature. This is related to the breaking of the rotational symmetry in the  $xy$ -plane. As this is also a continuous symmetry, Mermin-Wagner theorem can once again be applied and this long-range ordering can no longer be found at finite temperature. An additional Berezinskii-Kosterlitz-Thouless (BKT) transition at a critical temperature  $T_{BKT} > 0$  exists. Above this temperature, free vortex and anti-vortex excitations occur, which annihilate each other below the critical temperature and lead to a quasi-long-ranged ordered phase between  $T = 0$  and  $T = T_{BKT}$ , where the transverse spin correlation function decays algebraically. Furthermore, this phase can be characterized by a finite spin stiffness, which exhibits an universal jump at  $T = T_{BKT}$ . This will be the criteria to determine  $T_{BKT}$  in our QMC calculations.

## 4.2 Fermionization of the XXZ Model

We want to apply the FRG described in the next chapter to the XXZ model. Unfortunately, Wick's theorem [Wic50] cannot be used for spin systems due to the non-trivial commutation relations of spin-operators

$$\left[ S^\alpha, S^\beta \right] = i\epsilon^{\alpha\beta\gamma} S_\gamma, \quad \text{with } \alpha, \beta, \gamma \in [x, y, z] \quad (4.2.1)$$

so that a direct diagrammatic calculation is not possible. Various auxiliary-particle techniques have been used for spin systems, which have in common that the spin operators are replaced by fermionic or bosonic ones. Those fulfill canonical commutation relations and thus diagrammatic calculations become available. Probably, the most common auxiliary-particle techniques are the spin-wave theory [And52, Man91] and the hard-core boson Ansatz [Gia03]. In this thesis, we follow Reuther and Wölfle [Reu10]

and use the Abrisokov auxiliary-fermion representation [Abr65]. Two fermionic operators  $f_\uparrow$  and  $f_\downarrow$  are introduced per site rewriting the spin operators of site  $i$  as follows

$$S_i^\mu = \frac{1}{2} \sum_{\alpha\beta} f_{i\alpha}^\dagger \sigma_{\alpha\beta}^\mu f_{i\beta}, \quad (4.2.2)$$

with  $\mu \in [x, y, z]$  and  $\sigma^\mu$  being the standard Pauli matrices. The operators  $f$  fulfill fermionic commutation relations allowing to use Wick's theorem, but also double the local Hilbert space per lattice site from two to four states, which are labelled by

$$|0, 0\rangle, \quad |0, 1\rangle, \quad |1, 0\rangle, \quad |1, 1\rangle, \quad (4.2.3)$$

where the numbers are the occupations of up and down fermions. The two single-occupied states correspond to the physical states of the original model while the doubly and the unoccupied state are unphysical. One thus has also to introduce the constraint

$$Q_i = \sum_{\alpha} f_{i\alpha}^\dagger f_{i\alpha} \equiv 1, \quad (4.2.4)$$

which is always fulfilled *on average* for fermions at half-filling in the XXZ model, leading to a vanishing chemical potential  $\mu = 0$  for the auxiliary-fermions at temperature  $T = 0$  due to particle-hole symmetry. An exact treatment of this constraint is only possible for lattice models at finite temperature at the particle-hole symmetric point. Popov and Fedotov proposed to introduce a homogeneous imaginary chemical potential  $\mu_{PPV} = -\frac{i\pi T}{2}$  with the temperature  $T$  and a modification of the Hamiltonian

$$H^{PPV} = H - \mu^{PPV} \sum_i Q_i. \quad (4.2.5)$$

The expectation values of physical observables  $\mathcal{O}$  with respect to this new Hamiltonian and the entire Hilbert space are the same as for the original Hamiltonian and the physical Hilbert space [Pop88]. This occurs because the unphysical contributions cancel out for each lattice site exactly as in the partition function these contributions lead to  $\sum_{Q_i=0,2} e^{\beta\mu_{PPV}} = 1 + e^{i\pi} = 0^1$ . Although using this imaginary chemical potential or the vanishing potential at  $T = 0$  due to particle-hole symmetry seem to be equivalent at  $T = 0$ , this is not necessarily the case as the limit  $T \rightarrow 0$  while using an imaginary chemical potential does not always commute with the calculation of expectation values. Therefore, the constraint can only be taken into account on average neglecting the quantum fluctuations and the impact of this approximation has to be checked carefully.

---

<sup>1</sup>A more detailed discussion can be found in Appendix A of [Reu11a]





# Chapter 5

## Method: The Spin-FRG

In this chapter we will explain first why RG methods are often useful to tackle low-dimensional systems. Here, we focus on the FRG and sketch a short derivation of the infinite hierarchy of flow equations for the one particle irreducible (1PI) vertex functions. A complete derivation can be found in Ref. [Jak10a]. This infinite system of differential equations will be approximated with the Katanin truncation scheme. Afterwards, we will describe in detail how this scheme is applied to spin systems.

### 5.1 General Renormalization Group Idea

Quantum many-body systems in condensed matter physics have often a wide range of energy scales which have to be taken into account. Already the bare energy contributions to the Hamiltonian like the kinetic energy, the Coulomb interaction, magnetic interactions and so on can deviate in orders of magnitude. Further relevant scales, like single-particle excitation energies, the Kondo temperature and others are often even much smaller than the bare ones, e.g., the bare Coulomb interaction in cuprate high-temperature superconductors is larger than the transition temperature for superconductivity by a factor of 1000 [Met12]. Perturbative approaches, which tackle all these energy scales at once, often fail due to the emergence of infrared divergences especially in low dimensional systems, even if the expansion parameter is small [Hew93, Gia03]. Furthermore, the diversity of the relevant energy scales renders it nearly impossible to solve these microscopic models with a straightforward numerical method as a huge class of interesting phenomena only occurs at very low temperatures and exceedingly large system sizes. Due to these complications the idea came up to separately tackle the degrees of freedom of different energy scales successively by integrating them out from high to low [Wil74]. Various methods based on this so called RG-idea were formulated and we will outline one of these in the following, namely the FRG [Sal01, Met12].

The central idea of the FRG method is to split the free propagator of a system into two parts, one containing the high energy contributions and the other one the low ones, where high and low has to be regarded with respect to a cutoff parameter  $\Lambda$ . It depends on the scheme what is meant by energy contributions, e.g., one can consider the single-particle energy within the corresponding propagator, the frequency argument, the imaginary frequency and so on [Jak10a]. The high energy contributions are then absorbed by defining effective many-body interactions, which replace the bare ones, and the propagation of the system is restricted to the low energies. The calculation of the effective interactions does usually not suffer from the infrared divergences as no low energies are incorporated. Choosing  $\Lambda = \infty$  these effective interactions are equal to the bare ones, which is the starting point for most of the RG schemes.  $\Lambda$  is now lowered and the flow equations state how the effective interactions have to be modified to keep the physical variables unchanged during the flow. In this way the energy scales are incorporated into the effective interactions step by step and one gets closer and closer to the former infrared divergences in a controlled fashion.

## 5.2 Functional Renormalization Group Formalism

In the following we will present the fermionic formulation of a special RG method, namely the FRG, which has been successfully applied to various fermionic systems in equilibrium and non-equilibrium (see [Met12] and references therein). Due to the semi-group law of the RG [Sal01] the effective interactions described in the previous section are exactly the same as the connected amputated Green functions, where the bare propagator is replaced by the one containing only the low energy contributions, as used by Polchinski [Pol84]. One can also compute the flow of other Green or vertex functions and we will use the 1PI vertex functions  $\gamma_m$ , whose flow equations are usually derived via generating functionals [Wet93, Sal01] or alternatively on a diagrammatic level [Jak03, Jak07]. These derivations lead to an infinite hierarchy of differential equations

$$\partial_\Lambda \gamma_m^\Lambda = f_m(\{\gamma_n^\Lambda | n \leq m + 1\}), \quad (5.2.1)$$

where the functions  $f_m$  can be explicitly deduced, so that it is an exact reformulation of the full quantum many-body problem. This leads to the necessity of a truncation of the set of differential equations, which is commonly done by neglecting the flow of all vertex functions above a certain  $m_c$  (which is usually  $m_c = 1$  or  $m_c = 2$ ), and is obviously only valid if the neglected terms are and stay small during the flow. This is however difficult

to determine as only the truncated problem can be tackled. Within this approach, it is known that the important Ward-identities [War50] are violated. Another truncation scheme introduced by Katanin [Kat04] incorporating parts of  $\gamma_3$  into the flow of  $\gamma_2$  (instead of neglecting it completely) and neglecting all other contributions helps to fulfill Ward-identities to higher order. This truncation scheme will be discussed later. The 1PI vertex functions have major advantages: first, all closed propagator loops, meaning all parts leading to the infrared divergences, are incorporated and double-counting of reducible diagrams does not occur. Furthermore, the self-energy can be feed back in the RG flow non-perturbatively. Most importantly, the theory can be utilized directly to microscopic models with physical meaningful energy scales and is not limited to effective field theories, so that the full-fledged physics is accessible and not only the low-energy asymptotics. Additionally, different approximation schemes can be used at different energy scales so that one can combine the full power of all existing truncation schemes.

Within the FRG framework phase diagrams are accessible as competing instabilities in two-dimensional systems are signaled by a divergence of parts of the vertex functions. The  $\Lambda$ -scale, at which the vertex function diverge, is interpreted as the critical temperature of the system in Ref. [Reu11d] and we will check this assumption in the following within the XXZ-model described in chapter 4. A disadvantage of this divergence in the vertex functions is that the full solution at  $\Lambda = 0$  cannot be recovered, making it impossible to calculate quantitative observables like the ground-state energy.

### 5.3 Flow Equations

As already mentioned in the last section, the flow equations for the vertex functions can be derivated via generating functionals within the Matsubara formalism [Sal01], but one can also obtain them on a diagrammatic level [Jak03, Jak07], and we will sketch this in the following.

The  $n$ -particle vertex function is given as the sum of all 1PI diagrams  $d_n$ , which include  $n$  amputated incoming and  $n$  amputated outgoing lines. Each of these diagrams  $d_n$  consists of bare interactions connected by single-particle Green functions  $G^0$  as propagators [Jak10a]. An example for a diagram  $d_2$  is sketched in Fig. 5.1.

Introducing a sharp frequency cutoff in the bare propagator  $G^0$  in the Matsubara

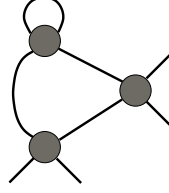


**Figure 5.1:** Example of a diagram contributing to the vertex function  $\gamma_2$ . The incoming and outgoing lines are amputated, the gray dots represent bare vertex functions and the connecting lines are dressed particle Green functions  $G^0$ .

formalism

$$G^0(i\omega) \rightarrow G^{0\Lambda}(i\omega) = \frac{\Theta(|\omega| - \Lambda)}{i\omega - \epsilon}, \quad (5.3.1)$$

all diagrams and vertex functions become also  $\Lambda$ -dependent. Calculating the diagrams  $d_n$  with the standard diagrammatic rules, e.g. [Bru04, Sch09a, Jak10a], the free propagators and therefore the  $\Lambda$ -dependence occur as products. Considering now the derivative of  $d_n$  with respect to  $\Lambda$  one gains a sum over all diagrams  $d'_n$ , which are equal to  $d_n$ , except for one Green function being replaced by its derivative. This derivative will be represented by a slanted line in the diagrams. To compute  $\partial_\Lambda \gamma_n^\Lambda$  one thus has to sum all diagrams  $d'_n$ , which result from crossing any line in any diagram  $d_n$ . Visualizing now these diagrams  $d'_n$  with leaving out the derivative of the propagator, it is easy to see that the remaining part stays connected as  $d_n$  was 1PI by definition, and furthermore it is a chain of irreducible subdiagrams connected by single lines which form a closed loop when reinserting the derivative. Adding up all  $d'_n$  with the same loop-structure, so differing only in the irreducible subdiagrams, one gets a loop of vertex functions. When further adding up those rings which are identical except for self-energy insertions, one achieves a dyson equation leading to full Green functions  $G$  and full Single Scale propagator

$$S^\Lambda = G^\Lambda \frac{d}{d\Lambda} (G^{0\Lambda})^{-1} G^\Lambda \quad (5.3.2)$$

connecting the vertex functions.

To sum up, for calculating the derivative of  $\gamma_n^\Lambda$  one has to draw all possible loops consisting of vertex functions  $\{\gamma_m^\Lambda | m \in \{2, \dots, m+1\}\}$  and connect those vertex functions with full Green functions  $G$  and exactly one Single Scale propagator  $S$ . Symmetry factors or other prefactors due to equivalent lines of diagrams are not needed due to the special loop structure and the distinguished position of  $S$  [Jak07, Jak10a]. A short summary of this procedure is depicted in Fig. 5.2.

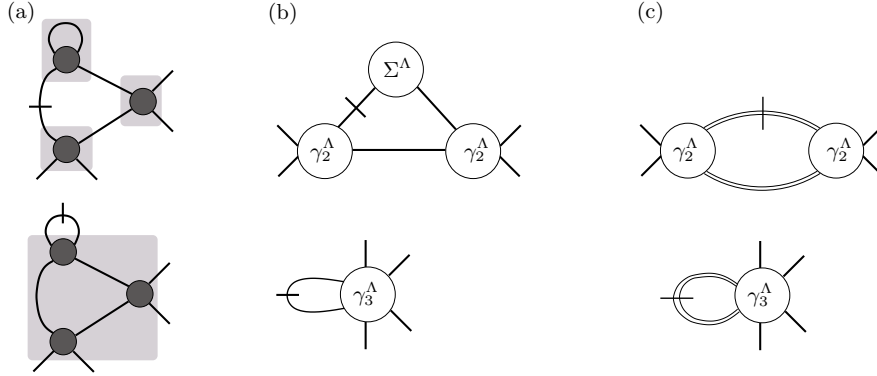


**Figure 5.2:** a) Two diagrams contributing to the derivative of the diagram  $d_2$  which is sketched in Fig. 5.1. The slanted line indicates the derivative of a free propagator. One recognizes the loop structure of vertex functions (shaded in gray) connected via propagators and exactly one derivative of it.

b) Summing up all diagrams with the same ring structure leads to diagrams with full vertex functions and self-energy insertions in the propagators. c) Adding up these self-energy insertions one gets the full propagators  $G$  and the Single Scale propagator  $S$ .

The flow equations for the vertex functions  $\gamma_1^\Lambda$  and  $\gamma_2^\Lambda$  are shown in Fig. 5.3 and for temperature  $T = 0$  read

$$\frac{d}{d\Lambda} \gamma_1^\Lambda(1', 1) = \frac{1}{2\pi} \sum_{2,2'} \gamma_2^\Lambda(1', 2'; 1, 2) S^\Lambda(2, 2') \quad (5.3.3)$$

$$\begin{aligned} \frac{d}{d\Lambda} \gamma_2^\Lambda(1', 2'; 1, 2) &= \frac{1}{2\pi} \sum_{3,3'} \gamma_3^\Lambda(1', 2', 3'; 1, 2, 3) S^\Lambda(3, 3') \\ &+ \frac{1}{2\pi} \sum_{3,3',4,4'} \left[ \gamma_2^\Lambda(1', 2'; 3, 4) \gamma_2^\Lambda(3', 4'; 1, 2) \right. \\ &\quad - \gamma_2^\Lambda(1', 4'; 1, 3) \gamma_2^\Lambda(3', 2'; 4, 2) - (3' \leftrightarrow 4'; 3 \leftrightarrow 4) \\ &\quad \left. + \gamma_2^\Lambda(2', 4'; 1, 3) \gamma_2^\Lambda(3', 1'; 4, 2) + (3' \leftrightarrow 4'; 3 \leftrightarrow 4) \right] \\ &\times G^\Lambda(3, 3') S^\Lambda(4, 4'), \end{aligned} \quad (5.3.4)$$

with the multi-indices  $1 = \{\omega, i, \alpha\}$  including the frequency  $\omega$ , the site index  $i$  and the spin  $\alpha$  of incoming or outgoing lines and the sum over 1 contains an integral over  $\omega_1$ , as well as a sum over  $i_1$  and  $\alpha_1$ .

## 5.4 Truncation Schemes

The solution of the infinite system of coupled differential equations for the vertex functions with the evaluation at  $\Lambda = 0$  would be the solution of the full-fledged many-body

The figure illustrates the flow equations for the self-energy  $\gamma_1$  and the two-particle vertex function  $\gamma_2$ . The first equation shows the derivative of the self-energy  $\frac{\partial}{\partial \Lambda}$  of a single vertex (represented by a circle with two external lines labeled 1' and 1) as equal to a diagram with a self-energy loop on the vertex. The second equation shows the derivative of the two-particle vertex function  $\frac{\partial}{\partial \Lambda}$  (represented by a circle with four external lines labeled 1', 1, 2, 2') as equal to a sum of diagrams: a self-energy loop on the vertex, a diagram with two vertices connected by two lines, and two diagrams with two vertices connected by two lines in different topologies.

**Figure 5.3:** Flow equations for the self-energy  $\gamma_1$  and the two-particle vertex function  $\gamma_2$ . The indices 1, 1', 2, 2' are multi-indices containing all relevant information of the incoming and outgoing lines (Sketch taken from Ref. [Jak10a]).

problem and is for almost all cases impossible. Hence, one needs truncation schemes yielding an easier set of differential equations which can be tackled at least numerically. As the differential equation for  $\gamma_n^\Lambda$  only contains  $\gamma_1^\Lambda$  up to  $\gamma_{n+1}^\Lambda$  and no vertex functions with higher particle numbers, the easiest way to get a closed set of equations is to neglect the flow of the vertex functions with indices larger than a critical index  $m$ . In this truncation scheme the Ward identities [War50] are not fulfilled and it was shown in earlier calculations that for spin systems a more involved truncation which does not violate the Ward identities in leading order [Kat04, Ens05] leads to better results [Reu10, Gö11]. Within this Katanin truncation-scheme parts of the flow of  $\gamma_3$  are also included and the flow equation for  $\gamma_2^\Lambda$  is modified by the replacement

$$S^\Lambda \rightarrow -\frac{d}{d\Lambda} G^\Lambda, \quad (5.4.1)$$

so  $\gamma_3$  still does not appear explicitly leaving a closed set of differential equations for  $\gamma_1$  and  $\gamma_2$ .

## 5.5 Extension to Spin Systems

Using a mapping of the XXZ model to a fermionic system allows to use the FRG introduced in the previous sections. Moreover, in the mapped XXZ model no weak coupling parameter for all regimes of  $\Delta$  exists in the Hamiltonian, in which one could expand the vertex functions. In this so called strong coupling limit a truncation of the flow equations cannot be substantiated mathematically. Nonetheless, we will use the Katanin truncation scheme as it led to reasonable results in former applications, see, e.g., [Reu10].

The self-energy, the full propagator and the Single Scale propagator are local in real space and spin conserving, so one can rewrite them

$$\gamma_1^\Lambda(1, 1') = \gamma_1^\Lambda(\omega_1) \delta(\omega_1 - \omega_{1'}) \delta_{i_1 i_{1'}} \delta_{\alpha_1 \alpha_{1'}} \quad (5.5.1)$$

and equivalently for  $G^\Lambda$  and  $S^\Lambda$ . Defining the self-energy  $\Sigma = -i\gamma_1$  and the two-particle vertex  $\Gamma = \gamma_2$  their flow equations read

$$\begin{aligned} \frac{d}{d\Lambda} \Sigma^\Lambda(1) &= -\frac{1}{2\pi} \sum_2 \Gamma^\Lambda(1, 2; 1, 2) S^\Lambda(\omega_2), \\ \frac{d}{d\Lambda} \Gamma^\Lambda(1', 2'; 1, 2) &= \frac{1}{2\pi} \sum_{3,4} \left\{ \Gamma^\Lambda(1', 2'; 3, 4) \Gamma^\Lambda(3, 4; 1, 2) \right. \\ &\quad - [\Gamma^\Lambda(1', 4; 1, 3) \Gamma^\Lambda(3, 2'; 4, 2) - (3 \leftrightarrow 4)] \\ &\quad \left. + [\Gamma^\Lambda(2', 4; 1, 3) \Gamma^\Lambda(3, 1'; 4, 2) - (3 \leftrightarrow 4)] \right\} \\ &\quad \times G^\Lambda(\omega_3) S^\Lambda(\omega_4). \end{aligned} \quad (5.5.2)$$

The full propagator and the Single Scale propagator are given as ( $\epsilon = 0$  in this case)

$$G^\Lambda(i\omega) = \frac{\Theta(|\omega| - \Lambda)}{i\omega - \Sigma^\Lambda(i\omega)}, \quad (5.5.4)$$

$$S^\Lambda(i\omega) = \frac{\delta(|\omega| - \Lambda)}{i\omega - \Sigma^\Lambda(i\omega)} + \left( \frac{d}{d\Lambda} \Sigma^\Lambda(i\omega) \right) \frac{\Theta(|\omega| - \Lambda)}{[i\omega - \Sigma^\Lambda(i\omega)]^2}. \quad (5.5.5)$$

The model under consideration has several symmetries. First of all, it is translational invariant, so that the vertex functions do only depend on the distance  $|\vec{i}_1 - \vec{i}_2|_1$  instead of the positions  $\vec{i}_1$  and  $\vec{i}_2$  themselves, with  $|\dots|_1$  meaning the one-norm defined as  $|\vec{a}|_1 = |a_x| + |a_y|$  in our two-dimensional system, and the self-energy is position-independent. The position vectors  $\vec{i}$  refer to an arbitrarily chosen reference spin and the distance between neighboring spins is defined as our natural unit of length. Fur-

thermore, as the mapped pseudo-model consists of fermions, the vertex functions have to be antisymmetric under particle exchange. Last but not least, the system exhibits a rotational invariance in the  $xy$ -plane. All in all, the vertex can be parametrized as

$$\Sigma^\Lambda(1) = \Sigma^\Lambda(\omega_1) \quad (5.5.6)$$

$$\begin{aligned} \Gamma^\Lambda(1', 2'; 1, 2) = & \left[ \Gamma_{z, |\vec{i}_1 - \vec{i}_2|_1}^\Lambda(\omega_{1'}, \omega_{2'}; \omega_1, \omega_2) \sigma_{\alpha_1' \alpha_1}^z \sigma_{\alpha_2' \alpha_2}^z \right. \\ & + \Gamma_{xy, |\vec{i}_1 - \vec{i}_2|_1}^\Lambda(\omega_{1'}, \omega_{2'}; \omega_1, \omega_2) \left( \sigma_{\alpha_1' \alpha_1}^x \sigma_{\alpha_2' \alpha_2}^x + \sigma_{\alpha_1' \alpha_1}^y \sigma_{\alpha_2' \alpha_2}^y \right) \\ & + \Gamma_{d, |\vec{i}_1 - \vec{i}_2|_1}^\Lambda(\omega_{1'}, \omega_{2'}; \omega_1, \omega_2) \delta_{\alpha_1' \alpha_1} \delta_{\alpha_2' \alpha_2} \left. \right] \times \delta_{i_1' i_1} \delta_{i_2' i_2} \\ - & \left[ \Gamma_{z, |\vec{i}_1 - \vec{i}_2|_1}^\Lambda(\omega_{1'}, \omega_{2'}; \omega_2, \omega_1) \sigma_{\alpha_1' \alpha_2}^z \sigma_{\alpha_2' \alpha_1}^z \right. \\ & + \Gamma_{xy, |\vec{i}_1 - \vec{i}_2|_1}^\Lambda(\omega_{1'}, \omega_{2'}; \omega_2, \omega_1) \left( \sigma_{\alpha_1' \alpha_2}^x \sigma_{\alpha_2' \alpha_1}^x + \sigma_{\alpha_1' \alpha_2}^y \sigma_{\alpha_2' \alpha_1}^y \right) \\ & + \Gamma_{d, |\vec{i}_1 - \vec{i}_2|_1}^\Lambda(\omega_{1'}, \omega_{2'}; \omega_2, \omega_1) \delta_{\alpha_1' \alpha_2} \delta_{\alpha_2' \alpha_1} \left. \right] \times \delta_{i_1' i_2} \delta_{i_2' i_1} \end{aligned} \quad (5.5.7)$$

in the following, where  $\Gamma_d$  contains the density-density interaction and  $\Gamma_z$  and  $\Gamma_{xy}$  the spin-spin interaction in  $z$ -direction and in the  $xy$ -plane, respectively. Due to energy conservation, for the frequencies the relation  $\omega_1 + \omega_2 = \omega_{1'} + \omega_{2'}$  has to hold. Therefore, it is common to define three 'Mandelstam'-variables  $s, t, u$  by

$$\begin{aligned} \omega_1 &= \frac{1}{2}(s - t + u) & \omega_{1'} &= \frac{1}{2}(s + t + u) \\ \omega_2 &= \frac{1}{2}(s + t - u) & \omega_{2'} &= \frac{1}{2}(s - t - u) \end{aligned} \quad (5.5.8)$$

and write the vertex functions in the form

$$\Gamma_{xy/z/d, |\vec{i}_1 - \vec{i}_2|_1}^\Lambda(\omega_{1'}, \omega_{2'}; \omega_1, \omega_2) \rightarrow \Gamma_{xy/z/d, |\vec{i}_1 - \vec{i}_2|_1}^\Lambda(s, t, u), \quad (5.5.9)$$

which satisfies the energy conservation implicitly. Inserting this parametrization into eq. (5.5.3) leads to the flow equations which will be solved numerically. Due to their length, we will only present them in appendix A.

We will now specify the initial conditions for  $\Sigma$  and  $\Gamma$  at the starting point of the flow  $\Lambda = \infty$ . By introducing the cutoff parameter  $\Lambda$  as shown in eq. 5.3.1, the bare propagator vanishes and only the bare two-particle interaction remains. The self-energy is obviously zero, as already the lowest order diagram contains one free propagator<sup>1</sup>

$$\Sigma^{\Lambda=\infty}(i\omega) = 0. \quad (5.5.10)$$

<sup>1</sup>Numerically, the flow has to start at a finite  $\Lambda$ . Consequences of this are discussed in Ref. [Jak10a].



The bare interaction has to be antisymmetrized as  $\Gamma^\Lambda(1', 2'; 1, 2)$  changes sign under the exchange of two incoming or outgoing particles, so it reads

$$\begin{aligned} \Gamma^{\Lambda=\infty}(1', 2'; 1, 2) = & J_{|\vec{i}_1 - \vec{i}_2|_1} \left[ \left( \frac{1}{4} \sigma_{\alpha_1' \alpha_1}^x \sigma_{\alpha_2' \alpha_2}^x + \frac{1}{4} \sigma_{\alpha_1' \alpha_1}^y \sigma_{\alpha_2' \alpha_2}^y + \frac{\Delta}{4} \sigma_{\alpha_1' \alpha_1}^z \sigma_{\alpha_2' \alpha_2}^z \right) \right. \\ & \times \delta_{i_1' i_1} \delta_{i_2' i_2} \\ & - \left( \frac{1}{4} \sigma_{\alpha_1' \alpha_2}^x \sigma_{\alpha_2' \alpha_1}^x + \frac{1}{4} \sigma_{\alpha_1' \alpha_2}^y \sigma_{\alpha_2' \alpha_1}^y + \frac{\Delta}{4} \sigma_{\alpha_1' \alpha_2}^z \sigma_{\alpha_2' \alpha_1}^z \right) \\ & \left. \times \delta_{i_1' i_2} \delta_{i_2' i_1} \right], \end{aligned} \quad (5.5.11)$$

where the Kronecker  $\delta$  prevent the fermionic hopping on the lattice. In the parametrized form this leads to

$$\Gamma_{xy, i_1 - i_2}^{\Lambda=\infty}(s, t, u) = \frac{1}{4} J_{|\vec{i}_1 - \vec{i}_2|_1}, \quad (5.5.12)$$

$$\Gamma_{z, i_1 - i_2}^{\Lambda=\infty}(s, t, u) = \frac{\Delta}{4} J_{|\vec{i}_1 - \vec{i}_2|_1}, \quad (5.5.13)$$

$$\Gamma_{d, i_1 - i_2}^{\Lambda=\infty}(s, t, u) = 0. \quad (5.5.14)$$

Regarding the symmetries of the initial conditions and the flow equations for the self-energy and the two-particle interaction with respect to the frequencies, it is obvious that the self-energy is an odd function. Furthermore, one can show that  $\Gamma$  is invariant under each of the transformations  $s \leftrightarrow -s$ ,  $t \leftrightarrow -t$  and  $u \leftrightarrow -u$  due to time-reversal invariance, particle-hole symmetry and antisymmetry by particle-exchange (see [Reu11a, Sä11]). Additionally,  $\Gamma_{xy}$  and  $\Gamma_z$  are invariant under  $s \leftrightarrow u$  and  $\Gamma_d$  changes sign under this transformation. These symmetries will be used to reduce the numerical effort by roughly a factor of 16.

## 5.6 Physical Observable: The Susceptibility

Our major physical observables under consideration are the static spin-spin correlation function  $\chi_{ij}(i\nu = 0)$  and the susceptibility  $\chi(q = \pi, \omega = 0)$ , as a divergence in these quantities would indicate a flow into a magnetically ordered phase. Following Reuther, Thomale and Trebst [Reu11d], the energy-scale, at which this divergence occur, is interpreted as the critical temperature of the system.



Using the symmetry properties of the vertex functions, this can be further simplified

$$\begin{aligned}
D_2^{zz} = & -2 \int_{\Lambda}^{\infty} \frac{d\omega_1}{2\pi} \int_{\Lambda}^{\omega_1} \frac{d\omega_2}{2\pi} \left[ \frac{1}{\omega_1 + i\Sigma(\omega_1)} \right]^2 \left[ \frac{1}{\omega_1 + i\Sigma(\omega_2)} \right]^2 \\
& \times \left\{ 4\Gamma_{z,|\vec{i}-\vec{j}|_1}^{\Lambda}(\omega_1 + \omega_2, 0, \omega_1 - \omega_2) \right. \\
& - \delta_{ij} \left[ \Gamma_{z,|\vec{i}-\vec{j}|_1}^{\Lambda}(\omega_1 + \omega_2, \omega_1 - \omega_2, 0) + \Gamma_{z,|\vec{i}-\vec{j}|_1}^{\Lambda}(\omega_1 - \omega_2, \omega_1 + \omega_2, 0) \right. \\
& - 2\Gamma_{xy,|\vec{i}-\vec{j}|_1}^{\Lambda}(\omega_1 + \omega_2, \omega_1 - \omega_2, 0) - 2\Gamma_{xy,|\vec{i}-\vec{j}|_1}^{\Lambda}(\omega_1 - \omega_2, \omega_1 + \omega_2, 0) \\
& \left. \left. + \Gamma_{d,|\vec{i}-\vec{j}|_1}^{\Lambda}(\omega_1 + \omega_2, \omega_1 - \omega_2, 0) + \Gamma_{d,|\vec{i}-\vec{j}|_1}^{\Lambda}(\omega_1 - \omega_2, \omega_1 + \omega_2, 0) \right] \right\}. \tag{5.6.4}
\end{aligned}$$

The calculation of  $D_2^{xx}$  yields

$$\begin{aligned}
D_2^{xx} = & -2 \int_{\Lambda}^{\infty} \frac{d\omega_1}{2\pi} \int_{\Lambda}^{\omega_1} \frac{d\omega_2}{2\pi} \left[ \frac{1}{\omega_1 + i\Sigma(\omega_1)} \right]^2 \left[ \frac{1}{\omega_1 + i\Sigma(\omega_2)} \right]^2 \\
& \times \left\{ 4\Gamma_{xy,|\vec{i}-\vec{j}|_1}^{\Lambda}(\omega_1 + \omega_2, 0, \omega_1 - \omega_2) \right. \\
& - \delta_{ij} \left[ -\Gamma_{z,|\vec{i}-\vec{j}|_1}^{\Lambda}(\omega_1 + \omega_2, \omega_1 - \omega_2, 0) - \Gamma_{z,|\vec{i}-\vec{j}|_1}^{\Lambda}(\omega_1 - \omega_2, \omega_1 + \omega_2, 0) \right. \\
& \left. \left. + \Gamma_{d,|\vec{i}-\vec{j}|_1}^{\Lambda}(\omega_1 + \omega_2, \omega_1 - \omega_2, 0) + \Gamma_{d,|\vec{i}-\vec{j}|_1}^{\Lambda}(\omega_1 - \omega_2, \omega_1 + \omega_2, 0) \right] \right\}. \tag{5.6.5}
\end{aligned}$$

In a next step, the static susceptibility can be computed from these quantities

$$\chi(\mathbf{q} = (\pi, \pi), i\nu = 0) = \sum_{\vec{i}} (-1)^{|\vec{i}|_1} \chi_{0|\vec{i}|_1}(i\nu = 0). \tag{5.6.6}$$

These quantities have only a physical interpretation at  $\Lambda = 0$ , but we will calculate them for finite  $\Lambda$  as well and interpret their divergence as sign of a magnetic instability of the system.

## 5.7 Other Methods

As we want to test the results calculated within the spin-FRG, we have to use also other methods to compare with. In this section, we will briefly describe those.

**Random Phase Approximation** The random phase approximation (RPA) is a widely used approximation scheme to compute, e.g., magnetic properties in condensed matter physics. It was introduced by Bohm and Pines in the early 1950's [Boh51, Pin52,

Boh53]. The individual spins or electrons are treated as they only interact with a total magnetic or electric field, which consists of an externally applied field and a screening potential due to the other spins or electrons. So the rest of the system is only treated on average and quantum fluctuations are neglected. By dropping some terms of the full set of FRG equations we can reproduce a single-channel summation of RPA character. We will present results of such restricted flows, where only specific terms of the t-channel are taken into account, which are the terms  $\sim \Gamma^\Lambda(1', 4; 1, 3)\Gamma^\Lambda(3, 2'; 4, 2) + (3 \leftrightarrow 4)$  of eq. (5.5.3). Details are explained in Ref. [Reu10]. The remaining terms can be investigated more carefully by using the parametrization (5.5.7). The  $\Gamma_{d,|\vec{i}-\vec{j}|}^\Lambda$  terms are initially zero and stay constant during the flow. Fourier-transforming the other vertex functions  $\Gamma_{xy/z,|\vec{i}-\vec{j}|}^\Lambda$  from  $|\vec{i}-\vec{j}|$  to the reciprocal vector  $\vec{q}$ , the t-channel can be split into a part which do not couple different  $\vec{q}$  and a part with an internal sum over another  $\vec{q}'$ . The second ones are vertex corrections and also dropped in our RPA scheme, but the first ones are bubble-like diagrams and lead to the flow equations for the vertices explicitly stated in Ref. [Reu10]. In the following comparison to the FRG results, we will discuss two versions of this RPA scheme. In the first one, the self-energy is completely neglected, and we will call this "RPA0". Including these self-energy contributions like in usual self-consistent RPA without cutoffs we call the "RPA+" scheme.

**Quantum Monte Carlo** A common starting point for numerical studies of interacting many-body systems is the path-integral formalism. As long as the system under consideration is not frustrated, so positive definiteness can be assured, unbiased QMC methods can be used to solve these problems numerically exact [Ass08]. In this thesis, we use comparative data for the critical temperature  $T_c$  in the vicinity of  $\Delta = 1$  calculated by Cuccoli *et al.* [Cuc03]. As we need an estimation of  $T_c$  in a wider range of  $\Delta$  to test the Spin-FRG, we use QMC simulations with the stochastic series expansion method [San99] with generalized directed loop updates [Syl02, Ale05]. Square lattices with periodic boundary conditions and edge length up to 32 spins are simulated and from these finite size data the critical temperature in the easy-axis regime  $\Delta > 1$  is obtained from a finite-size analysis based on the critical Binder ratio [Bin81]. For  $\Delta < 1$  the critical temperature is given by the jump in the spin stiffness, which is calculated from the measurement of the spin winding number fluctuations [Pol87]. We appreciate that Stefan Weßel<sup>2</sup> has provided the results of the QMC calculations presented in the following.

---

<sup>2</sup>Stefan Weßel, RWTH Aachen, Institute for Condensed Matter Physics

# Chapter 6

## Results

In this chapter, we present the numerical solution of the flow equations (5.5.2) and (5.5.3) with the initial conditions (5.5.14). In detail, we will show at first the flow of the susceptibility (5.6.6) and reproduce the phase transition at  $\Delta = 1$ . Afterwards, we investigate the critical scale  $\Lambda_c$ , at which the flow of the vertex function diverge, and compare this with the critical temperature of the XXZ model in various limits.

If it is not stated explicitly otherwise, we consider a square lattice with  $10 \times 10$  sites. The handling of the frequencies is comparable to the one of Reuther and Wölfle [Reu10], as we also use a logarithmic discretization of  $N_f = 30$  positive frequencies with  $\omega_{min} = 0.001J$  and  $\omega_{max} \approx 250J$ . Negative frequencies are included due to the symmetry relations of the vertex functions. So all in all, the full range of frequencies is covered where the frequencies with a small absolute value are treated in detail, as they mainly determine the low-energy behavior of the system, but also high frequencies larger than  $\Delta \times J$  are taken into account to capture the high-energy physics.

Of course this finite-size treatment of the XXZ Model and the frequency discretization are approximations which have to be tested, so we also present results for different lattice sizes and other frequency discretizations.

### 6.1 Susceptibility

As mentioned at the beginning of this chapter, we start with the discussion of the susceptibility for different values of  $\Delta$ . For  $\Delta > 1$  we expect a dominant correlation in  $z$ -direction leading to  $\chi^{zz} > \chi^{xx}$ . At the isotropic point  $\Delta = 1$ , the system is rotational invariant, so both susceptibilities should be equal, and for  $\Delta < 1$  the planar correlation becomes stronger than the axial one. These results were reproduced within our FRG calculations as one can see in Fig. 6.1.

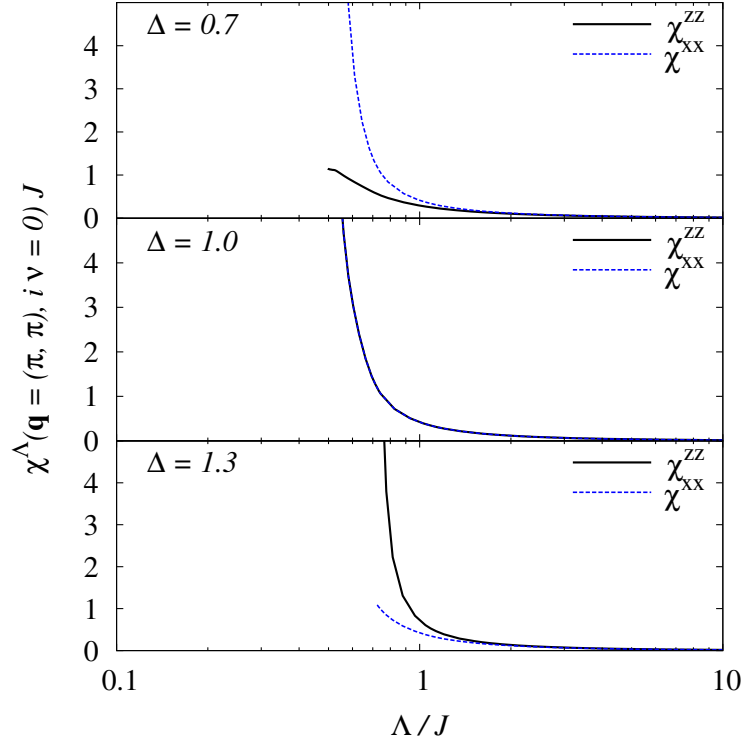


**Figure 6.1:** Flow of the static Néel susceptibility in  $z$ - and  $x$ -direction,  $\chi^{zz}$  and  $\chi^{xx}$  respectively, for different values of the anisotropy parameter  $\Delta$ . The existence of a phase transition at  $\Delta = 1$  can be confirmed, as for  $\Delta > 1$  a diverging  $\chi^{zz}$  characterizes an axial ordering, whereas for  $\Delta < 1$  the planar ordering dominates due to  $\chi^{xx} > \chi^{zz}$ .

In the easy-plane regime with  $\Delta = 0.7$ , the static Néel susceptibility  $\chi^{xx}$  diverges at  $\Lambda \approx 0.6J$ , whereas  $\chi^{zz}$  increases but remains finite. As mentioned earlier, these quantities have only a strict physical interpretation at  $\Lambda = 0$ , but the divergence of one component can be interpreted as a tendency to a magnetic ordering in this direction. Thus a planar ordering is obtained. Analogously, the diverging  $\chi^{zz}$  for  $\Delta = 1.3$  indicates an axial ordering in the system. For  $\Delta = 1$  both susceptibilities diverge simultaneously as expected. All in all, the phase transition at  $\Delta = 1$  from planar order ( $\Delta < 1$ ) to an axial ordering ( $\Delta > 1$ ) is obtained, but quantitative comparisons to other methods for the values of the susceptibility are not possible due to its divergence. Therefore, in a next step we try to connect the scale  $\Lambda_c$  at which the flow diverges with the critical temperature  $T_c$  of the system, as it is done by Reuther, Thomale and Trebst [Reu11d].

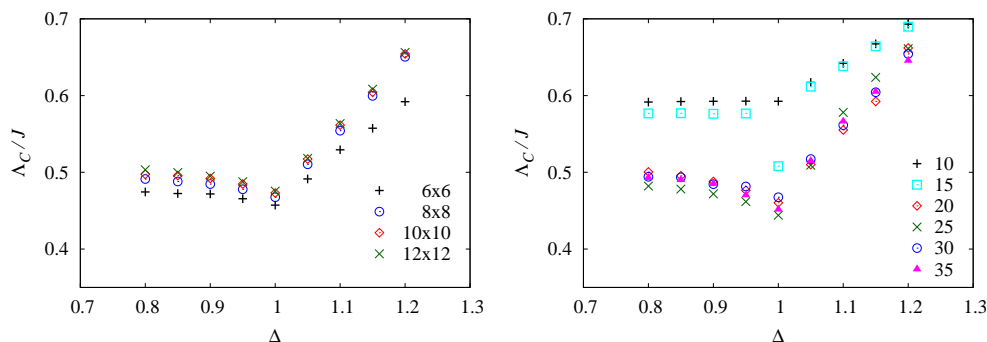


**Figure 6.2:** Left: Critical scale of the system for different lattice sizes.  $\Lambda_c$  seems to be nearly converged, only a mild effect of increasing with lattice size is obtained. Right: Critical scale for different amounts of frequencies used in the discretization of the flow equations. As long as enough frequencies are taken into account, the critical scale seems to be converged and does not show a monotonous behavior.

## 6.2 Finite Size and Frequency Discretization Effects

Before we compare the critical scale  $\Lambda_c$ , at which the flow of the vertex functions diverge, with the critical temperature of the system, we try to assess the effect of our finite system and the frequency discretization on this quantity. The results for various lattice sizes and different amounts of frequencies are shown in Fig. 6.2.

Although only lattices up to  $12 \times 12$  sites are studied due to the numerical effort of the method, the critical scale seems to be nearly converged in all regions of the anisotropy parameter  $\Delta$ . A mild finite-size effect is still visible and  $\Lambda_c$  seems to increase with system size. The number of positive frequencies  $N_f$  used in the FRG calculations show also no crucial effect on the critical scale, as long as enough frequencies  $N_f > 20$  are taken into account. Furthermore, in contrast to the system-size dependence, one cannot observe a monotonous dependence for the critical scale on the frequency discretization within the limitations of our test.

## 6.3 Critical Scale and Temperature

The critical scale  $\Lambda_c$  of the RG-flow is directly interpreted as the critical temperature  $T_c$  of the system by Reuther, Thomale and Trebst [Reu11d]. To check this interpretation, we first consider the Ising limit, meaning  $\Delta \rightarrow \infty$ , as the critical temperature for the phase transition into the ordered phase is exactly known  $T_c \approx 2.269\Delta J/4$  [Ons44]. The results in this limit are presented in Fig. 6.3.

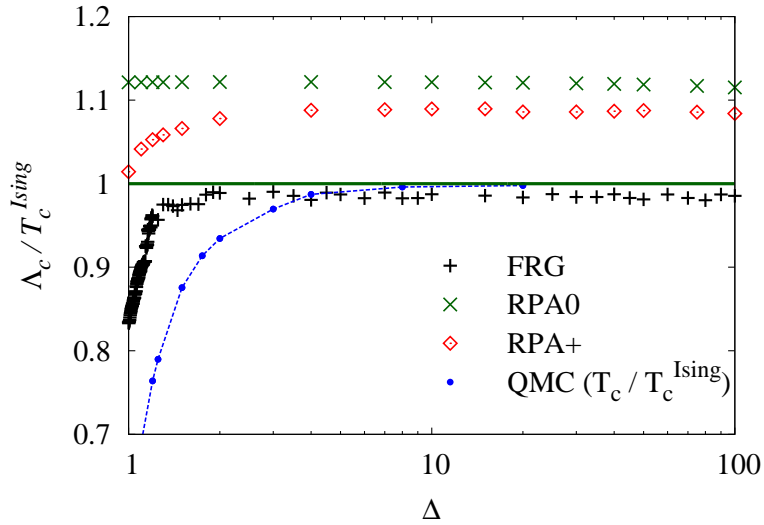


**Figure 6.3:** Critical scale  $\Lambda_c$  as a function of the anisotropy parameter  $\Delta$  for the different methods under consideration in this thesis. The spin-FRG is a distinct improvement of both RPA methods and the critical scale coincides with the critical temperature in the Ising limit  $\Delta \rightarrow \infty$  within the expected error due to various approximations.

The QMC data are numerically exact for this model due to the absence of frustration, as explained in the previous chapter. The values of the "RPA0", "RPA+" and "FRG" converge as a function of large  $\Delta$ , but their limits differ. From the comparison of the "RPA0" and the "RPA+" results we can conclude that the inclusion of the self-energy improves the results, but both methods lead to too large critical temperatures so that the ordering tendency of the system is overestimated. Concerning the various approximations within the spin-FRG calculations, the result in the Ising limit agrees rather well with the correct value, so that this method seems to be an improvement over the RPA. Furthermore, the interpretation of  $\Lambda_c$  as the critical temperature  $T_c$  might be a promising assumption at least in the Ising limit.

In a next step, we investigate the regime  $\Delta \approx 1$ , where we will show that this interpretation becomes invalid. In this regime, no analytic result for the critical temperature is known, so we will compare the results with those of the QMC analysis. Only at  $\Delta = 1$  the critical temperature has to vanish as the Mermin-Wagner theorem states the absence of a finite temperature phase transition in a model with a continuous symmetry. Remember that for  $\Delta < 1$  a continuous symmetry also exist, the rotational invariance in the  $xy$ -plane, but a BKT-transition occurs at finite temperature, whose critical temperature is calculated within the QMC analysis. The results for the various methods are shown in Fig. 6.4.



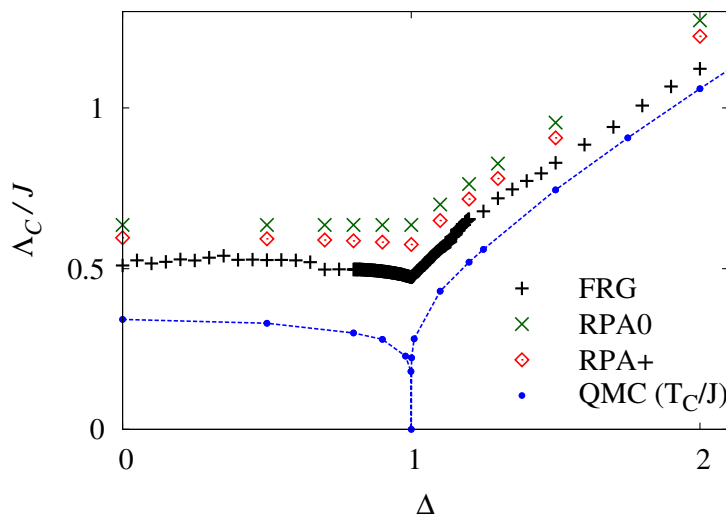


**Figure 6.4:** The spin-FRG is also an improvement of the RPA methods in the isotropic regime, but violates the Mermin-Wagner theorem at  $\Delta = 1$  significantly. The deviations between FRG results and the numerical exact estimations for  $T_c$  calculated with a QMC analysis are rather large, especially in the easy-plane regime.

Like in the Ising limit, the spin-FRG improves both RPA calculations, but the deviations to the QMC data are significantly larger than before. For  $\Delta \gtrsim 2$  the approximation of the critical temperature provides a reasonable estimate, but in the easy-plane regime it fails by roughly a factor of 2. The strongest deviations between spin-FRG and QMC data are around the isotropic point  $\Delta = 1$ . The QMC results reproduce the vanishing critical temperature, whereas the spin-FRG results stay finite and therefore violate the Mermin-Wagner theorem under the interpretation  $\Lambda_c = T_c$ . Taking a closer look at the RPA and the spin-FRG results in this regime, the "RPA0" without any self-energy inclusion does not show any special feature at  $\Delta = 1$  and the critical temperature is monotonically increasing with  $\Delta$ . The "RPA+" has a very tiny kink at this position, and a distinct kink appears in the FRG data which is again an improvement with respect to the RPA results. Nonetheless, the isotropic model is gapless and the critical temperature vanishes, so only the bare energy scale  $J$  exists. Therefore, the interpretation of  $\Lambda_c$  as any energy scale of the model fails at all. Concluding, important parts of the physics to describe the vanishing critical temperature at  $\Delta \approx 1$  correctly are obviously not captured in the spin-FRG scheme, so the interpretation of  $\Lambda_c$  as the critical temperature  $T_c$  of the system has to be taken with great caution.

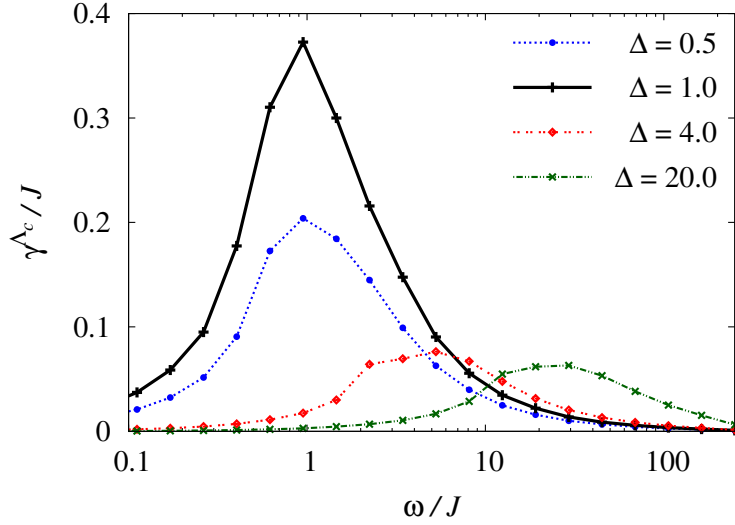


**Figure 6.5:** Auxiliary fermion self-energy near  $\Lambda = \Lambda_c$  for different values of the anisotropy parameter  $\Delta$ . It shows a peak structure with the maximum located at  $\omega \approx \Delta J$  at least for  $\Delta \geq 1$ .

## 6.4 Auxiliary Fermion Self-Energy

As explained previously, the difference between "RPA0" and "RPA+" is the generated self-energy of the auxiliary fermions. This leads to an improved description of the critical temperature at the isotropic point  $\Delta = 1$ , because the "RPA+" shows at least a weak kink in this parameter regime whereas the "RPA0" leads to a monotonically increasing critical temperature with  $\Delta$ . So probably a deeper analysis of this self-energy could shed light on the results of the spin-FRG.

Although this auxiliary fermion self-energy is not a physical quantity, as the auxiliary fermion Green function connects the physical Hilbert space with one fermion per site to the unphysical sector of doubly- or unoccupied lattice sites, we present in Fig. 6.5 the results of the spin-FRG for the frequency dependent self-energy  $\gamma^\Lambda(\omega)$  at the end of the RG-flow for different values of  $\Delta$ . One observes a peak structure with the maximum located at  $\omega \approx \Delta J$  at least for  $\Delta \geq 1$ .

The position of the peak differs qualitatively from the self-energy found in self-consistent RPA [Bri05], where the peak occurs near zero frequency. It has to be pointed out that the mismatch between the self-consistent RPA scheme and our "RPA+" could be the delayed generation of the self-energy in our implementation, although both approaches keep the same class of diagrams.

Even more accessible are the results for a two-site system. The exact form of the

auxiliary fermion self-energy can be computed by a Lehmann representation yields  $\gamma \sim 1/\omega$  [Reu11a]. The self-energy generated in our RG-flow shows the same structure as for the two-dimensional system, see Refs. [Gö11, Sä11]. A possible reason for this disagreement is an incorrect description of the small frequencies in our spin-FRG approach, which could originate from the frequency discretization with a finite  $\omega_{min}$ .

Based on this hypothesis, one could argue why the spin-FRG leads to a good approximation of the critical temperature at least in the Ising limit  $\Delta \rightarrow \infty$ . In this regime, the flow diverges at a larger scale of  $\Lambda$ . The self-energy enters into the flow only via the propagators  $\sim 1/[\omega + \gamma(\omega)]$ , so its precise form for  $\omega \geq \Lambda$  only weakly effects the results. For smaller values of  $\Delta$ , the flow reaches regimes where the self-energy becomes more and more important, so that the mismatch between the generated self-energy and the expected  $\sim 1/\omega$  behavior becomes relevant, leading to the failure of avoiding the divergence of the flow at a non-zero scale for  $\Delta = 1$ . This could be a qualitative explanation for the reasonable results in the Ising regime and the violation of the Mermin-Wagner theorem at the isotropic point.

An artificially stronger suppression of the auxiliary fermion spectral function at small frequencies could improve the results in self-consistent studies [Bri05]. Also in our spin-FRG scheme a larger self-energy around  $\omega \approx 0$  could lead to a vanishing critical temperature at the isotropic point and thus to the fulfillment of the Mermin-Wagner theorem. However, this would also strongly effect the estimations of the critical temperature for other values of  $\Delta$ , especially in the easy-plane where it would vanish.



# Chapter 7

## Conclusion

In this first part of the thesis, we compared the results of spin-FRG calculations with those of other methods, namely "RPA0", "RPA+" and QMC, to get a qualitative and quantitative assessment of the spin-FRG. Although the prediction for the phase transition of the XXZ model from planar to axial ordering at  $\Delta = 1$  could be reproduced, the interpretation of the critical scale  $\Lambda_c$  as the critical temperature  $T_c$  yields only good results in the strong Ising limit. Near the isotropic point this interpretation becomes unsatisfactory, as the Mermin-Wagner theorem was violated, and also in the easy-plane regime the critical temperature was overestimated by a factor of two. Furthermore, the self-energy of the auxiliary fermions was not generated correctly especially in the low frequency regime, leading to a divergent FRG-flow, as the self-energy was too weak to prevent this divergence.

Possible reasons for these problems are:

- It was stated that the low-energy part of the auxiliary fermion self-energy was generated too weak to prevent the divergence in the FRG-flow. A denser discretization of the frequencies would perhaps lead to better results, but the results presented in Fig. 6.2 at least do not suggest improvements due to a higher number of frequencies. Furthermore, at the isotropic point, excitations with an infinitesimal energy are possible, so that one would need a continuous treatment of the frequencies to cover the whole physics, which is numerically not possible.
- Another numerical issue is the necessity of treating a finite size system. Probably the long-wave physics is not included in our relatively small systems, so that the spin waves are too constrained. A counter-argument is given by Fig. 6.2 as the critical scale  $\Lambda_c$  increases with the system size for the models under consideration in our calculations and do not decrease as it is needed for fulfilling the Mermin-Wagner theorem.

- Another approximation was already addressed in section 4.2. The mapping from the spin-system to the fermionic one was only possible with the introduction of a constraint (eq. 4.2.4). For vanishing temperature, this constraint could only be fulfilled on average neglecting quantum fluctuations. The generated self-energy of these auxiliary fermions does not fit to the expected one and major changes to the formalism would be needed to alter this behavior. For finite temperatures the constraint can be surpassed by the introduction of an imaginary chemical potential [Pop88] which increases the numerical effort substantial as some of the presented symmetries are broken. Nevertheless, calculations for the Heisenberg model at finite temperature were done by Reuther [Reu11a], but no qualitative differences to the vanishing temperature results was found, so we do not expect that this projection is the main source of error.
- Within the FRG one sets up an infinite system of coupled differential equations, which was truncated after the four-point vertex in our study. For standard spin-Hamiltonians without a kinetic energy term, like the XXZ model, no small expansion parameter exists. Therefore, a truncation of the flow equations is a priori not controlled. Furthermore, in a bosonic description of  $O(3)$  models, the four-boson coupling needs to be included in the calculations to get a vanishing critical temperature to fulfill the Mermin-Wagner theorem. This four-boson coupling corresponds to a 1PI eight-fermion vertex which we do not include due to the truncation. So the interaction of low-lying spin fluctuations which suppress the zero-frequency ordering might not be incorporated correctly, which is also supported by the observation that the estimation of the critical temperature  $T_c$  in the easy-plane regime is worse than in the easy-axis regime, because the spin waves on the easy-plane side are gapless.

We conclude, the spin-FRG improves RPA calculations in the two dimensional quantum spin XXZ model and furthermore, it was possible to detect the quantum phase transition at  $\Delta = 1$ . The computed critical temperature in the Ising limit  $\Delta \rightarrow \infty$  coincides with the analytic solution and in the regime not too close to the isotropic point  $\Delta = 1$  the calculated critical scales were at least in the same order of magnitude as the estimations of the QMC analysis. However, at the isotropic point the spin-FRG predicts a finite critical temperature in violation of Mermin-Wagner theorem, which also destroys the quantitative validity in the vicinity of  $\Delta = 1$ . Additionally, due to the divergence in the RG-flow at finite  $\Lambda$ , no quantitative results for susceptibilities or correlation functions can be calculated and compared to other methods. These drawbacks of FRG calculations are already known in itinerant two-dimensional many

fermion systems [Met12] and the advanced approximation in the spin-FRG with the Katanin truncation, including the full self-energy feedback and frequency dependence of the vertices, cannot remedy this deficiency. All in all, the spin-FRG should only be used to explore phase diagrams whose competing ground states differ strongly, meaning a difference already in the correlation functions on short distances. These are the situations studied in most of the spin-FRG papers up to now.





# Real-Time RG Study of a Generic 2-Level Quantum Dot in the Coulomb Blockade Regime in Nonequilibrium

In the following chapters, we will apply the real time renormalization group to a generic quantum dot in the Coulomb blockade regime and compare the results for the stationary magnetization and current to those of a poor man's scaling-approach.

This part is based on Refs. [Gö15a, Gö15b].



# Chapter 8

## Motivation

Within recent years, the possibility to prepare and manipulate quantum systems has made enormous progress. One example for this is the field of ultra-cold atoms [Blo08], but also in other setups coherent quantum systems were realized, e.g., in single molecules in silicon structures [Pla12]. Furthermore, the manipulation of charge- [Pet04] and spin-degrees [Cra04, Pet05] of freedom in quantum dots (QDs) were successfully demonstrated already earlier. The ability to control these setups is one of the most important steps towards quantum computing, but it has also a variety of applications in nano-electronics and spintronics in general [Han07]. These open quantum systems show interesting many-body properties and coherent phenomena at low temperatures [And10, Sch11b]. We will focus on spin-dependent phenomena, as the elementary unit needed for quantum processing, the qubit, is often modeled by a single spin coupled to an infinite environment. Those can be described by a QD, which is tuned to the Coulomb blockade regime, such that the dot is occupied by a fixed number of charges and only other quantum numbers can be changed by an interaction with the environment. An example is the antiferromagnetic spin-1/2 Kondo model, which can be realized by a single-occupied dot, where this particle can fluctuate between two states. The investigation of this Kondo model has a long history [Hew93], and a milestone was reached by the prediction and experimental observation of universal conductance [Gla88, Ng88, GG98b, Cro98, Sim99]. Next to the broad studies of equilibrium properties of the Kondo model [Cos94, Gla05], also the non-equilibrium features at finite bias voltage and the time dynamics have been analyzed in weak [Ros01, Ros03, Keh05, Sch09b, Sch09c, Fri10, Ple10] and strong coupling [Jak10b, Eck10, Ple12, Smi13a, Smi13b, Rei14] as well as compared to experiments [Kre12, Klo13] with renormalization group (RG) methods. The isotropic Kondo model with unpolarized leads is only one special case of this QD setups with a particle fluctuating between two states. On the one hand, the leads can, e.g., be ferromagnetically with arbitrary spin orientations, on the other hand, the quantum numbers

labeling the dot levels do not have to belong to a physical spin but can also arise from different orbitals or mixtures of spin and orbital degrees of freedom in the presence of spin-orbit interaction. Thus, the tunneling matrices could be non spin-conserving. For these cases exchange fields are generated, and it has been found in equilibrium and the linear response regime that the universal properties of the Kondo model can be re-established, if one cancels those exchange fields by external ones. Within a numerical RG-approach, this could be confirmed for ferromagnetic leads with parallel or antiparallel orientations [Mar03b, Mar03a, Sin07], for orbital degrees of freedom on the dot and for Aharonov-Bohm geometries [Boe01, Boe02]. An analytical understanding was achieved by Kashcheyevs *et al.* [Kas07], as all these equilibrium models could be mapped to the anisotropic Kondo model. The studies concerning non-equilibrium situations focused on exchange fields generated by ferromagnetic leads [Kö03, Bra04, Wey07], spin-orbit interactions [Paa10], orbital fluctuations [Boe01, Boe02] or an additional Dzyaloshinskii-Moriya interaction [Ple11]. Up to now, all studies treated special cases of a pseudo spin-1/2 QD. In this thesis, we identify generic features, which are independent of the complexity of the geometry, special forms of the interactions or the polarizations of the leads.

As the dissipative environment coupled to the QD has a continuous spectrum, typically logarithmic divergences occur in all orders of perturbation theory. These are at large energies  $D \gg \Delta, 1/t$  powers of

$$J_0 \ln \frac{D}{\max\{\Delta, 1/t\}}, \quad (8.0.1)$$

where  $D$  is the band width of the reservoirs,  $J_0$  is an appropriately defined coupling constant between the reservoirs and the QD,  $\Delta$  contains all physical low-energy scales like the magnetic field, the temperature or the bias voltage, and  $t$  denotes the time variable. Furthermore, also divergences at long times  $t \gg 1/\Delta$  can occur, which are powers of  $J_0 \ln \Delta t$  [Kas13]. Perturbation theory breaks down if one of these parameters become of  $\mathcal{O}(1)$ , such that it is necessary to resum the leading logarithmic terms via some well-controlled weak-coupling RG method. Phenomenologically, one expects that the non-equilibrium setup leads to two new energy scales, the bias voltage  $V$  and the inverse time  $1/t$ , which could cut the RG-flow. One thus uses the usual poor man's scaling (PMS)-approach [And70, Hal78] to integrate out the high-energy contributions of the reservoirs step by step until the effective bandwidth becomes of the same order as  $\Lambda_c = \max\{\Delta, 1/t\}$ , which is the maximum of all physical energy scales of the system. Here, one stops the RG-flow and uses this renormalized couplings  $J_c$  as input parameters for a perturbation theory in  $J_c$ , which is at least well defined if  $J_c \ll 1$ . Although

this phenomenological ansatz is very appealing from a pragmatic point of view, it is important to check its validity by a comparison to a fully controlled microscopic approach. Therefore, many RG methods have been developed. Based on the functional renormalization group (FRG) [Met12], a quantum dot (QD) in a non-equilibrium setup has been treated in Ref. [Jak10b, Kar10], where one expands in the Coulomb interaction on the dot. Furthermore, also the flow-equation method [Weg00, Gl93, Gla94] was extended to treat this situation [Keh05, Fri10]. In this thesis, we will use the recently developed real time renormalization group (RTRG) [Sch09b]. It uses an expansion in the reservoir-dot hopping, such that it is formally close to the phenomenological poor man's scaling (PMS)-approach, which makes an analytical comparison between both ansatzes possible.



## Chapter 9

# Model: The Quantum Dot

In the first part of this chapter, we introduce a generic  $Z$ -level QD, which is coupled to an arbitrary number of non-interacting multi-channel metallic reservoirs by a generic tunneling matrix. We will show that only a specific combination of the reservoir density of states and the tunneling matrix occurs for observables supported on the local QD system. By utilizing that only this combination occurs, one can map the two-level QD to a pseudo spin-1/2 model with the spin on the dot and in the reservoirs pointing in arbitrary directions individually, which is equivalent to the Anderson impurity model with ferromagnetic leads. Afterwards, we will focus on the Coulomb blockade regime of this two-level QD with a fixed particle number  $N = 1$  on the dot. The effective Hamiltonian of this special case can be derived by a standard “Schrieffer-Wolff transformation” [Sch66], as explained in Ref. [Sch09b], and will be the starting point for our RG-approach in the next chapter. We will use the units  $\hbar = e = k_B = 1$ .

### 9.1 Generic Z-Level Quantum Dot Model

The generic  $Z$ -level interacting QD is coupled to an arbitrary number of reservoirs via tunneling processes. The Hamiltonian of this configuration is generically given by

$$H_{\text{tot}} = H_{\text{res}} + H_{\text{D}} + V, \quad (9.1.1)$$

where  $H_{\text{res}}$ ,  $H_{\text{D}}$  and  $V$  denote the reservoir, the dot and the tunneling part, respectively. The QD without the coupling to the reservoirs consists of  $Z$  single particle levels described by a complete set of quantum numbers (like the spin) and are labeled by  $l = 1, \dots, Z$  in the following. Therefore, the Hamiltonian containing an arbitrary

interaction can be written as

$$H_D = \sum_{l'} \epsilon_{l'} c_l^\dagger c_{l'} + \frac{1}{2} \sum_{l_1 l_2, l'_1 l'_2} v_{l_1 l_2, l'_1 l'_2} c_{l_1}^\dagger c_{l_2}^\dagger c_{l'_2} c_{l'_1}, \quad (9.1.2)$$

with the creation and annihilation field operators on the dot  $c_l^\dagger$  and  $c_l$ . This Hamiltonian can be diagonalized with the eigenenergies  $E_s$  and the corresponding eigenstates  $|s\rangle$ , to rewrite the Hamiltonian as

$$H_D = \sum_s E_s |s\rangle \langle s|. \quad (9.1.3)$$

The reservoirs are assumed to be infinitely large and consist of non-interacting fermions. Therefore, the Hamiltonian of this part reads

$$H_{\text{res}} = \sum_\alpha H_{\text{res}}^\alpha = \sum_{\alpha\nu\nu'k} \epsilon_{\nu\nu'}^{\alpha k} a_{\alpha\nu k}^\dagger a_{\alpha\nu'k} = \sum_{\alpha k} \underline{a}_{\alpha k}^\dagger \underline{\epsilon}^{\alpha k} \underline{a}_{\alpha k}, \quad (9.1.4)$$

with  $\alpha = 1, \dots, Z_{\text{res}}$  being the reservoir index,  $\nu = 1, \dots, Z_{\text{ch}}^\alpha$  the channel index, e.g., the spin, of the corresponding reservoir  $\alpha$ , and  $k$  represents a one-dimensional discrete index characterizing uniquely the energy dispersion of the reservoir bands. The corresponding creation and annihilation operators are  $a_{\alpha\nu k}^\dagger$  and  $a_{\alpha\nu k}$ . The column (row) vector  $\underline{a}_{\alpha k}^{(\dagger)}$  and the dispersion matrix  $\underline{\epsilon}^{\alpha k}$  are defined for a compactified notation w.r.t. the channel indices. As the reservoirs are non-interacting their density matrix in the isolated case can be described by a grandcanonical distribution function

$$\rho_{\text{res}}^{\text{eq}} = \prod_\alpha \rho_\alpha^{\text{eq}}, \quad \rho_\alpha^{\text{eq}} = \frac{1}{Z_\alpha} e^{-(H_{\text{res}}^\alpha - \mu_\alpha N_{\text{res}}^\alpha)/T_\alpha}, \quad (9.1.5)$$

with chemical potentials  $\mu_\alpha$  and temperatures  $T_\alpha$ , which could differ generically. Within this treatment of the reservoirs, spin-orbit effects and ferromagnetic leads are incorporated, as the reservoirs need not to be diagonal w.r.t. the channel index. To clarify the notation, the index  $\alpha$  denotes a specific reservoir with its temperature  $T_\alpha$  and chemical potential  $\mu_\alpha$  whereas the index  $\nu$  labels the bands within the same reservoir. Furthermore, we can also define for the density of states of the reservoirs a matrix representation

$$\underline{\rho}^\alpha(\omega) = \frac{1}{\rho_0} \sum_k \delta(\omega - \underline{\epsilon}^{\alpha k} + \mu_\alpha), \quad (9.1.6)$$

with some average density of states  $\rho_0$ .

Last but not least, the interaction  $V$  between the reservoirs and the dot has to be



specified. Again, we start with the generic form

$$V = \frac{1}{\sqrt{\rho_0}} \sum_{\alpha\nu kl} t_{\nu l}^{\alpha k} a_{\alpha\nu k}^\dagger c_l + \text{h.c.}, \quad (9.1.7)$$

with the tunneling matrix elements  $t_{\nu l}^{\alpha k}$ . The energy dependence of the tunneling matrix is taken into account for the general discussion of the model but will be neglected later. To shorten the notation, we introduce the  $Z_{\text{ch}}^\alpha \times Z$  matrix  $\underline{\underline{t}}^{\alpha k}$  with the matrix elements  $t_{\nu l}^{\alpha k}$  and rewrite  $V$  as

$$V = \frac{1}{\sqrt{\rho_0}} \sum_{\alpha k} \left\{ a_{\alpha k}^\dagger \underline{\underline{t}}^{\alpha k} \underline{c} + \underline{c}^\dagger \left( \underline{\underline{t}}^{\alpha k} \right)^\dagger a_{\alpha k} \right\}, \quad (9.1.8)$$

where  $\underline{c}$  is a vector w.r.t. the index  $l$ .

**Continuum Representation** After introducing the generic model, the question arises, if a mapping to an effective model with simpler matrix structures for the energy dispersion  $\underline{\underline{e}}^{\alpha k}$  with the matrix elements  $\epsilon_{\nu\nu'}^{\alpha k}$  and the tunneling matrix exists. Trivial unitary transformations in the channel space of the reservoirs are obviously possible, however, we will show that additionally the information can be shifted from the density of states of the reservoirs to the tunneling matrix and vice versa, as the observables under consideration depend only on a specific combination of those.

At this point, we switch to a continuum representation in the energy space of the reservoirs replacing the discrete (arbitrarily dense)  $k$  index to introduce the possibility for the system to relax into a steady-state without recurrence. Therefore, we have to switch to the basis, in which the hermitian matrix  $\underline{\underline{e}}^{\alpha k}$  is diagonal, to find a unique relationship between the discrete index  $k$  and the continuous variable  $\omega$ . We perform a unitary transformation  $\underline{\underline{U}}^{\alpha k}$  such that

$$\underline{\underline{e}}^{\alpha k} = \left( \underline{\underline{U}}^{\alpha k} \right)^\dagger \underline{\underline{\tilde{e}}}^{\alpha k} \underline{\underline{U}}^{\alpha k}, \quad (9.1.9)$$

with the diagonal matrix

$$\tilde{\epsilon}_{\nu\nu'}^{\alpha k} = \delta_{\nu\nu'} \tilde{\epsilon}_\nu^{\alpha k} \quad (9.1.10)$$

characterizing the energy-band dispersion for given reservoir and channel. With this dispersion relation the function  $k_\nu^\alpha(\omega)$  can be defined as the solution for  $k$  of the equation

$$\tilde{\epsilon}_\nu^{\alpha k} = \omega + \mu_\alpha \quad (9.1.11)$$

for given  $\alpha, \nu, \omega$ . Assuming  $\tilde{\epsilon}_\nu^{\alpha k}$  to be a monotonously increasing function of  $k$ , this solution is always unique. As a reservoir lead coupled to a QD is characterized by standing waves with quantum number  $k$  labeling the longitudinal direction, this monotony can always be achieved. Hence, all other quantum numbers like the transverse modes, the spin and further degeneracies are incorporated in the channel index  $\nu$ . Due to this unique relation between  $k$  and the energy dispersion, we can define a density of states in the diagonalized basis

$$\tilde{\rho}_\nu^\alpha(\omega) = \sum_k \delta(\omega - \tilde{\epsilon}_\nu^{\alpha k} + \mu_\alpha). \quad (9.1.12)$$

This density of states contains all information of  $\tilde{\epsilon}_\nu^{\alpha k}$  (up to a trivial shift of the  $k$ -indices) as one can first determine  $\omega_\nu^\alpha(k)$  from

$$\tilde{\epsilon}_\nu^{\alpha k} = \omega_\nu^\alpha(k) + \mu_\alpha, \quad (9.1.13)$$

then inverting this function obtaining  $k_\nu^\alpha(\omega)$ , and finally derivating this

$$\frac{1}{\delta k} \frac{d}{d\omega} k_\nu^\alpha(\omega) = \tilde{\rho}_\nu^\alpha(\omega), \quad (9.1.14)$$

with the constant distance between the discrete  $k$ -indices  $\delta k$ .

To complete the unitary transformation (9.1.9), we introduce the field operators and the tunneling matrix in this new basis by

$$\tilde{\underline{a}}_{\alpha k} = \underline{\underline{U}}^{\alpha k} \underline{a}_{\alpha k}, \quad (9.1.15)$$

$$\tilde{\underline{t}}^{\alpha k} = \underline{\underline{U}}^{\alpha k} \underline{t}^{\alpha k}, \quad (9.1.16)$$

and define also their continuum representation via

$$U_{\nu\nu'}^\alpha(\omega) = U_{\nu\nu'}^{\alpha k} \Big|_{k=k_\nu^\alpha(\omega)}, \quad (9.1.17)$$

$$\tilde{\underline{a}}_\alpha(\omega) = \frac{1}{\sqrt{\rho_0}} \sum_k \delta(\omega - \tilde{\epsilon}_\nu^{\alpha k} + \mu_\alpha) \tilde{\underline{a}}_{\alpha k}, \quad (9.1.18)$$

$$\tilde{\underline{a}}_\alpha^\dagger(\omega) = \frac{1}{\sqrt{\rho_0}} \sum_k \tilde{\underline{a}}_{\alpha k}^\dagger \delta(\omega - \tilde{\epsilon}_\nu^{\alpha k} + \mu_\alpha), \quad (9.1.19)$$

$$\tilde{t}_{\nu l}^\alpha(\omega) = \tilde{t}_{\nu l}^{\alpha k} \Big|_{k=k_\nu^\alpha(\omega)}. \quad (9.1.20)$$

The coupling between the dot and the reservoirs (9.1.8) can then be reformulated as

$$V = \sum_{\alpha} \int d\omega \left[ \tilde{a}_{\alpha}^{\dagger}(\omega) \tilde{t}_{\underline{\underline{\alpha}}}^{\alpha}(\omega) \underline{\underline{c}} + \underline{\underline{c}}^{\dagger} \tilde{t}_{\underline{\underline{\alpha}}}^{\alpha}(\omega)^{\dagger} \tilde{a}_{\alpha}(\omega) \right]. \quad (9.1.21)$$

Now we can transform back to the original basis by the definitions

$$\underline{a}_{\alpha}(\omega) = \underline{\underline{U}}^{\alpha}(\omega)^{\dagger} \tilde{a}_{\alpha}(\omega), \quad (9.1.22)$$

$$\underline{a}_{\alpha}^{\dagger}(\omega) = \tilde{a}_{\alpha}^{\dagger}(\omega) \underline{\underline{U}}^{\alpha}(\omega), \quad (9.1.23)$$

$$\underline{\rho}^{\alpha}(\omega) = \underline{\underline{U}}^{\alpha}(\omega)^{\dagger} \tilde{\rho}^{\alpha}(\omega) \underline{\underline{U}}^{\alpha}(\omega), \quad (9.1.24)$$

$$\underline{t}_{\underline{\underline{\alpha}}}^{\alpha}(\omega) = \underline{\underline{U}}^{\alpha}(\omega)^{\dagger} \tilde{t}_{\underline{\underline{\alpha}}}^{\alpha}(\omega), \quad (9.1.25)$$

with the tunneling part (9.1.21) becoming

$$V = \sum_{\alpha} \int d\omega \left[ \underline{a}_{\alpha}^{\dagger}(\omega) \underline{t}_{\underline{\underline{\alpha}}}^{\alpha}(\omega) \underline{\underline{c}} + \underline{\underline{c}}^{\dagger} \underline{t}_{\underline{\underline{\alpha}}}^{\alpha}(\omega)^{\dagger} \underline{a}_{\alpha}(\omega) \right]. \quad (9.1.26)$$

The correspondance between the quantities in the continuum description (9.1.22 - 9.1.25) to the discrete  $k$ -representation can be done by a straightforward calculation. For example, inserting eq. (9.1.15) into eq. (9.1.18) and this into eq. (9.1.22), one can use eq. (9.1.9) to show

$$\underline{a}_{\alpha}(\omega) = \frac{1}{\sqrt{\rho_0}} \sum_k \delta(\omega - \underline{\underline{\epsilon}}^{\alpha k} + \mu_{\alpha}) \underline{a}_{\alpha k}. \quad (9.1.27)$$

Equivalently, one can calculate

$$\underline{a}_{\alpha}^{\dagger}(\omega) = \frac{1}{\sqrt{\rho_0}} \sum_k \underline{a}_{\alpha k}^{\dagger} \delta(\omega - \underline{\underline{\epsilon}}^{\alpha k} + \mu_{\alpha}), \quad (9.1.28)$$

$$\underline{\rho}^{\alpha}(\omega) = \frac{1}{\rho_0} \sum_k \delta(\omega - \underline{\underline{\epsilon}}^{\alpha k} + \mu_{\alpha}), \quad (9.1.29)$$

$$t_{\nu l}^{\alpha}(\omega) = \sum_{\nu'} \left( \underline{\underline{U}}^{\alpha k} \right)_{\nu \nu'}^{\dagger} \left( \underline{\underline{U}}^{\alpha k} \underline{t}_{\underline{\underline{\alpha}}}^{\alpha k} \right)_{\nu' l} \Big|_{k=k_{\nu'}^{\alpha}(\omega)}. \quad (9.1.30)$$

The last deviation of the relation for the tunneling matrix is a little bit subtle since a unique connection between  $k$  and  $\omega$  only exists in the diagonalized basis, and as no explicit sum over  $k$  occurs on the r.h.s. of the equation, one needs to introduce two unitary matrices.

The whole information is now covered by the density of states  $\underline{\underline{\rho}}^{\alpha}(\omega)$  and the continuum representation of the tunneling matrix  $\underline{t}_{\underline{\underline{\alpha}}}^{\alpha}(\omega)$ .

**Hybridization Matrix** In this thesis, we study only physical quantities, which contain the dot degrees of freedom and the tunneling vertices. More specifically, we will investigate the reduced density matrix of the dot

$$\rho_D(t) = \text{Tr}_{\text{res}} \rho_{\text{tot}}(t) \quad (9.1.31)$$

and the expectation value of the particle current flowing from reservoir  $\alpha$  to the dot

$$I^\alpha(t) = -i \langle [H_{\text{tot}}, N_\alpha] \rangle(t) \quad (9.1.32)$$

$$= i \int d\omega \langle \underline{a}_\alpha^\dagger(\omega) \underline{t}_\alpha^\alpha(\omega) \underline{c} - \underline{c}^\dagger \underline{t}_\alpha^\alpha(\omega)^\dagger \underline{a}_\alpha(\omega) \rangle(t). \quad (9.1.33)$$

Furthermore, we are only interested in stationary properties. For  $t \rightarrow \infty$  the initial density matrix at time  $t = t_0$  is unimportant<sup>1</sup>, so we can choose it to be a product of an arbitrary dot density matrix and the equilibrium density matrix for the reservoirs

$$\rho_{\text{tot}}(t_0) = \rho_D(t_0) \rho_{\text{res}}^{\text{eq}}. \quad (9.1.34)$$

With these assumptions, one can expand in the tunneling part  $V$  and integrate out the reservoirs via Wick's theorem [Wic50] for which one needs to calculate pair contractions of the form

$$\underline{t}_\alpha^\alpha(\omega)^\dagger \overline{\underline{a}_\alpha(\omega, t) \underline{a}_{\alpha'}^\dagger(\omega', t')} \underline{t}_\alpha^\alpha(\omega'). \quad (9.1.35)$$

To evaluate this expression, we indicate some relations for the field operators in the continuum representation

$$[H_{\text{res}}, \underline{a}_\alpha(\omega)] = -(\omega + \mu_\alpha) \underline{a}_\alpha(\omega), \quad (9.1.36)$$

$$\underline{a}_\alpha(\omega, t) = e^{iH_{\text{res}}t} \underline{a}_\alpha(\omega) e^{-iH_{\text{res}}t} = e^{-i(\omega + \mu_\alpha)t} \underline{a}_\alpha(\omega), \quad (9.1.37)$$

$$\{ \underline{a}_\alpha(\omega), \underline{a}_{\alpha'}^\dagger(\omega') \} = \delta_{\alpha\alpha'} \delta(\omega - \omega') \underline{\rho}^\alpha(\omega), \quad (9.1.38)$$

$$\begin{aligned} \overline{\underline{a}_\alpha(\omega) \underline{a}_{\alpha'}^\dagger(\omega')} &= \text{Tr}_{\text{res}} \underline{a}_\alpha(\omega) \underline{a}_{\alpha'}^\dagger(\omega') \rho_{\text{res}}^{\text{eq}} \\ &= \delta_{\alpha\alpha'} \delta(\omega - \omega') \underline{\rho}^\alpha(\omega) [1 - f_\alpha(\omega)], \end{aligned} \quad (9.1.39)$$

$$\overline{\underline{a}_{\alpha'}^\dagger(\omega) \underline{a}_\alpha(\omega')} = \delta_{\alpha\alpha'} \delta(\omega - \omega') \underline{\rho}^\alpha(\omega) f_\alpha(\omega), \quad (9.1.40)$$

where  $[\cdot, \cdot]$  and  $\{\cdot, \cdot\}$  are the commutator and anticommutator, respectively, and  $f_\alpha(\omega) = (e^{\omega/T_\alpha} + 1)^{-1}$  denotes the Fermi distribution function. With this, the expression

<sup>1</sup>Only for some special points in the parameter space the initial condition affects the stationary state, like a completely decoupled dot level. These systems will not be discussed here.

(9.1.35) can be simplified to

$$\begin{aligned} \underline{t}^\alpha(\omega)^\dagger \overline{a_\alpha(\omega, t)}^\dagger a_{\alpha'}^\dagger(\omega', t') \underline{t}^{\alpha'}(\omega') &= \delta_{\alpha\alpha'} \delta(\omega - \omega') \underline{t}^\alpha(\omega)^\dagger \underline{\rho}^\alpha(\omega) \underline{t}^\alpha(\omega) \\ &\times [1 - f_\alpha(\omega)] e^{-i(\omega + \mu_\alpha)(t - t')}. \end{aligned} \quad (9.1.41)$$

Thus, the reservoirs only occur in the so called hybridization matrix, defined as

$$\underline{\Gamma}^\alpha(\omega) = 2\pi \underline{t}^\alpha(\omega)^\dagger \underline{\rho}^\alpha(\omega) \underline{t}^\alpha(\omega). \quad (9.1.42)$$

The prefactor  $2\pi$  is chosen by convention. This hybridization matrix is hermitian and a positive definite single-particle matrix in the dot space.<sup>2</sup>

At this point, we can conclude that all models with the same hybridization matrix (9.1.42) yield the same results for the physical observables studied in this thesis.

**Effective Channel-Diagonal Model** Taking a closer look at the hybridization matrix (9.1.42) it is obvious that the observables considered here are invariant not only under unitary transformations within the channel indices, but also under shift of parts of the tunneling matrix to the density of states or vice versa. For a physical interpretation of our generic model, we will first shift all information beside an overall scale  $t^\alpha(\omega)$  for each tunneling barrier into the density of states, leading to a so called “effective channel-diagonal model”. The hybridization matrix is given by

$$\underline{\Gamma}^\alpha(\omega) = 2\pi t^\alpha(\omega)^2 \underline{\rho}_{\text{eff}}^\alpha(\omega) = \frac{1}{Z} \Gamma^\alpha(\omega) \underline{\rho}_{\text{eff}}^\alpha(\omega) \quad (9.1.43)$$

with

$$\Gamma^\alpha(\omega) = 2\pi Z t^\alpha(\omega)^2 \quad (9.1.44)$$

describing the strength of the tunnel barrier  $\alpha$ . The effective tunneling matrix takes the form

$$\underline{t}_{\text{eff}}^\alpha(\omega) = t^\alpha(\omega) \underline{\mathbb{1}} \quad (9.1.45)$$

showing that one can perform a unitary transformation in the channel indices such that the effective number of channels  $Z_{\text{ch}}^\alpha$  in reservoir  $\alpha$  is the same as the number of dot levels  $Z$ . The corresponding effective density of states in the reservoirs can be

---

<sup>2</sup>For those familiar with the Keldysh formalism, the combination  $-\frac{i}{2}\underline{\Gamma}^\alpha(\omega)$  is the contribution of the noninteracting reservoir  $\alpha$  to the retarded self-energy after integrating it out.

diagonalized analogously to eq. (9.1.9) which leads to

$$\underline{\rho}_{\text{eff}}^{\alpha}(\omega) = \underline{U}_{\text{eff}}^{\alpha}(\omega) \dagger \tilde{\rho}_{\text{eff}}^{\alpha}(\omega) \underline{U}_{\text{eff}}^{\alpha}(\omega). \quad (9.1.46)$$

The matrix  $\tilde{\rho}_{\text{eff}}^{\alpha}(\omega)$  has real and positive eigenvalues since the hybridization matrix  $\underline{\Gamma}^{\alpha}(\omega)$  is hermitian and positive definite. Furthermore, the eigenvalues  $\tilde{\rho}_{\text{eff},\nu}^{\alpha}(\omega)$  characterize the polarization of the channels, which have been rotated in the  $Z$  dimensional space.

We will focus mainly on the two-level QD with  $Z = 2$ . This effective channel-diagonal model has a direct physical interpretation as an effective Anderson impurity model with ferromagnetic leads. The conserved channel index  $\nu \equiv l \equiv \sigma = \uparrow, \downarrow$  can be understood in terms of a pseudo-spin- $\frac{1}{2}$ . The dot Hamiltonian of this model can be written as an Anderson impurity model

$$H = \sum_{\sigma=\uparrow,\downarrow} \epsilon_{\sigma} c_{\sigma}^{\dagger} c_{\sigma} + U n_{\uparrow} n_{\downarrow}, \quad (9.1.47)$$

with  $n_{\sigma} = c_{\sigma}^{\dagger} c_{\sigma}$ , where the  $z$ -axis is chosen such that the effective magnetic field on the dot points in this direction. The unitary transformation matrix  $\underline{U}_{\text{eff}}^{\alpha}(\omega)$  has generically the form (up to a phase factor which can be included in  $t^{\alpha}$ )

$$\underline{U}_{\text{eff}}^{\alpha}(\omega) = e^{\frac{i}{2} \vec{\phi}_{\alpha}(\omega) \cdot \underline{\vec{\sigma}}}, \quad (9.1.48)$$

where the vector  $\vec{\phi}_{\alpha}(\omega)$  represents the rotation axis and the vector  $\underline{\vec{\sigma}} = (\underline{\sigma}_x, \underline{\sigma}_y, \underline{\sigma}_z)^T$  contains the Pauli matrices  $\sigma_i$ . The effective spin direction  $\vec{d}_{\alpha}(\omega)$  of reservoir  $\alpha$  can be computed from the rotation axis

$$\underline{R}(\vec{\phi}_{\alpha}(\omega)) \underline{e}_z = \vec{d}_{\alpha}(\omega), \quad (9.1.49)$$

where  $\underline{R}(\vec{\phi}_{\alpha}(\omega))$  is the rotation matrix in a 3-dimensional space with rotation axis  $\vec{\phi}_{\alpha}(\omega)$ .

To sum up, we derived a two-level QD coupled to ferromagnetic leads with a spin dependent density of states  $\tilde{\rho}_{\text{eff},\sigma=\uparrow,\downarrow}^{\alpha}(\omega)$  and spin polarization directions  $\vec{d}_{\alpha}(\omega)$ .

**Effective Normal Lead Model** As already mentioned earlier, the hybridization matrix determines the results of the physical observables described in this thesis. In the previous paragraph, the hopping matrix was shifted into the density of states, and here we will now alternatively shift the density of states in the tunneling matrix. We call

this the “effective normal lead model” and treat it in the next chapters. First, we need to diagonalize the hybridization matrix, which is done by the unitary transformation  $\underline{\underline{U}}_{\text{eff}}^\alpha$  defined in eq. (9.1.46). This leads to

$$\underline{\underline{\Gamma}}^\alpha(\omega) = \underline{\underline{U}}_{\text{eff}}^\alpha(\omega)^\dagger \underline{\underline{\tilde{\Gamma}}}^\alpha(\omega) \underline{\underline{U}}_{\text{eff}}^\alpha(\omega), \quad (9.1.50)$$

with the diagonal matrix  $\underline{\underline{\tilde{\Gamma}}}^\alpha(\omega)$  given by

$$\tilde{\Gamma}_{ll'}^\alpha(\omega) = \delta_{ll'} \tilde{\Gamma}_l^\alpha(\omega), \quad \tilde{\Gamma}_l^\alpha(\omega) = 2\pi \tilde{t}_l^\alpha(\omega)^2. \quad (9.1.51)$$

Furthermore, we find the relations

$$\Gamma^\alpha(\omega) = \sum_l \tilde{\Gamma}_l^\alpha(\omega) = Z 2\pi t^\alpha(\omega)^2, \quad (9.1.52)$$

$$\tilde{\Gamma}_l^\alpha(\omega) = \frac{1}{Z} \Gamma^\alpha(\omega) \tilde{\rho}_{l,\text{eff}}^\alpha(\omega). \quad (9.1.53)$$

With this, the hybridization matrix takes the form

$$\underline{\underline{\Gamma}}^\alpha(\omega) = 2\pi \underline{\underline{t}}_{\text{eff}}^\alpha(\omega)^\dagger \underline{\underline{t}}_{\text{eff}}^\alpha(\omega) \quad (9.1.54)$$

with an effective tunneling matrix whose elements read

$$t_{ll',\text{eff}}^\alpha(\omega) = \tilde{t}_l^\alpha(\omega) U_{ll',\text{eff}}^\alpha(\omega). \quad (9.1.55)$$

In this form, the density of states is a constant

$$\underline{\underline{\rho}}_{\text{eff}}^\alpha(\omega) = \rho_0 \underline{\underline{\mathbb{1}}}, \quad (9.1.56)$$

leading to an effective Hamiltonian for the reservoirs

$$H_{\text{res}}^{\text{eff}} = \sum_{\alpha\nu k} \epsilon_k a_{\alpha\nu k}^\dagger a_{\alpha\nu k}. \quad (9.1.57)$$

Again, the effective channel number  $Z_{\text{ch}}^{\text{eff}}$  coincides with the number of dot levels  $Z$ , and we will consider the case  $Z = 2$  and additionally neglect the frequency-dependence of the effective tunneling matrix and assume a vanishing temperature in all reservoirs  $T_\alpha = 0$  for the rest of this thesis. Within these assumptions, the eigenvalues of the hybridization matrix can be compactified to the form

$$\tilde{\Gamma}_l^\alpha(\omega) = \frac{1}{2} \Gamma^\alpha(\omega) (1 + lp_\alpha(\omega)), \quad (9.1.58)$$

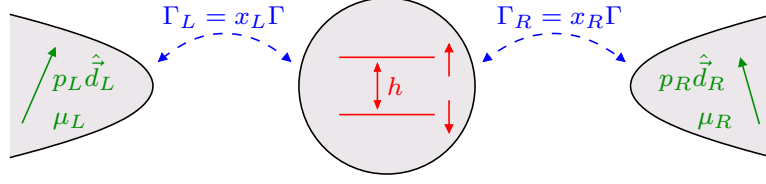


**Figure 9.1:** Sketch of the effective model of two ferromagnetic reservoirs  $\alpha = L, R$  coupled to a two-level QD via spin-conserving tunneling rates  $\Gamma_{L,R} = x_{L,R}\Gamma$ .  $\mu_{L,R}$  denote the chemical potentials and the polarizations of the reservoirs are characterized by their strength  $p_{L,R}$  and direction  $\hat{d}_{L,R}$ .  $h$  is the Zeeman-splitting of the dot.

where  $l = \pm$  and we defined the spin polarization

$$p_\alpha(\omega) = \frac{\tilde{\rho}_{\uparrow,\text{eff}}^\alpha - \tilde{\rho}_{\downarrow,\text{eff}}^\alpha}{\tilde{\rho}_{\uparrow,\text{eff}}^\alpha + \tilde{\rho}_{\downarrow,\text{eff}}^\alpha}. \quad (9.1.59)$$

The hybridization matrix can then be written in the form

$$\underline{\underline{\Gamma}}^\alpha(\omega) = \frac{1}{2}\Gamma^\alpha(\omega)\{\underline{\underline{1}} + p_\alpha(\omega)\hat{d}_\alpha(\omega) \cdot \underline{\underline{\sigma}}\}. \quad (9.1.60)$$

A sketch of this model for two external reservoirs is given in Fig. 9.1.

**Effective Tunneling-Hermitian Model** We also note a third possibility to encode the same information in the density of states and the tunneling matrix. One could again assume a constant density of states, but instead of eq. (9.1.55) we rewrite the tunneling matrix in a hermitian form by inserting an additional unitary transformation which does not change the hybridization matrix as it cancels out in eq. (9.1.54)

$$\underline{\underline{t}}_{\text{eff}}^\alpha(\omega) = \underline{\underline{U}}_{\text{eff}}^\alpha(\omega)^\dagger \tilde{\underline{\underline{t}}}^\alpha(\omega) \underline{\underline{U}}_{\text{eff}}^\alpha(\omega). \quad (9.1.61)$$

For the case  $Z = 2$  one can split  $\tilde{\underline{\underline{t}}}^\alpha(\omega)$  into

$$\tilde{\underline{\underline{t}}}^\alpha(\omega) = \lambda_1^\alpha(\omega)\underline{\underline{1}} - \lambda_2^\alpha(\omega)\underline{\underline{e}}_z \cdot \underline{\underline{\sigma}}, \quad (9.1.62)$$

with

$$\lambda_1^\alpha(\omega) = \frac{1}{2} [\tilde{t}_\downarrow^\alpha(\omega) + \tilde{t}_\uparrow^\alpha(\omega)], \quad (9.1.63)$$

$$\lambda_2^\alpha(\omega) = \frac{1}{2} [\tilde{t}_\downarrow^\alpha(\omega) - \tilde{t}_\uparrow^\alpha(\omega)], \quad (9.1.64)$$



leading to a tunneling matrix of the form

$$\underline{t}_{\text{eff}}^\alpha(\omega) = \lambda_1^\alpha(\omega)\underline{\mathbb{1}} - \lambda_2^\alpha(\omega)\vec{d}_\alpha(\omega) \cdot \underline{\vec{\sigma}}, \quad (9.1.65)$$

where we have used eq. (9.1.48). The  $\lambda_i^\alpha(\omega)$  are real numbers and  $\lambda_1^\alpha(\omega)$  is chosen to be larger than zero, and  $\vec{d}_\alpha(\omega)$  is the normalized spin polarization vector defined in eq. (9.1.49). This is exactly the model which was treated in Ref. [Ple11]. There, it was found that the vector  $\vec{d}_\alpha$  describes a Dzyaloshinskii-Moriya (DM)-interaction  $\sim \vec{d}_\alpha \cdot \vec{s}_\alpha \times \vec{S}$  between the reservoir spin  $\vec{s}_\alpha$  and the dot spin  $\vec{S}$  in the Coulomb blockade regime, which we will introduce in the next section. For this DM-vector we found another physical interpretation as it represents the direction of the spin polarization in the ferromagnetic leads when one shifts the hopping matrix into an effective density of states. Furthermore, the two parameters  $\lambda_i^\alpha(\omega)$  describes the square root of the average density of states of the two spin species in reservoir  $\alpha$  ( $\lambda_1^\alpha(\omega)$ ) and the difference of those ( $\lambda_2^\alpha(\omega)$ ).

## 9.2 Effective 2-Level QD with Fixed Particle Number N=1

From now on, we will consider a generic QD with  $Z = 2$  levels. We have shown in the previous section that this situation can be described by an Anderson impurity model with ferromagnetic leads. We shift the reservoir density of states into the tunneling matrix leading to the effective normal lead model, and furthermore neglect the frequency dependence of the tunneling matrix. Within this scheme, the tunneling matrix and the density of states are given by eq. (9.1.55) and eq. (9.1.56), respectively. The Hamiltonian in the continuum representation reads (omitting the index “eff” in the following)

$$H_{\text{tot}} = H_{\text{res}} + H_{\text{D}} + V, \quad (9.2.1)$$

$$H_{\text{res}} = \sum_{\alpha} \int d\omega (\omega + \mu_{\alpha}) \underline{a}_{\alpha}^{\dagger}(\omega) \underline{a}_{\alpha}(\omega), \quad (9.2.2)$$

$$H_{\text{D}} = \sum_{\sigma=\uparrow,\downarrow} \epsilon_{\sigma} c_{\sigma}^{\dagger} c_{\sigma} + U n_{\uparrow} n_{\downarrow}, \quad (9.2.3)$$

$$V = \sum_{\alpha} \int d\omega \left[ \underline{a}_{\alpha}^{\dagger}(\omega) \underline{g}^{\alpha} + (\underline{g}^{\alpha})^{\dagger} \underline{a}_{\alpha}(\omega) \right], \quad (9.2.4)$$

with the dot operator

$$\underline{g}^{\alpha} = \underline{t}_{\text{eff}}^{\alpha} \underline{c}, \quad (9.2.5)$$

and its anticommutation relation

$$\left\{ \underline{g}^\alpha, \left( \underline{g}^{\alpha'} \right)^\dagger \right\} = \underline{t}^\alpha \left( \underline{t}^{\alpha'} \right)^\dagger. \quad (9.2.6)$$

The equations (9.1.38 - 9.1.40) simplify to

$$\left\{ \underline{a}_\alpha(\omega), \underline{a}_{\alpha'}^\dagger(\omega') \right\} = \delta_{\alpha\alpha'} \delta(\omega - \omega') \underline{\mathbb{1}}, \quad (9.2.7)$$

$$\overline{a_{\alpha\sigma}(\omega) a_{\alpha'\sigma'}^\dagger(\omega')} = \delta_{\alpha\alpha'} \delta_{\sigma\sigma'} \delta(\omega - \omega') [1 - f_\alpha(\omega)], \quad (9.2.8)$$

$$\overline{a_{\alpha\sigma}^\dagger(\omega) a_{\alpha'\sigma'}(\omega')} = \delta_{\alpha\alpha'} \delta_{\sigma\sigma'} \delta(\omega - \omega') f_\alpha(\omega), \quad (9.2.9)$$

and the tunneling matrix can be written as

$$t_{\sigma\sigma'}^\alpha = \tilde{t}_\sigma^\alpha U_{\sigma\sigma'}^\alpha \quad (9.2.10)$$

$$= \tilde{t}_\sigma^\alpha \left[ \cos\left(\frac{\phi_\alpha}{2}\right) \delta_{\sigma\sigma'} + i \sin\left(\frac{\phi_\alpha}{2}\right) \hat{\phi}_\alpha \cdot \underline{\vec{\sigma}}_{\sigma\sigma'} \right] \quad (9.2.11)$$

with  $\phi_\alpha = |\vec{\phi}_\alpha|$ ,  $\vec{\phi}_\alpha = \phi_\alpha \hat{\phi}_\alpha$  which is defined by eq. (9.1.49). The density of states of the two spin directions in the corresponding reservoir  $\alpha$  is given by  $\tilde{\rho}_\sigma^\alpha = (\tilde{t}_\sigma^\alpha/t^\alpha)^2$ . The hybridization matrix (9.1.60) simplifies to

$$\underline{\Gamma}^\alpha(\omega) = \frac{1}{2} \Gamma^\alpha \left\{ \underline{\mathbb{1}} + p_\alpha \vec{d}_\alpha \cdot \underline{\vec{\sigma}} \right\}. \quad (9.2.12)$$

Furthermore, we introduce the notations

$$\Gamma^\alpha = \text{Tr}_\sigma \underline{\Gamma}^\alpha = \sum_\sigma \Gamma_\sigma^\alpha, \quad (9.2.13)$$

$$\underline{\Gamma} = \sum_\alpha \underline{\Gamma}^\alpha, \quad (9.2.14)$$

$$\Gamma_\sigma^\alpha = \Gamma_{\sigma\sigma}^\alpha, \quad (9.2.15)$$

$$\Gamma = \sum_\sigma \Gamma_\sigma = \sum_\sigma \Gamma_{\sigma\sigma}. \quad (9.2.16)$$

We define now the single particle energies  $\epsilon_\sigma$  of the dot levels

$$\epsilon_\sigma = \epsilon + \frac{1}{2} \sigma h_0, \quad (9.2.17)$$

with  $\sigma = \uparrow \downarrow \equiv \pm$  and the bare magnetic field chosen in  $z$ -direction  $h_0$ . The average charge excitation energies  $D_\pm$  from the single occupied dot to the double occupied one

or from an empty dot to the single occupied one, respectively, read

$$D_+ = \epsilon + U \quad \text{and} \quad D_- = -\epsilon. \quad (9.2.18)$$

Here, we have set the average chemical potential to zero

$$\mu = \frac{1}{Z_{\text{res}}} \sum_{\alpha} \mu_{\alpha} = 0, \quad (9.2.19)$$

otherwise the term  $\epsilon$  would be replaced by  $\epsilon - \mu$  in the definition of  $D_{\pm}$ . These average charge excitation energies need to be much larger than all other bare energy scales of the system

$$D_{\pm} \gg |\hbar_0|, |\mu_{\alpha}|, \Gamma^{\alpha}, \quad (9.2.20)$$

as we consider the Coulomb blockade regime with fixed particle number  $N = \sum_{\sigma} c_{\sigma}^{\dagger} c_{\sigma} = 1$  from now on, where only cotunneling processes via virtual intermediate states lead to spin fluctuations. Pair tunneling is neglected because of the assumption of a strong repulsive Coulomb interaction.

To derive the effective Hamiltonian of this model, we perform a Schrieffer-Wolff transformation [Sch66]. This is done by introducing an operator  $S$  being first order in  $V$  and defining the effective Hamiltonian

$$H_{\text{tot}}^{\text{eff}} = e^S H_{\text{tot}} e^{-S} = (1 + S + \dots) (H_0 + V) (1 - S + \dots) \quad (9.2.21)$$

$$= H_0 + V + [S, H_0] + [S, V] + \frac{1}{2} [S, [S, H_0]] + \mathcal{O}(S^3) \quad (9.2.22)$$

where  $H_0 = H_{\text{res}} + H_{\text{D}}$ . Furthermore,  $S$  is chosen such that  $H_{\text{tot}}^{\text{eff}}$  does not contain any terms linear in  $V$ , meaning  $V = -[S, H_0]$ , leading to

$$H_{\text{tot}}^{\text{eff}} = H_0 + \frac{1}{2} [S, V] + \mathcal{O}(S^3). \quad (9.2.23)$$

The virtual process of an electron hopping from the reservoir to the dot and back can be written as [Kor07]

$$g_{\alpha\sigma, \alpha'\sigma'}^+(\omega, \omega') = \frac{1}{2} \sum_{\sigma_1 \sigma'_1} c_{\sigma_1}^{\dagger} c_{\sigma'_1} \langle \sigma_1 | g_{\sigma}^{\alpha} (g_{\sigma'}^{\alpha'})^{\dagger} | \sigma'_1 \rangle \times \left( \frac{1}{\omega + \mu_{\alpha} + \sigma_1 \frac{\hbar_0}{2} - D_+} + \frac{1}{\omega' + \mu_{\alpha'} + \sigma'_1 \frac{\hbar_0}{2} - D_+} \right), \quad (9.2.24)$$

and the contrary one from the dot to the reservoir and back

$$g_{\alpha\sigma,\alpha'\sigma'}^-(\omega,\omega') = \frac{1}{2} \sum_{\sigma_1\sigma'_1} c_{\sigma_1}^\dagger c_{\sigma'_1} \langle \sigma_1 | (g_{\sigma'}^{\alpha'})^\dagger g_{\sigma}^{\alpha} | \sigma'_1 \rangle \times \left( \frac{1}{\omega + \mu_\alpha - \sigma_1 \frac{\hbar\omega_0}{2} + D_-} + \frac{1}{\omega' + \mu_{\alpha'} - \sigma'_1 \frac{\hbar\omega_0}{2} + D_-} \right). \quad (9.2.25)$$

With this, the effective interaction in the subspace  $N = 1$  is given by

$$V_{\text{eff}} = \sum_{\alpha\sigma\alpha'\sigma'} \int d\omega d\omega' \left[ g_{\alpha\sigma,\alpha'\sigma'}^+(\omega,\omega') a_{\alpha\sigma}^\dagger(\omega) a_{\alpha'\sigma'}(\omega') - g_{\alpha\sigma,\alpha'\sigma'}^-(\omega,\omega') a_{\alpha'\sigma'}(\omega') a_{\alpha\sigma}^\dagger(\omega) \right]. \quad (9.2.26)$$

Defining the normal ordering  $: \mathcal{O} :$  of a product of two operators  $a$  and  $b$

$$: ab := ab - \overline{ab} \quad (9.2.27)$$

the total effective Hamiltonian can be rewritten using (9.2.8) and (9.2.9)

$$H_{\text{tot}}^{\text{eff}} = H_{\text{res}} + H_{\text{eff}} + V_{\text{eff}}, \quad (9.2.28)$$

$$H_{\text{eff}} = H_{\text{D}} + \sum_{\eta\alpha\sigma} \int d\omega \eta f(\eta\omega) g_{\alpha\sigma,\alpha\sigma}^\eta(\omega,\omega), \quad (9.2.29)$$

$$V_{\text{eff}} = \sum_{\alpha\sigma\alpha'\sigma'} \int d\omega d\omega' : \underline{a}_\alpha^\dagger(\omega) \underline{\hat{g}}^{\alpha\alpha'}(\omega,\omega') \underline{a}_{\alpha'}(\omega') :, \quad (9.2.30)$$

with the dimensionless vertex operator matrix

$$\hat{g}_{\sigma\sigma'}^{\alpha\alpha'}(\omega,\omega') = \hat{g}_{\alpha\sigma,\alpha'\sigma'}(\omega,\omega') = \sum_{\eta} g_{\alpha\sigma,\alpha'\sigma'}^\eta(\omega,\omega'). \quad (9.2.31)$$

**Effective Dot Hamiltonian** In a next step, we calculate the additional terms to the dot Hamiltonian, which lead to corrections to the level splitting and generate transition matrix elements between the levels. As we assume a vanishing temperature  $T_\alpha = 0$  for all reservoirs, the Fermi distribution function reduces to a step function, leading to a trivial frequency integral. It is formally divergent in the uv-limit, and we will split it at some high-frequency  $D$  into the low-frequency regime from 0 to  $D$  and the high one from  $D$  to  $\infty$ . For this high-energy part of the integral, one can approximate the denominator in (9.2.24) and (9.2.25) by  $D$ . The remaining sums can be performed leading to a constant in the Coulomb blockade regime, yielding an infinite constant for the integral, which will be neglected from now on. The low-frequency contribution

reads

$$H_{\text{eff}} = H_D + \frac{1}{2} \sum_{\alpha\sigma} \sum_{\sigma_1\sigma'_1} c_{\sigma_1}^\dagger c_{\sigma'_1} \left\{ \langle \sigma_1 | g_\sigma^\alpha (g_\sigma^\alpha)^\dagger | \sigma'_1 \rangle \ln \left| \frac{D_+ - \mu_\alpha - \sigma_1 \frac{h_0}{2}}{D} \right| \right. \\ \left. + \langle \sigma_1 | (g_\sigma^\alpha)^\dagger g_\sigma^\alpha | \sigma'_1 \rangle \ln \left| \frac{D_- + \mu_\alpha - \sigma_1 \frac{h_0}{2}}{D} \right| \right\} + \text{h.c.} \quad (9.2.32)$$

As long as its large enough, the high energy scale  $D$  can be chosen arbitrarily, as the contributions from  $\ln D$  give only additional irrelevant constants. To this end, we define

$$\frac{1}{D} = \frac{1}{2} \left( \frac{1}{D_+} + \frac{1}{D_-} \right) = \frac{U}{2|\epsilon|(\epsilon + U)}. \quad (9.2.33)$$

From the definition of  $g_\sigma^\alpha$  (9.2.5) and the hybridization matrix (9.1.54) we can evaluate the matrix elements in eq. (9.2.32)

$$\sum_{\sigma} \{g_\sigma^\alpha, (g_\sigma^\alpha)^\dagger\} = \text{Tr} \underline{t}^\alpha (\underline{t}^\alpha)^\dagger = \frac{\Gamma^\alpha}{2\pi}, \quad (9.2.34)$$

$$\langle \sigma_1 | \sum_{\sigma} (g_\sigma^\alpha)^\dagger g_\sigma^\alpha | \sigma'_1 \rangle = \frac{1}{2\pi} \Gamma_{\sigma_1\sigma'_1}^\alpha. \quad (9.2.35)$$

With these, eq. (9.2.32) can be transformed to (again, some irrelevant constants are left out)

$$H_{\text{eff}} = H_D + \frac{1}{4\pi} \sum_{\alpha,\sigma,\sigma'} \sigma c_\sigma^\dagger c_{\sigma'} \Gamma_{\sigma\sigma'}^\alpha \ln \left| \frac{D_- + \mu_\alpha - \sigma' \frac{h_0}{2}}{D_+ - \mu_\alpha + \sigma' \frac{h_0}{2}} \right| \\ + \frac{1}{4\pi} \sum_{\alpha,\sigma \neq \sigma'} c_\sigma^\dagger c_{\sigma'} \Gamma_{\sigma\sigma'}^\alpha \left[ \ln \left| \frac{D_- + \mu_\alpha - \sigma \frac{h_0}{2}}{D_+ - \mu_\alpha - \sigma \frac{h_0}{2}} \right| + (\sigma \rightarrow \sigma') \right]. \quad (9.2.36)$$

Using  $D_\pm \gg |\mu_\alpha|, |h_0|$  the logarithms can be expanded

$$\ln \left| \frac{D_- + \mu_\alpha - \sigma' \frac{h_0}{2}}{D_+ - \mu_\alpha + \sigma' \frac{h_0}{2}} \right| \approx \ln \frac{D_-}{D_+} + 2 \frac{\mu_\alpha}{D} - \sigma' \frac{h_0}{D}, \quad (9.2.37)$$

$$\ln \left| \frac{D_- + \mu_\alpha - \sigma \frac{h_0}{2}}{D_+ - \mu_\alpha - \sigma \frac{h_0}{2}} \right| \approx \ln \frac{D_-}{D_+} + 2 \frac{\mu_\alpha}{D} + \frac{1}{2} \left( \frac{1}{D_+} - \frac{1}{D_-} \right) \sigma h_0, \quad (9.2.38)$$

which leads to the result for the effective Hamiltonian

$$H_{\text{eff}} = \frac{1}{2} h_0' \sum_{\sigma} \sigma c_\sigma^\dagger c_\sigma + \Delta_0 c_\uparrow^\dagger c_\downarrow + \Delta_0^* c_\downarrow^\dagger c_\uparrow, \quad (9.2.39)$$

with longitudinal and transverse fields

$$h'_0 = h_0 + \frac{\Gamma_\uparrow - \Gamma_\downarrow}{2\pi} \ln \frac{D_-}{D_+} + \frac{1}{\pi} \sum_\alpha (\Gamma_\uparrow^\alpha - \Gamma_\downarrow^\alpha) \frac{\mu_\alpha}{D} - \frac{\Gamma}{2\pi} \frac{h_0}{D}, \quad (9.2.40)$$

$$\Delta_0 = \frac{\Gamma_{\uparrow\downarrow}}{2\pi} \ln \frac{D_-}{D_+} + \frac{1}{\pi} \sum_\alpha \Gamma_{\uparrow\downarrow}^\alpha \frac{\mu_\alpha}{D}, \quad (9.2.41)$$

where we have chosen the external magnetic field in  $z$ -direction.

The Hamiltonian can also be written in the form

$$H_{\text{eff}} = h_0 \left( 1 - \frac{\Gamma}{2\pi D} \right) S^z + \frac{1}{\pi} \sum_\alpha \left( \frac{1}{2} \ln \frac{D_-}{D_+} + \frac{\mu_\alpha}{D} \right) \underline{c}^\dagger \Gamma_\alpha \underline{c} \quad (9.2.42)$$

$$= \vec{h}_{\text{eff}}^{(0)} \cdot \vec{S}, \quad (9.2.43)$$

with the effective exchange field

$$\vec{h}_{\text{eff}}^{(0)} = h_0 \left( 1 - \frac{\Gamma}{2\pi D} \right) \vec{e}_z + \frac{1}{\pi} \sum_\alpha \left( \frac{1}{2} \ln \frac{D_-}{D_+} + \frac{\mu_\alpha}{D} \right) \Gamma_\alpha p_\alpha \hat{d}_\alpha. \quad (9.2.44)$$

The first term  $\sim h_0$  on the r.h.s. of this equation contains a  $\mathcal{O}(\Gamma)$  correction to the bare magnetic field of the dot and is independent of the spin polarization in the leads. The second one contains the contribution of the spin polarizations of the reservoirs, which generate individual exchange fields pointing into the corresponding direction of the polarization axis  $\hat{d}_\alpha$ . This contribution is also of  $\mathcal{O}(\Gamma)$  and has already been derived and discussed in Ref. [Bra04] for the case  $h_0 = 0$  and a finite temperature  $T \gg \Gamma$ .

**Particle-Hole Symmetric Point** Investigating eq. (9.2.44) carefully, one can extract that the effective magnetic field is dominated by the terms  $\sim \Gamma \ln \frac{D_-}{D_+} \sim J_0 D$  if  $|D_+ - D_-| \sim D \gg |\mu_\alpha|, |h_0|$  with some characteristic exchange coupling  $J_0 \sim \Gamma/D$ , if one does not consider particle-hole symmetry  $D_+ = D_-$ . These large contributions would dominate the physics of the system, and higher order renormalization effects, which we will show are  $\sim J|\mu_\alpha|, Jh_0$  with the renormalized coupling constant  $J$  given in lowest order perturbation theory by  $J_0$ , would be negligible. Furthermore, terms  $\sim J_0 D$  would crucially depend on the definition of the high-frequency cutoff scale  $D$ , i.e. are nonuniversal contributions. Therefore, to consider a well defined effective model with universal low-energy behavior and making a renormalization group approach applicable, we will study the model at the particle-hole symmetric point

$$D_+ = D_- = D, \quad \Leftrightarrow \quad 2\epsilon + U = 0. \quad (9.2.45)$$

As already explained, this effective model is only valid in the low-energy regime compared to the charge excitation energy  $D$  of the dot. So, an additional cutoff for the reservoir frequencies  $\omega \equiv \epsilon_k - \mu_\alpha$  on the scale of  $D$  has to be introduced, which is chosen by convenience as a Lorentz-function

$$D(\omega) = \frac{D^2}{D^2 + \omega^2}. \quad (9.2.46)$$

This artificially introduced cutoff scale has nothing to do with the physical band width of the reservoir spectrum and is only needed for a well defined effective model. Of course, we have to show that the low-energy physics is universal and does not depend on the specific form of the chosen cutoff function.

**Compactification of the Effective Dot Hamiltonian and the Effective Interaction** With this high-frequency cutoff, or to be more precise with the claimed independence of the low-energy physics of the effective model of this cutoff, the vertex operator matrix  $\underline{\hat{g}}^{\alpha\alpha'}$  defined in eq. (9.2.31) can be simplified. In the denominators of eqs. (9.2.24) and (9.2.25) we need only the excitation energies  $D_+$  and  $D_-$ . Using (9.2.5) we obtain the frequency-independent result

$$\underline{\hat{g}}^{\alpha\alpha'} \approx -\frac{1}{D} \left[ \underline{g}^\alpha, \left( \underline{g}^{\alpha'} \right)^\dagger \right] = -\frac{1}{D} \underline{t}^\alpha [\underline{c}, \underline{c}^\dagger] \left( \underline{t}^{\alpha'} \right)^\dagger. \quad (9.2.47)$$

Inserting this equation into eq. (9.2.30) one derives a series of terms involving spin-spin and spin-charge interactions which has been treated in Ref. [Ple11]. However, we will keep the vertex in the form (9.2.47) as it is more compact. Performing the trace over the reservoir spin index and considering  $\alpha = \alpha'$  we get

$$\text{Tr}_\sigma \underline{\hat{g}}^{\alpha\alpha} = \frac{1}{\pi D} \underline{c}^\dagger \Gamma^\alpha \underline{c} - \frac{\Gamma^\alpha}{2\pi D}. \quad (9.2.48)$$

Therefore, the effective dot Hamiltonian (9.2.42) can be written as (again, an irrelevant constant has been neglected)

$$H_{\text{eff}} = h_0 \left( 1 - \frac{\Gamma}{2\pi D} \right) S^z + \sum_\alpha \mu_\alpha \text{Tr}_\sigma \underline{\hat{g}}^{\alpha\alpha}. \quad (9.2.49)$$

We will show later that the form of the second term on the r.h.s. of this equation stays unchanged during the RG flow if one replaces the vertex operator matrix by a

renormalized one. We can also use

$$[c, c^\dagger] = -2\underline{\underline{\sigma}} \cdot \vec{S}, \quad (9.2.50)$$

to rewrite eq. (9.2.47)

$$\begin{aligned} \underline{\underline{\hat{g}}}^{\alpha\alpha'} &\approx \frac{2}{D} t^\alpha \underline{\underline{\sigma}} \left( t^{\alpha'} \right)^\dagger \cdot \vec{S} \\ &= \underline{\underline{J}}^{\alpha\alpha'} \cdot \vec{S} \end{aligned} \quad (9.2.51)$$

with

$$\underline{\underline{J}}^{\alpha\alpha'} = \frac{2}{D} t^\alpha \underline{\underline{\sigma}} \left( t^{\alpha'} \right)^\dagger. \quad (9.2.52)$$

This form will be later used for the RG-treatment of the model.

The effective interaction (9.2.30) can be written in a more convenient form by antisymmetrizing the sequence of the two field operators via

$$g_{\eta\alpha\sigma, \eta'\alpha'\sigma'} = \delta_{\eta, -\eta'} \begin{cases} \hat{g}_{\alpha\sigma, \alpha'\sigma'} & \text{for } \eta = +, \\ -\hat{g}_{\alpha'\sigma', \alpha\sigma} & \text{for } \eta = -, \end{cases} \quad (9.2.53)$$

$$a_{\eta\alpha\sigma}(\omega) = \begin{cases} a_{\alpha\sigma}^\dagger(\omega) & \text{for } \eta = + \\ a_{\alpha\sigma}(\omega) & \text{for } \eta = - \end{cases}. \quad (9.2.54)$$

The effective interaction can then be represented as

$$V_{\text{eff}} = \frac{1}{2} g_{11'} : a_1 a_{1'} :, \quad (9.2.55)$$

where we sum/integrate implicitly over the multi-indices

$$1 \equiv \eta\alpha\sigma\omega, \quad 1' \equiv \eta'\alpha'\sigma'\omega'. \quad (9.2.56)$$



## Chapter 10

# Method: Real-Time Renormalization Group

Here, we will present the technical details to tackle the effective Anderson impurity model with ferromagnetic leads, derived in the previous chapter. The standard quantum field theoretical approach to systems in nonequilibrium is based on the Keldysh-formalism [Kel75, Hau08, Dan84, Ram86], where the field operators are integrated out via Wick's theorem or the path integral formalism [Neg88]. We cannot adopt these methods here, as the dot Hamiltonian could contain arbitrary interaction parts which need not to be quadratic, so Wick's theorem is not applicable. Due to this, only the reservoir degrees of freedom can be integrated out and the coupling vertex  $g_{1\dots n}$  remains as an operator. Furthermore, we will not expand the time evolution on the Keldysh contour, but we will introduce superoperators in Liouville space with the advantage that the two branches of the Keldysh contour can be taken together in a compact form. So at first, we reduce the problem to calculate the density matrix of the system to the derivation of an effective Liouvillian, where we integrate out the reservoir degrees of freedom. In a next step we can show that a perturbative treatment of this Liouvillian encounters the problem of logarithmic divergences, making a RG-ansatz necessary. Therefore, we derive the flow equations in the E-flow scheme of the RTRG and perform a weak coupling expansion. All these steps are simultaneously done for the Liouvillian itself to determine the reduced density matrix and the current kernel to calculate the stationary current through the system. This method was successfully applied to the Kondo model in and out of equilibrium for weakly and strongly coupled reservoirs [Sch09b, Sch09c, Ple12]. Also the time dynamics of those systems and extensions to the Dzyakoshinskii-Moriya-Kondo model were investigated [Ple10, Ple11, Rei14]. Additionally, the RTRG was adapted to the spin-1/2 and spin-1 Kondo model for a multi-channel setup [Hö12b, Hö12a, Hö14]. Furthermore, the properties of the spin

boson model were calculated [Kas13, Ken13].

## 10.1 Dot Density Matrix in Liouville Space

The main task of this thesis is to calculate the stationary density matrix of the effective Anderson impurity model with ferromagnetic leads, which has been derived in the previous chapter. So we start our considerations with the von-Neumann equation

$$\dot{\rho}(t) = -i[H, \rho(t)], \quad (10.1.1)$$

with the initial condition given at time  $t = t_0$  by eq. (9.1.34)

$$\rho(t_0) = \rho_D(t_0)\rho_{res}^{eq}. \quad (10.1.2)$$

For a time-independent Hamiltonian, it can be formally solved by a forward time evolution  $e^{-iH(t-t_0)}$  acting from the left on the initial density matrix and a backward time evolution  $e^{iH(t-t_0)}$  acting from the right. Defining a Liouville superoperator  $Lb = [H, b]$  acting on an arbitrary operator  $b$  in the Hilbert space, this can also be written as

$$\rho(t) = e^{-iH(t-t_0)}\rho(t_0)e^{iH(t-t_0)} = e^{-iL(t-t_0)}\rho(t_0). \quad (10.1.3)$$

The effect of an Liouville superoperator can be understood by a comparison to a “normal” Hilbert operator  $b$ . Given an orthonormal basis in Hilbert space defined by the ket-vectors  $|n\rangle$ , the matrix element  $b_{mn}$  is defined as the projection of  $b|n\rangle$  to the state  $|m\rangle$

$$b_{mn} = \langle m|b|n\rangle. \quad (10.1.4)$$

For the Liouville space, one can also define a Liouville ket-vector  $|mn\rangle_L$ , which is an operator in Hilbert space

$$|mn\rangle_L = |m\rangle\langle n|, \quad (10.1.5)$$

so that the matrix elements of a Liouville superoperator are given by

$$\begin{aligned} A_{mn,m'n'} &= {}_L\langle mn|A|m'n'\rangle_L = \text{Tr} [ |n\rangle\langle m| (A|m'\rangle\langle n'|) ] \\ &= \langle m| (A|m'\rangle\langle n'|) |n\rangle \end{aligned} \quad (10.1.6)$$

which can be interpreted as the projection of  $A|m'n'\rangle_L = A|m'\rangle\langle n'|$  to the state  $|mn\rangle_L = |m\rangle\langle n|$ . Products of a Liouville superoperator  $A$  and a Hilbert operator  $b$  or a second Liouville superoperator  $B$  are given by

$$\begin{aligned} (Ab)_{mn} &= \langle m| Ab |n\rangle \\ &= \sum_{m'n'} \langle m| (A|m'\rangle\langle m'| b |n'\rangle\langle n'|) |n\rangle \\ &= \sum_{m'n'} A_{mn,m'n'} b_{m'n'}, \end{aligned} \tag{10.1.7}$$

$$\begin{aligned} (AB)_{mn,m'n'} &= \langle m| (AB|m'\rangle\langle n'|) |n\rangle \\ &= \sum_{m''n''} \langle m| [A|m''\rangle\langle m''| (B|m'\rangle\langle n'|) |n''\rangle\langle n''|] |n\rangle \\ &= \sum_{m''n''} A_{mn,m''n''} B_{m''n'',m'n'}. \end{aligned} \tag{10.1.8}$$

A full Liouville superoperator basis and some useful relations are given in appendix B. After this short definition of the Liouville space, we return to the formal solution of the time-dependent density matrix (10.1.3). In the same way, as the total effective Hamiltonian defined in eq. (9.2.28) was split into a reservoir, a dot and an interaction part, the Liouvillian can also be splitted into

$$L_{\text{res}}b = [H_{\text{res}}, b], \quad L_{\text{D}}b = [H_{\text{eff}}, b], \quad L_{\text{V}}b = [V_{\text{eff}}, b]. \tag{10.1.9}$$

Analogue to the Hamiltonian, the parts  $L_{\text{res}}$  and  $L_{\text{D}}$  are easy to deal with as the reservoirs are noninteracting and the eigenstates and -energies of the uncoupled QD are known exactly. To express  $L_{\text{V}}$  in the Liouville space, we have to introduce dot superoperators and lead superoperators

$$G_{11'}^{pp'} b = \delta_{pp'} \begin{cases} g_{11'} b & \text{for } p = +, \\ -b g_{11'} & \text{for } p = -, \end{cases} \tag{10.1.10}$$

$$J_1^p b = \begin{cases} a_1 b & \text{for } p = +, \\ b a_1 & \text{for } p = -, \end{cases} \tag{10.1.11}$$

where the indices  $p$  and  $p'$  denote the corresponding time evolution on the Keldysh-contour with  $p = +$  being the forward time evolution and  $p = -$  the backward one. The effective interaction (9.2.55) can then be expressed in Liouville space by

$$L_{\text{V}} = \frac{1}{2} p' G_{11'}^{pp'} : J_1^p J_1^{p'} : \tag{10.1.12}$$

where the implicit summation over the multi-indices 1 and 1' is extended to the additional summation over  $p$  and  $p'$ .

We now return to the calculation of the central object of this thesis, the reduced density matrix of the dot. The reservoir information are included by tracing out their degrees of freedom, leading to an integro-differential equation in real-time space. By convenience, we perform a Laplace transformation to map the convolutions in real-time to products in the Laplace variable, which leads to

$$\begin{aligned}\rho_{\text{D}}(E) &= \int_{t_0}^{\infty} dt e^{iE(t-t_0)} \rho_{\text{D}}(t) \\ &= \text{Tr}_{\text{res}} \frac{i}{E - L(E)} \rho_{\text{D}}(t_0) \rho_{\text{res}},\end{aligned}\quad (10.1.13)$$

with  $\text{Im}(E) > 0$ . As we are only interested in the stationary state properties of the system, we consider the case  $E = i\eta$  with  $\eta$  being some infinitesimal positive quantity, as the stationary state density matrix  $\rho_{\text{D}}^{\text{st}} = \lim_{t \rightarrow \infty} \rho_{\text{D}}(t)$  can be computed from

$$\rho_{\text{D}}^{\text{st}} = -i \lim_{E \rightarrow i\eta} E \rho_{\text{D}}(E). \quad (10.1.14)$$

Eq. (10.1.13) is in general still not exactly solvable, so we now insert the splitted form of the Liouvillian and expand in terms of the exchange interaction  $L_V$

$$\rho_{\text{D}}(E) = i \text{Tr}_{\text{res}} \sum_{n=0}^{\infty} \left( \frac{1}{E - L_{\text{res}} - L_{\text{D}}} L_V \right)^n \frac{1}{E - L_{\text{res}} - L_{\text{D}}} \rho_{\text{D}}(t_0) \rho_{\text{res}}. \quad (10.1.15)$$

## 10.2 Wick's Theorem

To proceed with the evaluation of the reduced density matrix, the trace over the reservoir degrees of freedom in eq. (10.1.15) is performed. It is equivalent to the calculation of an expectation value with respect to the grandcanonical density matrix  $\rho_{\text{res}}^{\alpha}$  of the noninteracting reservoirs, for which Wick's theorem [Wic50] is the method of choice. It will be applied to the fermionic lead superoperators  $J_1^p$  and the reservoir Hamiltonian  $H_{\text{res}}$ , but does not act on the dot operators  $G_{11'}^{pp'}$  and the dot Hamiltonian  $H_{\text{D}}$ <sup>1</sup>. The idea of Wick's theorem is that expectation values like

$$\langle p'_1 : J_1^{p_1} J_{1'}^{p'_1} : p'_2 : J_2^{p_2} J_{2'}^{p'_2} : \cdots p'_n : J_n^{p_n} J_{n'}^{p'_n} : \rangle_{\rho_{\text{res}}} \quad (10.2.1)$$

<sup>1</sup>The extension of Wick's theorem to superoperators is discussed in Ref. [Rei09].

can be evaluated by adding up all possible decompositions of the superoperator product into pairwise contractions. Hereby, one has to regard the constraint that no superoperators of the same block :  $J_1^{p_i} J_{i'}^{p'_i}$  : are contracted to each other, which is forbidden due to the normal ordering. The pair contraction of two reservoir superoperators  $J_1^p$  and  $J_{1'}^{p'}$  is defined by

$$\gamma_{11'}^{pp'} := \overline{J_1^p J_{1'}^{p'}} = p' \text{Tr}_{\text{res}} \left\{ J_1^p J_{1'}^{p'} \rho_{\text{res}} \right\} = p' \delta_{1\bar{1}'} \rho_{\text{res}}(\omega) f(p' \eta \omega) =: \delta_{1\bar{1}'} \gamma^{p'}(\eta \omega), \quad (10.2.2)$$

where the evaluation of the trace was performed in Ref. [Rei09].  $f(\omega)$  denotes the Fermi distribution function and  $\delta_{1\bar{1}'} = \delta_{\eta-\eta'} \delta(\omega - \omega') \delta_{\alpha\alpha'} \delta_{\sigma\sigma'}$ . With this, eq. (10.2.1) can be evaluated considering the following rules

1. Contract all pairs of superoperators  $J_i^{p_i}$  without contracting those which occur in the same normal-ordered block.
2. Disentangle the contractions to a product of n contractions by commuting the superoperators without changing the order of two superoperators which are contracted. Every commutation of neighboring  $J$ 's yields a minus sign.
3. Calculate the value of the contractions according to eq. (10.2.2).
4. Repeat all previous steps for every possible pairing of the superoperators and sum up the resulting terms.

An example calculation following these rules is given by

$$\begin{aligned} \langle p'_1 : J_1^{p_1} J_{1'}^{p'_1} : p'_2 : J_2^{p_2} J_{2'}^{p'_2} : \rangle_{\rho_{\text{res}}} &= \overline{J_1^{p_1} J_{1'}^{p'_1} J_2^{p_2} J_{2'}^{p'_2}} + \overline{J_1^{p_1} J_{1'}^{p'_1} J_2^{p_2} J_{2'}^{p'_2}} \\ &= - \overline{J_1^{p_1} J_2^{p_2} J_{1'}^{p'_1} J_{2'}^{p'_2}} + \overline{J_1^{p_1} J_2^{p_2} J_{1'}^{p'_1} J_{2'}^{p'_2}} \\ &= - \gamma_{12}^{p_1 p_2} \gamma_{1'2'}^{p'_1 p'_2} + \gamma_{12'}^{p_1 p_2} \gamma_{1'2}^{p'_1 p'_2}. \end{aligned} \quad (10.2.3)$$

To apply Wick's theorem to eq. (10.1.15), in a first step the lead superoperators  $J_1^p$  have to be shifted to the right, so commutators between  $J_1^p$  and  $L_{\text{res}}$  have to be computed. A straightforward calculation yields [Rei09]

$$[J_1^p, L_{\text{res}}]b = \begin{cases} [a_1, H_{\text{res}}]b = -x_1 a_1 b & \text{for } p = +, \\ b[a_1, H_{\text{res}}] = -x_1 b a_1 & \text{for } p = -, \end{cases} \quad (10.2.4)$$

with  $x_1 = \eta_1(\omega_1 + \mu_{\alpha_1}) = \bar{\omega}_1 + \bar{\mu}_1$ . For the resolvents follow

$$J_1^p J_{1'}^{p'} \frac{1}{E - L_{\text{res}} - L_D} = \frac{1}{E + x_1 + x_{1'} - L_{\text{res}} - L_D} J_1^p J_{1'}^{p'}. \quad (10.2.5)$$

By using the fact

$$\langle J_1^p J_{1'}^{p'} \rangle_{\rho_{\text{res}}} = \overline{J_1^p J_{1'}^{p'}} \sim \delta_{\eta\bar{\eta}'} \delta_{\alpha\alpha'} \delta_{\sigma\sigma'} \delta(\omega - \omega'), \quad (10.2.6)$$

which follows from eq. (9.2.9), it can be concluded that

$$x_1 + x_{1'} = 0 \quad \text{if} \quad \overline{J_1^p J_{1'}^{p'}} \neq 0. \quad (10.2.7)$$

With this information, eq. (10.2.5) can be extended to the normal-ordered product

$$: J_1^p J_{1'}^{p'} : \frac{1}{E - L_{\text{res}} - L_D} = \frac{1}{E + x_1 + x_{1'} - L_{\text{res}} - L_D} : J_1^p J_{1'}^{p'} :, \quad (10.2.8)$$

occurring in the perturbative expansion of the reduced density matrix  $\rho_D(E)$  (10.1.15). To sum up all energy shifts in each resolvent which occur due to the commutation of the lead superoperators and the resolvents, it follows again from eq. (10.2.7) that only those contractions lead to an energy shift, where one superoperator left from the resolvent is connected with one to the right of it. We denote the shift in the resolvent after the  $j$ -th coupling superoperator  $G_{jj'}^{p_j p'_j}$  by  $X_j$  with  $X_0 = 0$ . Furthermore, due to  $\text{Tr}_{\text{res}} L_{\text{res}} = 0$ , the reservoir Liouvillian  $L_{\text{res}}$  can be omitted in the denominators of this equation, so that eq. (10.1.15) becomes

$$\rho_D(E) = i \sum_{n=0}^{\infty} \frac{1}{2^n} \left( \prod_{j=1}^n \frac{1}{E + X_{j-1} - L_D} G_{jj'}^{p_j p'_j} \right) \frac{1}{E - L_D} \rho_D(t_0) \langle \prod_{j=1}^n p'_j : J_j^{p_j} J_{j'}^{p'_j} : \rangle_{\rho_{\text{res}}}, \quad (10.2.9)$$

where empty products are defined as one, i.e.,  $\prod_{j=1}^0 \dots = 1$ . To simplify the calculation, it can be shown that all decompositions of reservoir superoperators, which only differ by an exchange of the contraction partners of the two lead superoperators in one vertex, are equal. Therefore, only one of these contributions has to be calculated and the prefactor  $\frac{1}{2^n}$  is reduced to  $\frac{1}{S}$ , where the symmetry factor  $S = 2^m$  with  $m$  being the number of pairs of vertices which are contracted twice to each other. A more detailed analysis of this can be found in Ref. [Rei09].

To sum up, the  $n$ -th order contribution to eq. (10.2.9) is given by

$$\frac{i}{S}(-1)^{N_{\text{perm}}} \left( \prod \gamma \right) \frac{1}{E - L_D} G \frac{1}{E + X_1 - L_D} G \cdots G \frac{1}{E + X_n - L_D} G \frac{1}{E - L_D} \rho_D(t_0). \quad (10.2.10)$$

For all diagrams, each element in this equation can be obtained by the diagrammatic rules defined in Ref. [Sch09b], where:

- $S = 2^m$  is the symmetry factor and  $m$  denotes the number of pairs of vertices which are contracted twice with each other.
- $N_{\text{perm}}$  is the number of permutations needed to disentangle the pair contractions of superoperators.
- $\gamma = \gamma_{11'}^{pp'}$  is the contraction with adequate indices  $1, 1', p, p'$ .
- $G = G_{11'}^{pp'}$  is the coupling superoperator acting on the dot.
- $X_j$  is the energy shift in the resolvent due to contractions of two superoperators, with one being left and the other one right of the resolvent.
- One has to sum or integrate up over all occurring indices.

It is now convenient to define the irreducible kernel  $\Sigma(E)$ , which is the sum over all possible combinations of connected diagrams [Sch09b, Sch09c]. The  $n$ -th order contribution reads

$$\Sigma(E)^{(n)} \rightarrow \frac{1}{S}(-1)^{N_{\text{perm}}} \left( \prod \gamma \right)_{\text{connected}} G \frac{1}{E + X_1 - L_D} G \cdots G \frac{1}{E + X_n - L_D} G. \quad (10.2.11)$$

With this, we can rewrite eq. (10.2.9)

$$\begin{aligned} \rho_D(E) &= \frac{i}{E - L_D} \sum_{n=0}^{\infty} \left( \Sigma(E) \frac{1}{E - L_D} \right)^n \rho_D(t_0) \\ &= \frac{i}{E - L_D^{\text{eff}}(E)} \rho_D(t_0), \end{aligned} \quad (10.2.12)$$

with the effective dot-Liouvillian

$$L_D^{\text{eff}}(E) = L_D + \Sigma(E) \quad (10.2.13)$$

and  $L_D = -2\hbar_{\text{eff}} \cdot \underline{L}^2$  in the Liouville basis for the 2-level QD defined in appendix B. In addition, a partial resummation by taking all closed subdiagrams between two fixed vertices together, where only contractions connecting vertices between the two fixed ones occur, is possible. Schoeller and Reininghaus showed [Sch09c] that this leads to the replacement

$$\frac{1}{E + X_i - L_D} \rightarrow \frac{1}{E + X_i - L_D^{\text{eff}}(E + X_i)} =: \Pi(E + X_i), \quad (10.2.14)$$

where we defined the resolvent  $\Pi(E)$ . It has the advantage of a smaller number of diagrams which has to be taken into account, but the disadvantage that  $\Sigma(E)$  can only be calculated self-consistently.

Multiplying the representation of the stationary density matrix in eq. (10.1.14) by  $i\eta - L_D^{\text{eff}}(i\eta)$  from the left and using eq. (10.2.12), it is easy to verify that the stationary density matrix yields the kinetic equation

$$L_D^{\text{eff}}(i\eta)\rho_D^{\text{st}} = 0, \quad (10.2.15)$$

so we only have to calculate the eigenvector in Liouville space to the eigenvalue  $0^+$  of the effective dot Liouvillian  $L_D^{\text{eff}}$ . Inserting eq. (10.2.11) into eq. (10.2.13), the conditional equation to calculate the effective dot Liouvillian can be visualized in a diagrammatic expression

$$L_D^{\text{eff}}(E) = L_D + \frac{1}{2} \left[ \text{diagram 1} \right] + \left[ \text{diagram 2} \right] + \mathcal{O}(G^4). \quad (10.2.16)$$

which contains all diagrams up to third order in the bare vertices. The occurring elements in this diagrammatic expression and all following ones are summarized in tab. 10.1. From this diagrammatic series it is obvious that the frequency integrations in the first diagram over the resolvent  $\Pi \sim \frac{1}{\omega + \omega' + \dots}$  leads to logarithms, which diverge in the scaling limit  $D \rightarrow \infty$  at the upper boundary. Therefore, the evaluation of these diagrams is still impossible<sup>2</sup> and we will use a RG-treatment in the following to tackle this problem. The lower boundary of the integral cannot lead to divergences, as the eigenvalue zero of the Liouvillian can be disregarded in terms of the form

$$f(L_D^{\text{eff}}(E))G_{11'}^{pp} \quad (10.2.17)$$

with an arbitrary function  $f$  and all other eigenvalues lead to a finite contribution to the lower boundary [Rei09].

<sup>2</sup>A more rigorous proof of this statement can be found, e.g., in [Sch11a].



Symbol	Name	Rule
	Bare two-point vertex $G_{11'}^{(0)}$	Indices which are contracted with each other are fixed to $1 \leftrightarrow \bar{1}$
	Effective two-point vertex $G_{12}(E, X_i)$	$X_i$ is determined from the resolvent to its left
	Resolvent $\Pi(E + X_i)$	$X_i$ is determined by a vertical cut through the contractions
	$\frac{\partial}{\partial E}\Pi(E + X_i)$	Derivative of the resolvent with respect of $E$
	Contraction $\gamma_{11'}^{pp'}(\omega)$	Integrate over $\omega$
	Contraction $\gamma_{11'}^{pp'}(\omega)$	Outgoing line of a vertex
	Derivative $\frac{d}{d\bar{\omega}}\gamma_{11'}^{pp'}(\omega)$	Derivative of the Fermi function $f(\bar{\omega})$

**Table 10.1:** This table contains a summary of objects occurring in the diagrammatic expressions used in this thesis. The indices 1 and 1' are chosen appropriate to the left and right connection.

### 10.3 Current

In addition to the stationary density matrix of the dot, we want to calculate the expectation value of the stationary current  $I^{\gamma, \text{st}}$  from reservoir  $\gamma$  into the dot. Therefore, we define the current operator  $I^\gamma(t)_H$  for reservoir  $\gamma$  in the Heisenberg picture which is given by the change of the particle number  $N_\gamma(t)_H$  in the corresponding reservoir

$$I^\gamma(t)_H = -\frac{d}{dt}N_\gamma(t)_H = -i[H, N_\gamma(t)_H]. \quad (10.3.1)$$

Changing to the Schrödinger picture and using the fact that only the interaction  $V$  changes the particle number in the reservoirs yields

$$I^\gamma = -i[V, N_\gamma]. \quad (10.3.2)$$

Analog to eq. (9.2.55) this can be expressed as [Sch09c]

$$I^\gamma = \frac{1}{2}i\gamma_{11'}^\gamma : a_1 a_{1'} :, \quad (10.3.3)$$

with

$$i\gamma_{11'}^\gamma = -2ic_{11'}^\gamma g_{11'}, \quad (10.3.4)$$

$$c_{11'}^\gamma = -\frac{1}{2}(\eta\delta_{\alpha\gamma} + \eta'\delta_{\alpha'\gamma}). \quad (10.3.5)$$

Next, we perform the same steps as for the dot density matrix. In the Liouville space, this leads to

$$(I^\gamma)_{11'}^{pp'} = c_{11'}^\gamma \delta_{pp'} p G_{11'}^{pp'} \quad (10.3.6)$$

$$L_{I^\gamma} = \frac{1}{2} p' (I^\gamma)_{11'}^{pp'} : J_1^p J_{1'}^{p'} : \quad (10.3.7)$$

and the expectation value of the current reads

$$\langle I^\gamma \rangle(t) = \text{Tr}_D \text{Tr}_{\text{res}} (-i L_{I^\gamma}) e^{-iL(t-t_0)} \rho_D(t_0) \rho_{\text{res}}. \quad (10.3.8)$$

The Laplace-transformation with the expansion in  $L_V$  leads to

$$\langle I^\gamma \rangle(E) = \text{Tr}_D \text{Tr}_{\text{res}} L_{I^\gamma} \frac{1}{E - L} \rho_D(t_0) \rho_{\text{res}}, \quad (10.3.9)$$

Finally, the current can be expressed as [Rei09]

$$\langle I^\gamma \rangle(E) = -i \text{Tr}_D \{ \Sigma^\gamma(E) \rho_D(E) \}, \quad (10.3.10)$$

where  $\Sigma^\gamma(E)$  is equivalent to  $\Sigma(E)$  with the first vertex  $G_{11'}^{pp'}$  being replaced by the current vertex  $(I^\gamma)_{11'}^{pp'}$ . Considering the stationary value, it can be determined from

$$I^{\gamma, \text{st}} = -i \text{Tr}_D \{ \Sigma^\gamma(i\eta) \rho_D^{\text{st}} \}. \quad (10.3.11)$$

## 10.4 Different RG Schemes

As it was shown in the previous sections, the perturbative expansion of the Liouvillian in bare vertices leads to logarithmic divergent frequency integrals, i.e., the  $n$ -th order contribution contains divergences of the form  $\ln^k \left( \frac{D}{\max\{|E|, \Delta\}} \right)$  with  $k \leq n - 1$  and  $\Delta = T, V, \dots$  is some physical energy scale except of  $E$ . To solve this problem, we will mention here two different RG-schemes.

**Lambda-Flow** In this scheme, the idea is to integrate out the reservoir energy scales step by step. Therefore, one introduces a high-energy cutoff parameter  $\Lambda$  in the contraction (10.2.2) by

$$\gamma_{11', \Lambda}^{pp'} = \begin{cases} p' \delta_{1\bar{1}'} \rho_{\text{res}}(\omega) f_\alpha(p' \eta \omega) & \text{for } \Lambda = \infty \\ 0 & \text{for } \Lambda = 0 \end{cases}, \quad (10.4.1)$$

i.e.,  $\gamma_{11',\Lambda}^{pp'}$  flows from its original value down to zero. An example of this could be an imaginary frequency cutoff in the Fermi distribution function  $f_\alpha(\omega)$

$$f_\alpha(\omega)_\Lambda = -T_\alpha \sum_{|\omega_n^\alpha| < \Lambda} e^{i\omega_n^\alpha \eta} \frac{1}{\omega - i\omega_n^\alpha}, \quad (10.4.2)$$

with the Matsubara frequencies  $\omega_n^\alpha = (2n + 1)\pi T_\alpha$  and the temperature  $T_\alpha$ . This scheme was successfully supplied to the Kondo model in Refs. [Sch09b, Sch09c] in the weak-coupling regime.

**E-Flow** In the E-Flow scheme, which we will apply to the generic two-level QD in this thesis, the Laplace variable  $E$  itself will be used as flow parameter. It was developed by Pletyukhov and Schoeller [Ple12] and is based on the idea that instead of expanding the effective Liouvillian in bare vertices, we expand its second derivative in effective vertices, where we will show that this leads to convergent frequency integrals. These effective vertices are defined as the sum over all connected diagrams with two outgoing lines. From the perturbative series of the kernel  $\Sigma$  (10.2.11) it can be seen that the Laplace variable  $E$  always occurs in combination with the internal frequencies and a shift due to the chemical potentials of the form  $E_{12\dots n} + \sum_{i=1}^n \bar{\omega}_i$  with  $E_{12\dots n} := E + \sum_{i=1}^n \bar{\mu}_i$ , so the imaginary part of  $E$  acts as a high-energy cutoff. Thus, for large enough  $E$  all logarithmic divergences are of the form  $\ln^k \left( \frac{D}{-iE} \right)$ , where we have chosen  $-iE$  in the argument so that the branch cuts point into the negative imaginary axis. Furthermore, a derivative with respect to  $E$  raises the exponent of the denominator in the resolvents by one. Thus, for the Liouvillian, where two frequency integrations have to be performed for the lowest order diagram, a second derivative would lead to a term  $\sim \omega^{-3}$ , which does not lead to logarithmic divergences. With this, the limit  $D \rightarrow \infty$  can be performed safely leading to universal results which do not depend on the precise form of the high-energy cutoff in the distribution function of the reservoirs. The resulting RG-equations can be symbolically written as

$$\frac{\partial^2}{\partial E^2} L_D^{\text{eff}}(E) = \mathcal{F}_L \{ L_D^{\text{eff}}(E_{12\dots n}), G_{\text{eff}}(E_{12\dots n'}) \}, \quad (10.4.3)$$

$$\frac{\partial}{\partial E} G_{\text{eff}}(E) = \mathcal{F}_G \{ L_D^{\text{eff}}(E_{12\dots n}), G_{\text{eff}}(E_{12\dots n'}) \}, \quad (10.4.4)$$

where the functionals  $F_{L/G}$  depend only on the effective Liouvillian and an effective two-point vertex  $G_{11',\text{eff}}^{pp'}$  and will be determined in the next sections.

## 10.5 Derivation of Flow Equations in the E-Flow Scheme

From now on, we will omit the index 'eff' as we always discuss the effective quantities  $L_D^{\text{eff}}$  and  $G_{\text{eff}}$  unless it is stated otherwise by an extra index (0). We start to derive the basic RG-equations (10.4.3) and (10.4.4) and use the diagrammatic expression of the effective Liouvillian in terms of the bare vertices (10.2.16) as our starting point. We already summed up those subdiagrams, where only contractions connecting vertices between two fixed vertices occur, so that the resolvent between the remaining vertices is given by  $\Pi$  defined in eq. (10.2.14). In the same way as it was done for the effective Liouvillian, one can also set up a diagrammatic series for the effective vertex  $G_{1\dots n}^{p_1\dots p_n}(E)$ , which is defined as the sum of all connected diagrams with  $n$  free lines. The diagrammatic series is exactly the same as for the effective Liouvillian with the additional conditions: [Rei14]

1. All outgoing lines are directed to the right and their frequencies and chemical potentials have to be included in the resolvents.
2. The diagram gets a factor of  $(-1)^P$ , where  $P$  is the number of permutations needed to transform the sequence of external indices  $P_1, P_2, \dots, P_n$  to  $1, 2, \dots, n$ .
3. When the outgoing lines belong to different vertices, one has to sum over all permutations of the external lines. When they belong to the same vertex, the corresponding diagram is to be computed once only.
4. As the vertices are normal ordered, a vertex cannot be contracted with itself.

For the two-point vertex, these rules give up to second order

$$\begin{aligned}
 G_{12}^{p_1 p_2}(E) - G_{12}^{(0)p_1 p_2} &= \text{Diagram} - (1 \leftrightarrow 2) \\
 &= \gamma^{\bar{p}_3}(\bar{\omega}_3) G_{13}^{(0)p_1 p_3} \Pi(E + X_{13}) G_{32}^{(0)\bar{p}_3 p_2} - (1 \leftrightarrow 2), \quad (10.5.1)
 \end{aligned}$$

where  $\bar{x} = \eta x$  and an implicit summation/integration over the internal frequencies and further indices is assumed, but not over the external ones. After defining these effective vertices, we turn back to the initial question how to perform the limit  $D \rightarrow \infty$  without the problem of divergent frequency integrals. This divergence can be estimated easily by counting the number of integrations and resolvents in each diagram. For the leading order diagram contributing to the Liouvillian, we have two internal frequency integrations and only one resolvent, so we need two derivatives with respect to the

Laplace variable  $E$  to obtain a convergent result. For the effective two-point vertex, we only have one integration and one resolvent (10.5.1), so a first derivative is sufficient. Performing the  $E$ -derivative to the Liouvillian (10.2.16), it can only act on the resolvent  $\Pi$  between the bare vertices. Choosing a specific resolvent for the derivative, the diagrams can be classified by the number of contractions running over this resolvent. By cutting those contractions, the diagrams split into two parts, and one can subsequently resum all connected diagrams to the left and to the right of the resolvent. With this resummation, one gets the effective vertices and no contraction is left which connects vertices only to the left or only to the right of the resolvent. In the remaining diagrams all contractions need to connect effective vertices which are on different sides of the resolvent which is differentiated. With this, we derived a diagrammatic series consisting only of effective vertices and all frequency integrals are convergent. For the second derivative of the Liouvillian and the first derivative of the effective two-point vertex those read up to  $\mathcal{O}(J^3)$  (with  $J$  defining the leading order of  $G_{12}$ ): [Rei14]

$$\frac{1}{2} \frac{\partial^2}{\partial E^2} L(E) = \frac{1}{2} \frac{1}{2} \left[ \text{Diagram 1} + \text{Diagram 2} \right] + \mathcal{O}(J^4) \tag{10.5.2}$$

$$\begin{aligned} \frac{\partial}{\partial E} G_{12}^{p_1 p_2}(E) = & \left[ \text{Diagram 3} - (1 \leftrightarrow 2) \right] + \frac{1}{2} \text{Diagram 4} + \frac{1}{2} \text{Diagram 5} \\ & + \left[ \text{Diagram 6} + \text{Diagram 7} - (1 \leftrightarrow 2) \right] + \mathcal{O}(J^4). \end{aligned} \tag{10.5.3}$$

Here, the prefactors arising from the symmetry factor  $S$  or from the  $E$ -derivatives  $\frac{1}{n!} \partial_E^n$  are written explicitly. From the diagrams we can see that all frequency integrations converge in the limit  $D \rightarrow \infty$  even if one neglects the frequency dependence of the two-point vertices, so this additional frequency dependence can be calculated perturbatively. Furthermore, one has to be careful with the higher-order diagrams, as the contribution to  $G_{12}^{p_1 p_2}(E)$  in  $\mathcal{O}(J^4)$  contains the four-point vertex like, e.g.,

$$\text{Diagram 8} \tag{10.5.4}$$

If one would neglect the frequency dependence of both effective vertices here, the frequency integration would diverge as there are two integrations and only one resolvent

and one derivative present. But one can show that all  $n$ -point vertices with  $n > 2$  can be expressed in terms of the two-point vertices with convergent frequency integrations [Rei14]. The limit  $D \rightarrow \infty$  can now be performed and the Liouvillian and the effective two-point vertex contain the band width  $D$  only implicitly by the initial conditions at  $E \sim iD$ ,<sup>3</sup> which will be determined later.

## 10.6 Frequency Integrals

In a next step, we want to evaluate the frequency integrations. As the resolvents depend only on the sum of the Laplace variable  $E$  and the frequencies  $\bar{\omega}_i = \eta_i \omega_i$ , we can replace the derivative with respect to  $E$  by a frequency derivative, and then apply an integration by parts. Here, we have to assume that the effective vertices can also contain a frequency dependence, so that for example the first term of eq. (10.5.3) reads

$$\begin{aligned}
 \text{Diagram 1} &= - \text{Diagram 2} - \text{Diagram 3} - \text{Diagram 4} \\
 &= - \text{Diagram 5} - \text{Diagram 6} - \text{Diagram 7}
 \end{aligned} \tag{10.6.1}$$

The diagrams consist of two vertices labeled 1 and 2. Diagram 1 shows a contraction between the two vertices with a red slash on the internal line. Diagrams 2-4 show similar contractions but with a red 'X' on the internal line, indicating a derivative. Diagrams 5-7 show more complex contractions involving multiple lines and vertices.

where the cross indicates a derivative with respect to the frequency  $\bar{\omega}$  of the corresponding contraction or vertex. From the first to the second line we have used the antisymmetry relation  $G_{12}^{p_1 p_2}(E, \bar{\omega}_1, \bar{\omega}_2) = -G_{21}^{p_2 p_1}(E, \bar{\omega}_2, \bar{\omega}_1)$  and

$$\text{Diagram 8} = \text{Diagram 9} + \mathcal{O}(J^3) \tag{10.6.2}$$

Diagram 8 shows a vertex labeled 12 with a red 'X' on the internal line. Diagram 9 shows a contraction between two vertices labeled 1 and 2 with a red slash on the internal line.

$$\text{Diagram 10} = \text{Diagram 11} + \mathcal{O}(J^3), \tag{10.6.3}$$

Diagram 10 shows a vertex labeled 21 with a red 'X' on the internal line. Diagram 11 shows a contraction between two vertices labeled 2 and 1 with a red slash on the internal line.

which can be derived analogously to eq. (10.5.3) [Rei14]. The first term of eq. (10.5.2) can be treated analogously, here two integration by parts lead to

$$\begin{aligned}
 \text{Diagram 12} &= \text{Diagram 13} + 2 \text{Diagram 14} + 2 \text{Diagram 15} + \mathcal{O}(J^4) \\
 &= \text{Diagram 16} - 4 \text{Diagram 17} + \mathcal{O}(J^4).
 \end{aligned} \tag{10.6.4}$$

Diagram 12 shows a contraction between two vertices with a red slash on the internal line. Diagram 13 shows a contraction with a red 'X' on the internal line. Diagrams 14 and 15 show similar contractions with red 'X' marks. Diagram 16 shows a contraction with a red slash on the internal line. Diagram 17 shows a contraction with a red slash on the internal line and a red 'X' on the external line.

<sup>3</sup>As mentioned earlier, the logarithmic divergences have the form  $\ln^k \left( \frac{D}{-iE} \right)$ , so the perturbative series at  $E = i\Lambda_0 \sim iD$  can be calculated without such problems.

Inserting these results into eqs. (10.5.3) and (10.5.2) many terms cancel each other, leading to the final third-order RG-equations

$$\frac{\partial^2}{\partial E^2} L(E) = \frac{1}{2} \text{diag} + \mathcal{O}(J^4) \quad (10.6.5)$$

$$\frac{\partial}{\partial E} G_{12}^{p_1 p_2}(E) = - \left[ \text{diag}_1 - (1 \leftrightarrow 2) \right] - \frac{1}{2} \text{diag}_{12} + \mathcal{O}(J^4). \quad (10.6.6)$$

The frequency derivative in the contractions acts only on the Fermi functions, and it is convenient to decompose those into a symmetric and an antisymmetric part by

$$f(\omega) = \frac{1}{2} + f^a(\omega), \quad (10.6.7)$$

so that the contraction can be split

$$\gamma^{p'}(\bar{\omega}) = p' \gamma^s(\bar{\omega}) + \gamma^a(\bar{\omega}) \quad (10.6.8)$$

with

$$\gamma^s(\bar{\omega}) = \frac{1}{2} D(\bar{\omega}), \quad \gamma^a(\bar{\omega}) = f^a(\bar{\omega}) D(\bar{\omega}). \quad (10.6.9)$$

This has the advantage that in the limit  $D \rightarrow \infty$  the index  $p'$  is split from the frequency dependent part. In particular, the frequency integrations in eqs. (10.6.5) and (10.6.6) are calculated by closing the integration path in the upper half of the complex plane. As the resolvents and the vertices are analytic there [Sch09b], only the poles of the contraction remain, which are given by the Matsubara poles of the antisymmetric part of the Fermi function. Hence, the symmetric part does not contribute and can be neglected in the RG-equations, it only has to be taken into account for the initial conditions. Furthermore, also the  $p'$ -dependence of the remaining antisymmetric contraction vanishes, so that the sum over the indices  $p$  can be performed, leading to the fact that only averaged vertices  $G_{12} = \sum_{p_1 p_2} G_{12}^{p_1 p_2}$  occur in the differential equations. Additionally, the frequency derivative of the antisymmetric contraction at vanishing temperature  $T = 0$  gives

$$\frac{\partial}{\partial \bar{\omega}} \gamma^a(\bar{\omega}) = f'(\bar{\omega}) = -\delta(\bar{\omega}), \quad (10.6.10)$$

such that those integrations become trivial. With all these information, the differential equations are finally given by

$$\frac{\partial^2}{\partial E^2} L(E) = \frac{1}{2} G_{12}(E) \Pi(E_{12}) G_{\bar{2}\bar{1}}(E_{12}), \quad (10.6.11)$$

$$\frac{\partial}{\partial E} G_{12}(E) = G_{13}(E) \Pi(E_{13}) G_{\bar{3}\bar{2}}(E_{13}) - G_{23}(E) \Pi(E_{23}) G_{\bar{3}\bar{1}}(E_{23}) \quad (10.6.12)$$

$$- \frac{i}{2} \int_0^\infty d\omega G_{34}(E) \Pi(E_{34} + i\omega) G_{12}(E_{34}) \Pi(E_{1234} + i\omega) G_{\bar{4}\bar{3}}(E_{1234}).$$

The differential equations for the current vertex  $I_{12}^\gamma(E)$  and the current kernel  $\Sigma^\gamma(E)$  are exactly the same but one replaces the first vertex on the r.h.s. by the current vertex.

## 10.7 RG-Equations for Slowly Varying Parts

Following Ref. [Kas13] it is helpful to split the kernels in parts which only vary slowly with respect to the Laplace variable  $E$

$$L(E) = L_\Delta(E) + EL'(E), \quad (10.7.1)$$

$$\Sigma^\gamma(E) = \Sigma_\Delta^\gamma(E) + E\Sigma'^\gamma(E), \quad (10.7.2)$$

where  $L_\Delta(E)$  and  $\Sigma_\Delta^\gamma(E)$  are proportional to some physical low-energy scale  $\Delta \sim \mu_\alpha, h$  and  $L'(E)$  and  $\Sigma'^\gamma(E)$  are dimensionless. In Ref. [Kas13], the differential equations for those quantities were derived up to order  $\mathcal{O}(J^2)$  and we will generalize this to the subleading order  $\mathcal{O}(J^3)$ . The main idea is to write the second derivative of the Liouvillian as first derivatives of  $L_\Delta(E)$  and  $L'(E)$  in the form

$$\frac{\partial^2}{\partial E^2} L(E) = \frac{\partial}{\partial E} L'(E) + \frac{\partial}{\partial E} \left[ \frac{\partial}{\partial E} L_\Delta(E) + E \frac{\partial}{\partial E} L'(E) \right]. \quad (10.7.3)$$

To this end we define the following quantities

$$Z'(E) = \frac{1}{1 - L'(E)}, \quad (10.7.4)$$

$$\chi_{12}^\Delta(E) = \underbrace{\bar{\mu}_{12}}_{=\bar{\mu}_1 + \bar{\mu}_2} - Z'(E_{12}) L_\Delta(E_{12}), \quad (10.7.5)$$

showing that the resolvent can be written as

$$\Pi(E_{12}) = \frac{1}{E + \chi_{12}^\Delta(E)} Z'(E_{12}). \quad (10.7.6)$$



We perform all the following steps only for the Liouvillian, but they can be simultaneously done for the current kernel if one replaces the first vertex by the current vertex. By adding terms which only contribute to  $\mathcal{O}(J^4)$ , eq. (10.6.11) can be rewritten to

$$\begin{aligned} \frac{\partial^2}{\partial E^2} L(E) = & \frac{1}{2} G_{12}(E) \Pi(E_{12}) G_{\bar{2}\bar{1}}(E_{12}) \\ & - G_{12}(E) \Pi(E_{12}) G_{\bar{2}3}(E_{12}) Z'(E_{13}) G_{\bar{3}\bar{1}}(E_{13}) \\ & - G_{12}(E) Z'(E_{12}) G_{\bar{2}3}(E_{12}) \Pi(E_{13}) G_{\bar{3}\bar{1}}(E_{13}) \\ & + \frac{\partial}{\partial E} \left[ \frac{1}{2} G_{12}(E) Z'(E_{12}) G_{\bar{2}\bar{1}}(E_{12}) \right. \\ & \left. - 2G_{12}(E) Z'(E_{12}) G_{\bar{2}3}(E_{12}) Z'(E_{13}) G_{\bar{3}\bar{1}}(E_{13}) \right] + \mathcal{O}(J^4). \end{aligned} \quad (10.7.7)$$

Hereby, the second and third term are canceled by the  $E$ -derivative of the vertices of the fourth term (up to higher orders) and the last term is of higher order and has only been added to show that  $L_\Delta(E)$  contains only terms proportional to  $\Delta$  and not to the Laplace variable  $E$  itself. By comparison, we find up to  $\mathcal{O}(J^3)$ :

$$\begin{aligned} \frac{\partial}{\partial E} L'(E) = & \frac{1}{2} G_{12}(E) \Pi(E_{12}) G_{\bar{2}\bar{1}}(E_{12}) - G_{12}(E) \Pi(E_{12}) G_{\bar{2}3}(E_{12}) Z'(E_{13}) G_{\bar{3}\bar{1}}(E_{13}) \\ & - G_{12}(E) Z'(E_{12}) G_{\bar{2}3}(E_{12}) \Pi(E_{13}) G_{\bar{3}\bar{1}}(E_{13}), \end{aligned} \quad (10.7.8)$$

$$\begin{aligned} \frac{\partial}{\partial E} L_\Delta(E) + E \frac{\partial}{\partial E} L'(E) = & \frac{1}{2} G_{12}(E) Z'(E_{12}) G_{\bar{2}\bar{1}}(E_{12}) \\ & - 2G_{12}(E) Z'(E_{12}) G_{\bar{2}3}(E_{12}) Z'(E_{13}) G_{\bar{3}\bar{1}}(E_{13}), \end{aligned} \quad (10.7.9)$$

and with eq. (10.7.6)

$$\begin{aligned} \frac{\partial}{\partial E} L_\Delta(E) = & \frac{1}{2} G_{12}(E) \frac{\chi_{12}^\Delta(E)}{E + \chi_{12}^\Delta(E)} Z'(E_{12}) G_{\bar{2}\bar{1}}(E_{12}) \\ & - G_{12}(E) \frac{\chi_{12}^\Delta(E)}{E + \chi_{12}^\Delta(E)} Z'(E_{12}) G_{\bar{2}3}(E_{12}) Z'(E_{13}) G_{\bar{3}\bar{1}}(E_{13}) \\ & - G_{12}(E) Z'(E_{12}) G_{\bar{2}3}(E_{12}) \frac{\chi_{13}^\Delta(E)}{E + \chi_{13}^\Delta(E)} Z'(E_{13}) G_{\bar{3}\bar{1}}(E_{13}), \end{aligned} \quad (10.7.10)$$

$$\begin{aligned} \frac{\partial}{\partial E} L'(E) = & \frac{1}{2} G_{12}(E) \frac{1}{E + \chi_{12}^\Delta(E)} Z'(E_{12}) G_{\bar{2}\bar{1}}(E_{12}) \\ & - G_{12}(E) \frac{1}{E + \chi_{12}^\Delta(E)} Z'(E_{12}) G_{\bar{2}3}(E_{12}) Z'(E_{13}) G_{\bar{3}\bar{1}}(E_{13}) \\ & - G_{12}(E) Z'(E_{12}) G_{\bar{2}3}(E_{12}) \frac{1}{E + \chi_{13}^\Delta(E)} Z'(E_{13}) G_{\bar{3}\bar{1}}(E_{13}). \end{aligned} \quad (10.7.11)$$

**Initial Conditions** As we set up the differential equations in the last sections, we have to specify next their initial conditions. We have to consider the lowest order diagrams for the effective Liouvillian and the two-point vertex and insert the unrenormalized values for the Liouvillian (B.1.8) and the vertices on the r.h.s of these equations, obtaining for  $D \gg \Delta$  [Sch09b]

$$\begin{aligned} L(E) &= L^{(0)} + \frac{1}{2} G_{12}^{(0)} \int \int d\omega d\omega' \frac{\gamma^p(\omega) \gamma^p(\omega')}{E_{12} - L^{(0)} + \omega + \omega'} G_{21}^{(0)pp} \\ &= L^{(0)} + \frac{1}{2} G_{12}^{(0)} \left[ -ip \frac{\pi}{2} (E_{12} - L^{(0)}) + (E_{12} - L^{(0)}) \ln \frac{-i(E_{12} - L^{(0)})}{D} \right. \\ &\quad \left. + \frac{1}{4} \left( \frac{\pi^2}{4} - 3 \right) (E_{12} - L^{(0)}) - p \frac{\pi}{2} D \right] G_{21}^{(0)pp}, \end{aligned} \quad (10.7.12)$$

$$\begin{aligned} G_{12}(E) &= G_{12}^{(0)} + \left\{ G_{13}^{(0)} \int d\omega \frac{\gamma^p(\omega)}{E_{13} - L^{(0)} + \omega} G_{32}^{(0)pp} - (1 \leftrightarrow 2) \right\} \\ &= G_{12}^{(0)} + \left\{ G_{13}^{(0)} \left[ -i \frac{\pi}{2} p + \ln \frac{-i(E_{13} - L^{(0)})}{D} \right] G_{32}^{(0)pp} - (1 \leftrightarrow 2) \right\}. \end{aligned} \quad (10.7.13)$$

The last two terms of eq. (10.7.12) are nonuniversal, i.e. they depend on the special choice of the cutoff function. The term linear in  $D$  will be discussed in detail later (see section 12.5), and we will show that it will vanish for a generic two-level QD. Concentrating on universal physics, we will omit all nonuniversal terms in the following. The logarithms can also be neglected, as they are small at  $E \sim iD$ . Defining

$$\tilde{G}_{12}^{(0)} = \sum_{p=\pm} p G_{12}^{(0)pp} \quad (10.7.14)$$

we find the initial conditions at  $E = i\Lambda_0 \sim iD$

$$L_{\Delta} \Big|_{E=i\Lambda_0} = L^{(0)} - i \frac{\pi}{4} G_{12}^{(0)} \left( \bar{\mu}_{12} - L^{(0)} \right) \tilde{G}_{21}^{(0)}, \quad (10.7.15)$$

$$L' \Big|_{E=i\Lambda_0} = -i \frac{\pi}{4} G_{12}^{(0)} \tilde{G}_{21}^{(0)}, \quad (10.7.16)$$

$$\Sigma_{\Delta}^{\gamma} \Big|_{E=i\Lambda_0} = -i \frac{\pi}{4} I_{12}^{\gamma(0)} \left( \bar{\mu}_{12} - L^{(0)} \right) \tilde{G}_{21}^{(0)}, \quad (10.7.17)$$

$$\Sigma'^{\gamma} \Big|_{E=i\Lambda_0} = -i \frac{\pi}{4} I_{12}^{\gamma(0)} \tilde{G}_{21}^{(0)}, \quad (10.7.18)$$

$$G_{12} \Big|_{E=i\Lambda_0} = G_{12}^{(0)} - i \frac{\pi}{2} \left[ G_{13}^{(0)} \tilde{G}_{32}^{(0)} - (1 \leftrightarrow 2) \right], \quad (10.7.19)$$

$$I_{12}^{\gamma} \Big|_{E=i\Lambda_0} = I_{12}^{\gamma(0)} - i \frac{\pi}{2} \left[ I_{13}^{\gamma(0)} \tilde{G}_{32}^{(0)} - (1 \leftrightarrow 2) \right]. \quad (10.7.20)$$

## 10.8 Weak Coupling Expansion

We now discuss the analytic solution of the RG-equations in the weak-coupling regime, which is defined as

$$\Lambda_c = \max\{|\mu_\alpha|, |h|\} \gg T_K, \quad (10.8.1)$$

with some low-energy scale  $T_K$ , called the Kondo-temperature, where the renormalized couplings become of  $\mathcal{O}(1)$  when  $\mu_\alpha = h = 0$ . This means that the couplings are still small for  $|E| \geq \Lambda_c$  if one is not too close to the branching points of the resolvent  $\Pi(E)$ . Following Ref. [Sch09c] we split the regime where we want to solve the RG-equations into a high- and a low-energy part separated by  $\Lambda_c$ . Starting the flow at  $E = i\Lambda_0$  and being interested in the stationary properties given at  $E = 0$ , it is convenient to rewrite the Laplace-variable  $E \rightarrow E + i\Lambda$  and integrate from  $\Lambda = \Lambda_0$  to  $\Lambda = 0$  and finally set  $E = 0$ .<sup>4</sup>

**Solution in the High-Energy Regime** In the regime  $\Lambda > \Lambda_c$  we define a reference solution, denoted by a superscript (1), in which all physical energy scales and  $E$  are set to zero. We furthermore neglect the weak frequency dependence of  $L_\Delta$  and  $Z'$  in the last term of eq. (10.6.12) such that the frequency integration can be performed easily. The RG-equations for  $L^{(1)}$ ,  $Z'^{(1)}$  and  $G_{12}^{(1)}$  read

$$\frac{\partial}{\partial \Lambda} L^{(1)} = \frac{1}{2\Lambda} G_{12}^{(1)} Z'^{(1)} G_{21}^{(1)} - \frac{2}{\Lambda} G_{12}^{(1)} G_{23}^{(1)} G_{31}^{(1)} + \mathcal{O}(J^4), \quad (10.8.2)$$

$$\frac{\partial}{\partial \Lambda} Z'^{(1)} = Z'^{(1)} \frac{\partial}{\partial \Lambda} L^{(1)} Z'^{(1)} + \mathcal{O}(J^4), \quad (10.8.3)$$

$$\frac{\partial}{\partial \Lambda} G_{12}^{(1)} = \frac{1}{\Lambda} G_{13}^{(1)} Z'^{(1)} G_{32}^{(1)} - \frac{1}{\Lambda} G_{23}^{(1)} Z'^{(1)} G_{31}^{(1)} - \frac{1}{2\Lambda} G_{34}^{(1)} G_{12}^{(1)} G_{43}^{(1)} + \mathcal{O}(J^4), \quad (10.8.4)$$

and their initial conditions depend only on the initial coupling vertex  $g_{12}$  but not on the other physical parameters of the system, whereas  $L_\Delta^{(1)}$

$$\frac{\partial}{\partial \Lambda} L_\Delta^{(1)} = \frac{1}{2\Lambda} G_{12}^{(1)} \chi_{12}^{(1)} Z'^{(1)} G_{21}^{(1)} - \frac{1}{\Lambda} G_{12}^{(1)} \chi_{12}^{(1)} G_{23}^{(1)} G_{31}^{(1)} - \frac{1}{\Lambda} G_{12}^{(1)} G_{23}^{(1)} \chi_{13}^{(1)} G_{31}^{(1)} + \mathcal{O}(J^4) \quad (10.8.5)$$

with  $\chi_{12}^{(1)} = E_{12} - Z'^{(1)} L_\Delta^{(1)}$  contains also the initial dot Hamiltonian and the chemical potentials. Again, the differential equations for the reference solution of the current vertex  $I_{12}^{\gamma(1)}$  and the current kernels  $\Sigma^{\gamma(1)}$  and  $\Sigma_\Delta^{\gamma(1)}$  can be obtained by replacing the

<sup>4</sup>Within this scheme, one could also calculate the time evolution of a system, see Ref. [Rei14].

first vertex with the current vertex.

In a next step, we calculate the next correction to the reference solution and denote it by a superscript (2). With  $\frac{1}{\Lambda}J^2 \sim \frac{d}{d\Lambda}J$  we find for the low-energy scale  $\Delta \sim \mu_\alpha, h$  the approximation

$$\frac{1}{\Lambda}J^n \sim \frac{d}{d\Lambda}J^{n-1}, \quad (10.8.6)$$

$$\begin{aligned} \frac{\Delta}{\Lambda^2}J^n &\sim \left( \frac{d}{d\Lambda} \frac{\Delta}{\Lambda} \right) J^n \\ &\sim \frac{d}{d\Lambda} \frac{\Delta}{\Lambda} J^n + \frac{\Delta}{\Lambda} J^{n-1} \frac{d}{d\Lambda} J \\ &\sim \frac{d}{d\Lambda} \frac{\Delta}{\Lambda} J^n + \frac{\Delta}{\Lambda^2} J^{n+1}, \end{aligned} \quad (10.8.7)$$

so terms on the r.h.s. of the RG-equations with a prefactor  $\frac{1}{\Lambda}$  become one order less in  $J$  after the integration, those with a prefactor  $\frac{\Delta}{\Lambda^2}$  remain of the same order. We can furthermore use

$$\frac{1}{\Lambda - i\chi_{12}} = \frac{1}{\Lambda} + \mathcal{O}\left(\frac{\Delta}{\Lambda^2}\right), \quad (10.8.8)$$

$$G_{12}(E_{1\dots n} + i\Lambda) = G_{12}(i\Lambda) + \mathcal{O}\left(\frac{\Delta}{\Lambda}J^2\right), \quad (10.8.9)$$

to neglect all low energy scales in the arguments of all quantities and it is thus sufficient to consider only the lowest order of the RG-equations (10.7.10), (10.7.11) and (10.6.12). The first correction can then be determined by replacing all quantities by their reference solution, leading to

$$\frac{\partial}{\partial\Lambda}L_\Delta^{(2)} = \frac{1}{2}G_{12}^{(1)}\chi_{12}^{(1)} \left( \frac{1}{\Lambda - i\chi_{12}^{(1)}} - \frac{1}{\Lambda} \right) G_{21}^{(1)}, \quad (10.8.10)$$

$$\frac{\partial}{\partial\Lambda}L'^{(2)} = \frac{1}{2}G_{12}^{(1)} \left( \frac{1}{\Lambda - i\chi_{12}^{(1)}} - \frac{1}{\Lambda} \right) G_{21}^{(1)}, \quad (10.8.11)$$

$$\frac{\partial}{\partial\Lambda}G_{12}^{(2)} = G_{13}^{(1)} \left( \frac{1}{\Lambda - i\chi_{13}^{(1)}} - \frac{1}{\Lambda} \right) G_{32}^{(1)} - (1 \leftrightarrow 2). \quad (10.8.12)$$

We can integrate those by using

$$\begin{aligned} \left( \frac{1}{\Lambda - i\chi_{12}^{(1)}} - \frac{1}{\Lambda} \right) J^2 &= \frac{d}{d\Lambda} \left( \ln \frac{\Lambda - i\chi_{12}^{(1)}}{\Lambda} J^2 \right) \\ &+ \mathcal{O}\left( \frac{1}{\Lambda} \frac{d\chi_{12}^{(1)}}{d\Lambda} J^2 \right) + \mathcal{O}\left( \ln \frac{\Lambda - i\chi_{12}^{(1)}}{\Lambda} J \frac{dG}{d\Lambda} \right) \end{aligned} \quad (10.8.13)$$

together with

$$\frac{1}{\Lambda} \frac{d\chi_{12}^{(1)}}{d\Lambda} J^2 \sim \frac{\chi_{12}^{(1)}}{\Lambda^2} J^4, \quad (10.8.14)$$

$$\ln \frac{\Lambda - i\chi_{12}^{(1)}}{\Lambda} J \frac{dG}{d\Lambda} \sim \frac{\chi_{12}^{(1)}}{\Lambda^2} J^3 \quad (10.8.15)$$

so that we can neglect those contributions. We finally get for the first correction to the reference solution up to  $\mathcal{O}(J^2)$

$$L_{\Delta}^{(2)} = \frac{1}{2} G_{12}^{(1)} \chi_{12}^{(1)} \ln \frac{\Lambda - i\chi_{12}^{(1)}}{\Lambda} G_{21}^{(1)}, \quad (10.8.16)$$

$$L'^{(2)} = Z'^{(2)} = \frac{1}{2} G_{12}^{(1)} \ln \frac{\Lambda - i\chi_{12}^{(1)}}{\Lambda} G_{21}^{(1)}, \quad (10.8.17)$$

$$G_{12}^{(2)} = G_{13}^{(1)} \ln \frac{\Lambda - i\chi_{13}^{(1)}}{\Lambda} G_{32} - (1 \leftrightarrow 2). \quad (10.8.18)$$

**Solution in the Low-Energy Regime** The previously defined reference solution and the first correction to it will be used as initial condition at  $\Lambda = \Lambda_c$ . We solve the RG-equations (10.7.10), (10.7.11) and (10.6.12) in the regime  $\Lambda < \Lambda_c$  perturbatively in the reference solution  $G_{12}^{(1)c} = G_{12}^{(1)}|_{\Lambda=\Lambda_c}$ . This perturbative series is well defined as the logarithmic divergences are summed up in the reference solution and the couplings are still small due to the weak-coupling condition. The lowest order contributions are already  $\mathcal{O}(J_c^2)$  so it is enough to consider only the lowest order diagrams for the RG-equations and replace all quantities by their reference solution evaluated at  $\Lambda = \Lambda_c$ . The remaining  $\Lambda$ -dependence is contained in the resolvent, which can be integrated via

$$\frac{1}{\Lambda - i\chi_{12}^{(1)c}} = \frac{d}{d\Lambda} \ln \frac{\Lambda - i\chi_{12}^{(1)c}}{\Lambda_c}. \quad (10.8.19)$$

So we find the final result valid for  $\Lambda < \Lambda_c$

$$L_{\Delta}(E + i\Lambda) = L_{\Delta}^{(1)c} + \frac{1}{2} G_{12}^{(1)c} \chi_{12}^{(1)c} \ln \frac{\Lambda - i\chi_{12}^{(1)c}}{\Lambda_c} G_{21}^{(1)c}, \quad (10.8.20)$$

$$L'(E + i\Lambda) = L'^{(1)c} + \frac{1}{2} G_{12}^{(1)c} \ln \frac{\Lambda - i\chi_{12}^{(1)c}}{\Lambda_c} G_{21}^{(1)c}, \quad (10.8.21)$$

$$Z'(E + i\Lambda) = Z'^{(1)c} + \frac{1}{2} G_{12}^{(1)c} \ln \frac{\Lambda - i\chi_{12}^{(1)c}}{\Lambda_c} G_{21}^{(1)c}, \quad (10.8.22)$$

$$G_{12}(E + i\Lambda) = G_{12}^{(1)c} + G_{13}^{(1)c} \ln \frac{\Lambda - i\chi_{13}^{(1)c}}{\Lambda_c} G_{32}^{(1)c} - (1 \leftrightarrow 2). \quad (10.8.23)$$

A modification of the definition of  $\Lambda_c$  by a factor of  $\mathcal{O}(1)$  would not change the solution up to  $\mathcal{O}(J_c^2)$  as the changes would cancel. Again, the current vertex and the current kernels could be calculated analogously by replacing the first vertex by the current vertex.

## 10.9 Summary of the RTRG

We are interested in the stationary properties of the system determined by eqs. (10.2.15) and (10.3.11) in leading and next-leading order, so we only need to calculate the Liouvillian and the current kernel at  $E = 0$ . With the decompositions (10.7.1) and (10.7.2) it is obvious that all these information are contained in  $L_\Delta$  and  $\Sigma_\Delta^\gamma$ . Therefore, we solve the differential equations in the high-energy regime (10.8.3 - 10.8.5) with the initial conditions (10.7.15, 10.7.19) and  $Z^{(1)}|_{\Lambda=\Lambda_0} = 1$  to determine the reference solutions  $L_\Delta^{(1)}$ ,  $G_{12}^{(1)}$  and  $Z^{(1)}$  and insert them into the equation (10.8.20), where we set finally  $E + i\Lambda = 0$ . The same is done for  $\Sigma_\Delta^\gamma$  by replacing the first vertex by the current vertex.  $L'$  and  $\Sigma'^\gamma$  have not to be calculated explicitly as  $L'$  only contributes implicitly due to the  $Z'$ -factor and  $\Sigma'^\gamma$  does not contribute at all. Furthermore, we need this  $Z'$ -factor only up to  $\mathcal{O}(J)$  because it always occurs in combination with at least two vertex functions in the differential equations under consideration.

## 10.10 Poor Man's Scaling

In the next chapter, we will compare our results to those of a PMS-approach [And70, Hal78]. Therefore, we shortly define what can be understood as a PMS-solution of the system under consideration. Instead of our RG-equations in the high-energy regime, within a PMS-approach one expands the Liouvillian in bare vertices (similar to eq. 10.7.12) and replaces the bare vertices with effective ones. These can be calculated in Hilbert-space via

$$\frac{d}{d\Lambda} g_{12}^{\text{PMS}} = \frac{1}{\Lambda} [g_{13}^{\text{PMS}} g_{32}^{\text{PMS}} - (1 \leftrightarrow 2)] \quad (10.10.1)$$

which yields for the vertices in Liouville space

$$\frac{d}{d\Lambda} G_{12}^{\text{PMS}} = \frac{1}{\Lambda} G_{13}^{\text{PMS}} G_{32}^{\text{PMS}} - (1 \leftrightarrow 2), \quad (10.10.2)$$

$$\frac{d}{d\Lambda} \tilde{G}_{12}^{\text{PMS}} = \frac{1}{\Lambda} \left( G_{13}^{\text{PMS}} \tilde{G}_{32}^{\text{PMS}} - \tilde{G}_{23}^{\text{PMS}} G_{31}^{\text{PMS}} \right), \quad (10.10.3)$$

which is identical to the leading order of eq. (10.8.4). The flow parameter  $\Lambda$  runs from  $\Lambda_0$  to  $\Lambda_c$ . For the low-energy regime one uses the same perturbative expansion as in the RTRG and inserts the previously calculated vertices as the reference solution.





## Chapter 11

# Comparison between RTRG and PMS

To compare the RTRG-results with those of a PMS-approach, we follow Ref. [Sch09b, Sch09c] and separate the part of the reference solutions for the vertex and the current vertex in the regime  $\Lambda > \Lambda_c$  which arises due to the  $\mathcal{O}(J^2)$  part of the initial condition. In the same sense, we isolate the contributions of those to the Liouvillian and the current kernel. With this splitting, we will show that the RTRG-calculations for the Liouvillian reproduce the PMS-solution exactly up to  $\mathcal{O}(J^2)$  for our two-level system but additionally generate an effective magnetic field. For the current kernel, we are able to show that the outcome of both methods coincide.

### 11.1 Splitting of the Vertex Functions

We start with the set of differential equations for the needed reference solutions in the regime  $\Lambda > \Lambda_c$  derived in the previous chapter which read up to  $\mathcal{O}(J^3)$

$$\frac{\partial}{\partial \Lambda} G_{12}^{(1)} = \frac{1}{\Lambda} G_{13}^{(1)} Z'^{(1)} G_{32}^{(1)} - \frac{1}{\Lambda} G_{23}^{(1)} Z'^{(1)} G_{31}^{(1)} - \frac{1}{2\Lambda} G_{34}^{(1)} G_{12}^{(1)} G_{43}^{(1)}, \quad (11.1.1)$$

$$\frac{\partial}{\partial \Lambda} I_{12}^{\gamma(1)} = \frac{1}{\Lambda} I_{13}^{\gamma(1)} Z'^{(1)} G_{32}^{(1)} - \frac{1}{\Lambda} I_{23}^{\gamma(1)} Z'^{(1)} G_{31}^{(1)} - \frac{1}{2\Lambda} I_{34}^{\gamma(1)} G_{12}^{(1)} G_{43}^{(1)}, \quad (11.1.2)$$

$$\frac{\partial}{\partial \Lambda} L_{\Delta}^{(1)} = \frac{1}{2\Lambda} G_{12}^{(1)} \chi_{12}^{(1)} Z'^{(1)} G_{21}^{(1)} - \frac{1}{\Lambda} G_{12}^{(1)} \chi_{12}^{(1)} G_{23}^{(1)} G_{31}^{(1)} - \frac{1}{\Lambda} G_{12}^{(1)} G_{23}^{(1)} \chi_{13}^{(1)} G_{31}^{(1)}, \quad (11.1.3)$$

$$\frac{\partial}{\partial \Lambda} \Sigma_{\Delta}^{\gamma(1)} = \frac{1}{2\Lambda} I_{12}^{\gamma(1)} \chi_{12}^{(1)} Z'^{(1)} G_{21}^{(1)} - \frac{1}{\Lambda} I_{12}^{\gamma(1)} \chi_{12}^{(1)} G_{23}^{(1)} G_{31}^{(1)} - \frac{1}{\Lambda} I_{12}^{\gamma(1)} G_{23}^{(1)} \chi_{13}^{(1)} G_{31}^{(1)}, \quad (11.1.4)$$

$$\frac{\partial}{\partial \Lambda} Z'^{(1)} = \frac{1}{2\Lambda} G_{12} G_{21} + \mathcal{O}(J^3). \quad (11.1.5)$$

The initial conditions are given by

$$G_{12}^{(1)}|_{E=i\Lambda_0} = G_{12}^{(0)} - i\frac{\pi}{2} \left[ G_{13}^{(0)} \tilde{G}_{32}^{(0)} - (1 \leftrightarrow 2) \right], \quad (11.1.6)$$

$$I_{12}^{\gamma(1)}|_{E=i\Lambda_0} = I_{12}^{\gamma(0)} - i\frac{\pi}{2} \left[ I_{13}^{\gamma(0)} \tilde{G}_{32}^{(0)} - (1 \leftrightarrow 2) \right], \quad (11.1.7)$$

$$L_{\Delta}^{(1)}|_{E=i\Lambda_0} = L^{(0)} - i\frac{\pi}{4} G_{12}^{(0)} \left( \bar{\mu}_{12} - L^{(0)} \right) \tilde{G}_{21}^{(0)}, \quad (11.1.8)$$

$$\Sigma_{\Delta}^{\gamma(1)}|_{E=i\Lambda_0} = -i\frac{\pi}{4} I_{12}^{\gamma(0)} \left( \bar{\mu}_{12} - L^{(0)} \right) \tilde{G}_{21}^{(0)}, \quad (11.1.9)$$

$$Z^{(1)}|_{E=i\Lambda_0} = 1, \quad (11.1.10)$$

with

$$G_{12}^{(0)} = [g_{12}^{(0)}, \cdot] = -2\vec{J}_{12} \cdot \underline{L}^2, \quad (11.1.11)$$

$$\tilde{G}_{12}^{(0)} = \{g_{12}^{(0)}, \cdot\} = \vec{J}_{12} \cdot (\underline{L}^1 + \underline{L}^3), \quad (11.1.12)$$

$$I_{12}^{\gamma(0)} = c_{12}^{\gamma} \{g_{12}^{(0)}, \cdot\} = c_{12}^{\gamma} \vec{J}_{12} \cdot (\underline{L}^1 + \underline{L}^3), \quad (11.1.13)$$

$$L^{(0)} = -2\vec{h}_{\text{eff}} \cdot \underline{L}^2, \quad (11.1.14)$$

and  $\vec{J}_{12}$  given by eq. (9.2.52). The superoperators  $\underline{L}^i$  and their algebra is defined in App. B.

In a first step, we perform the occurring  $\eta$ -sums. As the bare vertex contains a  $\delta_{\eta-\eta'}$  (9.2.53), this parametrization is conserved during the flow. From now on, all occurring vertices have the indices  $\eta = +$  and  $\eta' = -$  and the multi-indices  $1, 1'$  etc. do not longer contain those<sup>1</sup>. Furthermore, as mentioned before, we split

$$G_{12}^{(1)} = G_{12}^{(1_1)} + iG_{12}^{(1_2)}, \quad (11.1.15)$$

$$I_{12}^{\gamma(1)} = I_{12}^{\gamma(1_1)} + iI_{12}^{\gamma(1_2)}, \quad (11.1.16)$$

$$L_{\Delta}^{(1)} = L_{\Delta}^{(1_1)} + L_{\Delta}^{(1_2)}, \quad (11.1.17)$$

$$\Sigma_{\Delta}^{\gamma(1)} = \Sigma_{\Delta}^{\gamma(1_1)} + \Sigma_{\Delta}^{\gamma(1_2)} \quad (11.1.18)$$

<sup>1</sup>The vertices with  $\eta = -$  and  $\eta' = +$  are rewritten with eq. (B.4.2) to vertices, where the first  $\eta$ -index is positive.

where the  $(1_1)$  parts can contain  $\mathcal{O}(J)$  contributions, whereas the  $(1_2)$  parts are at least of  $\mathcal{O}(J^2)$ . The differential equations for these new defined quantities are given by

$$\Lambda \frac{\partial}{\partial \Lambda} G_{12}^{(1_1)} = G_{13}^{(1_1)} Z'^{(1)} G_{32}^{(1_1)} - G_{32}^{(1_1)} Z'^{(1)} G_{13}^{(1_1)} - G_{34}^{(1_1)} G_{12}^{(1_1)} G_{43}^{(1_1)}, \quad (11.1.19)$$

$$\Lambda \frac{\partial}{\partial \Lambda} G_{12}^{(1_2)} = G_{13}^{(1_1)} G_{32}^{(1_2)} + G_{13}^{(1_2)} G_{32}^{(1_1)} - G_{32}^{(1_1)} G_{13}^{(1_2)} - G_{32}^{(1_2)} G_{13}^{(1_1)}, \quad (11.1.20)$$

$$\begin{aligned} \Lambda \frac{\partial}{\partial \Lambda} L_{\Delta}^{(1_1)} &= \mu_{12} G_{12}^{(1_1)} Z'^{(1)} G_{21}^{(1_1)} - G_{12}^{(1_1)} Z'^{(1)} L_{\Delta}^{(1_1)} Z'^{(1)} G_{21}^{(1_1)} \\ &\quad - (\mu_{12} + \mu_{13}) \left( G_{12}^{(1_1)} G_{23}^{(1_1)} G_{31}^{(1_1)} + G_{21}^{(1_1)} G_{32}^{(1_1)} G_{13}^{(1_1)} \right) \\ &\quad + G_{12}^{(1_1)} \left\{ G_{23}^{(1_1)}, L_{\Delta}^{(1_1)} \right\} G_{31}^{(1_1)} - G_{21}^{(1_1)} \left\{ G_{32}^{(1_1)}, L_{\Delta}^{(1_1)} \right\} G_{13}^{(1_1)}, \end{aligned} \quad (11.1.21)$$

$$\begin{aligned} \Lambda \frac{\partial}{\partial \Lambda} L_{\Delta}^{(1_2)} &= i\mu_{12} \left( G_{12}^{(1_1)} G_{21}^{(1_2)} + G_{12}^{(1_2)} G_{21}^{(1_1)} \right) \\ &\quad - iG_{12}^{(1_1)} L_{\Delta}^{(0)} G_{21}^{(1_2)} - iG_{12}^{(1_2)} L_{\Delta}^{(0)} G_{21}^{(1_1)}, \end{aligned} \quad (11.1.22)$$

$$\Lambda \frac{\partial}{\partial \Lambda} Z'^{(1)} = G_{12}^{(1_1)} G_{21}^{(1_1)}, \quad (11.1.23)$$

and the flow equations for  $I_{12}^{\gamma(1_1)}$ ,  $I_{12}^{\gamma(1_2)}$ ,  $\Sigma_{\Delta}^{\gamma(1_1)}$  and  $\Sigma_{\Delta}^{\gamma(1_2)}$  are analogue with the first vertex replaced by the current vertex. The initial conditions read

$$G_{12}^{(1_1)} \Big|_{E=i\Lambda_0} = G_{12}^{(0)}, \quad (11.1.24)$$

$$G_{12}^{(1_2)} \Big|_{E=i\Lambda_0} = -i\frac{\pi}{2} \left[ G_{13}^{(0)} \tilde{G}_{32}^{(0)} - G_{32}^{(0)} \tilde{G}_{13}^{(0)} \right], \quad (11.1.25)$$

$$I_{12}^{\gamma(1_1)} \Big|_{E=i\Lambda_0} = I_{12}^{\gamma(0)}, \quad (11.1.26)$$

$$I_{12}^{\gamma(1_2)} \Big|_{E=i\Lambda_0} = -i\frac{\pi}{2} \left[ I_{13}^{\gamma(0)} \tilde{G}_{32}^{(0)} - I_{32}^{\gamma(0)} \tilde{G}_{13}^{(0)} \right], \quad (11.1.27)$$

$$L_{\Delta}^{(1_1)} \Big|_{E=i\Lambda_0} = L^{(0)}, \quad (11.1.28)$$

$$L_{\Delta}^{(1_2)} \Big|_{E=i\Lambda_0} = -i\frac{\pi}{2} G_{12}^{(0)} \left( \mu_{12} - L_{\Delta}^{(0)} \right) \tilde{G}_{21}^{(0)}, \quad (11.1.29)$$

$$\Sigma_{\Delta}^{\gamma(1_1)} \Big|_{E=i\Lambda_0} = 0, \quad (11.1.30)$$

$$\Sigma_{\Delta}^{\gamma(1_2)} \Big|_{E=i\Lambda_0} = -i\frac{\pi}{2} I_{12}^{\gamma(0)} \left( \mu_{12} - L^{(0)} \right) \tilde{G}_{21}^{(0)}. \quad (11.1.31)$$

## 11.2 Analytic Evaluation of the Differential Equations

Here, we analyze the differential equations for the Liouvillian and the current derived in the previous section. The hermicity of the effective Hamiltonian (9.2.43) and the relation  $g_{12}^\dagger = g_{21}$  in Hilbert space leads to the following relations for the initial conditions of the vertex superoperators

$$G_{12}^{(1_1),\dagger} \Big|_{\Lambda_0} = G_{21}^{(1_1)} \Big|_{\Lambda_0}, \quad (11.2.1)$$

$$I_{12}^{\gamma(1_1),\dagger} \Big|_{\Lambda_0} = - I_{21}^{\gamma(1_1)} \Big|_{\Lambda_0}, \quad (11.2.2)$$

where we have defined the adjoint of a superoperator in Liouville space as  $(A^\dagger)_{ss',\bar{s}\bar{s}'} = A_{\bar{s}\bar{s}',ss'}^*$ . For the Liouvillian, the current kernel and the  $Z$ -factor in leading order this results in

$$L_\Delta^{(1_1),\dagger} \Big|_{\Lambda_0} = L_\Delta^{(1_1)} \Big|_{\Lambda_0}, \quad (11.2.3)$$

$$\Sigma_\Delta^{\gamma(1_1),\dagger} \Big|_{\Lambda_0} = - \Sigma_\Delta^{\gamma(1_1)} \Big|_{\Lambda_0}, \quad (11.2.4)$$

$$Z^{(1),\dagger} \Big|_{\Lambda_0} = Z^{(1)} \Big|_{\Lambda_0}. \quad (11.2.5)$$

All these relations are preserved under the RG-flow for an arbitrary number of dot levels. For the two-level system under consideration in this thesis, we can show with this hermicity and eqs. (B.4.4) and (B.4.6) that the Liouvillian  $L^{(1_1)}$  has the structure

$$L_\Delta^{(1_1)} = \begin{pmatrix} 0 & 0 & -\phi^* & \phi \\ 0 & 0 & \phi^* & -\phi \\ -\phi & \phi & h & 0 \\ \phi^* & -\phi^* & 0 & -h \end{pmatrix} \quad (11.2.6)$$

$$= [H^{(1)}, \cdot], \quad (11.2.7)$$

where the basis in Liouville space is chosen as  $|\uparrow\uparrow\rangle, |\downarrow\downarrow\rangle, |\uparrow\downarrow\rangle, |\downarrow\uparrow\rangle$  and

$$H^{(1)} = \begin{pmatrix} \frac{h}{2} & \phi \\ \phi^* & -\frac{h}{2} \end{pmatrix} = \vec{h} \cdot \vec{S}, \quad (11.2.8)$$

with the generated magnetic field  $\vec{h} = (2\text{Re}(\phi), 2i\text{Im}(\phi), h)^T$ . So the contribution of  $L_\Delta^{(1_1)}$  is a renormalization of the effective magnetic field, which is a priori not captured in the PMS-calculations.

At first glance, integrating the differential equation for  $\Sigma_{\Delta}^{\gamma(1_1)}$  seems to produce terms  $\sim \mathcal{O}(J)$  for the current, which could not be captured within a PMS-approach. To investigate those, we first have to analyze  $I_{12}^{\gamma(1_1)}$ . The form of the initial condition (11.1.13) is preserved under the RG-flow in leading order<sup>2</sup> with the same  $\vec{J}_{12}$  as in eq. (11.1.11). The terms, which could lead to  $\mathcal{O}(J)$ -contributions to the current are given by

$$\Lambda \frac{\partial}{\partial \Lambda} \Sigma_{\Delta}^{\gamma(1_1)} = \mu_{12} I_{12}^{\gamma(1_1)} G_{21}^{(1_1)} - I_{12}^{\gamma(1_1)} L_{\Delta}^{(0)} G_{21}^{(1_1)} + \mathcal{O}(J^3). \quad (11.2.9)$$

The first part of the r.h.s. gives

$$\begin{aligned} \mu_{12} I_{12}^{\gamma(1_1)} G_{21}^{(1_1)} &= -2\mu_{12} c_{\alpha_1 \alpha_2}^{\gamma} J_{12}^i J_{21}^j (L_i^1 + L_i^3) L_j^2 \\ &= i\epsilon_{ijk} \mu_{12} c_{\alpha_1 \alpha_2}^{\gamma} J_{12}^i J_{21}^j L_k^1 \\ &= i\epsilon_{ijk} \mu_{12} c_{\alpha_1 \alpha_2}^{\gamma} J_{21}^i J_{12}^j L_k^1 \\ &= 0, \end{aligned} \quad (11.2.10)$$

where we have relabeled  $1 \leftrightarrow 2$  and used  $\mu_{12} = -\mu_{21}$ ,  $c_{\alpha_1 \alpha_2}^{\gamma} = -c_{\alpha_2 \alpha_1}^{\gamma}$ . For the evaluation of the second part, we choose the magnetic field in  $z$ -direction, which leads to

$$\begin{aligned} I_{12}^{\gamma(1_1)} L_{\Delta}^{(0)} G_{21}^{(1_1)} &= 4hc_{\alpha_1 \alpha_2}^{\gamma} J_{12}^i J_{21}^j (L_i^1 + L_i^3) L_z^2 L_j^2 \\ &= hc_{\alpha_1 \alpha_2}^{\gamma} J_{12}^i J_{21}^j (\delta_{jz} L_i^1 - \delta_{ij} L_z^1) \end{aligned} \quad (11.2.11)$$

where this expression has only contributions  $\sim L_x^1, L_y^1$ . To compute the current, we have to multiply this current kernel with the density matrix. When the magnetic field points in  $z$ -direction and is of  $\mathcal{O}(1)$  (otherwise, this contribution would be either way of higher order), the diagonal parts of the density matrix are of  $\mathcal{O}(1)$  and the off-diagonal are of higher order. As  $L_x^1$  and  $L_y^1$  act only on the off-diagonal matrix elements, the expression  $\Sigma_{\Delta}^{\gamma(1_1)} \rho$  does not have any contributions linear in  $J$ . Nevertheless, the second order contributions to  $\Sigma_{\Delta}^{\gamma(1_1)}$  could lead to a current, which would not be included in a PMS-approach. To discuss this, we computed the (1<sub>1</sub>), (1<sub>2</sub>) and (3) part of the current for two different generic models (see Fig. 11.1). The (3) part denotes the contribution from the low-energy regime  $\Lambda < \Lambda_c$ . Obviously, the (1<sub>1</sub>) contribution to the total current is of higher order in  $J$  than both others, such that it can be neglected completely.

---

<sup>2</sup>The higher order contributions can differ significantly from this form, as also contributions to  $I_{\alpha\alpha}^{\gamma}$  can arise.

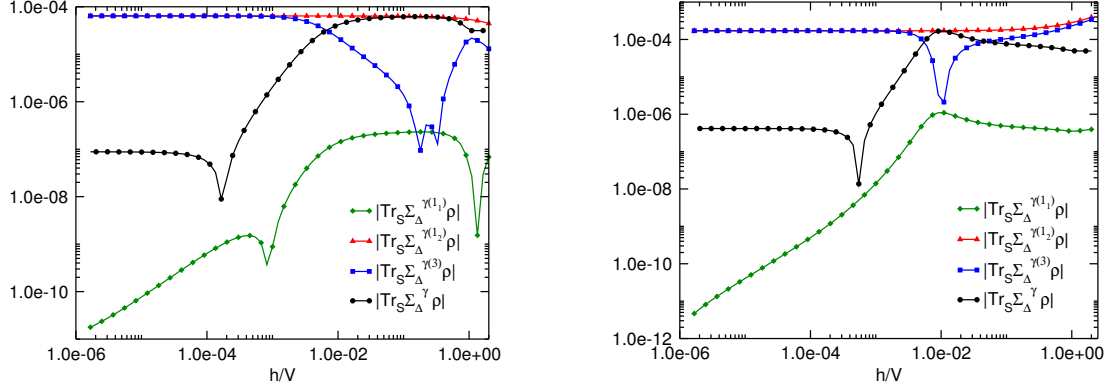


**Figure 11.1:** Decomposition of the various contributions to the current for two different generic two-level QDs to show that the  $\Sigma_{\Delta}^{(1)}$  part is of higher order and therefore can be neglected. In the left plot, the QD is coupled to two spinless reservoirs with  $t_1^L = 10^{-2}(-0.3377 + 1.4355i)$ ,  $t_2^L = 10^{-2}(1.7754 + 0.4888i)$ ,  $t_1^R = 10^{-2}(-0.5989 - 0.7406i)$  and  $t_2^R = 10^{-2}(1.6641 + 0.4501i)$ , and in the right one, the hopping amplitudes read  $t_1^L = 10^{-2}(0.3381 - 0.9112i)$ ,  $t_2^L = 10^{-2}(-2.0778 - 0.0993i)$ ,  $t_1^R = 10^{-2}(-1.4489 + 1.1025i)$  and  $t_2^R = 10^{-2}(-0.8992 + 0.5443i)$ . In both cases, the amplitude of the hopping matrix elements are chosen such that  $J \approx 0.01$ .

After discussing the contributions of the  $(1_1)$ -parts, in a next step we investigate  $L_{\Delta}^{(1_2)}$ . We first evaluate the differential equation for  $G^{(1_1)}$ . Starting this discussion by splitting

$$G_{12}^{(1_1)} = G_{12}^{(1_{1a})} + G_{12}^{(1_{1b})}, \quad (11.2.12)$$

where  $G_{12}^{(1_{1a})} \sim J$  and  $G_{12}^{(1_{1b})} \sim J^2$ , the differential equation for  $G^{(1_{1a})}$  reads

$$\Lambda \frac{dG_{12}^{(1_{1a})}}{d\Lambda} = G_{13}^{(1_{1a})} G_{32}^{(1_{1a})} - G_{32}^{(1_{1a})} G_{13}^{(1_{1a})} + \mathcal{O}(J^3), \quad (11.2.13)$$

with the initial condition  $G_{12}^{(1_{1a})}|_{E=i\Lambda_0} = [g_{12}^{(1)}, \cdot]$ . Comparing with the PMS-equations (10.10.1) and (10.10.2), which are identical to those of the RTRG in leading order, it is easy to verify that  $G_{12}^{(1_{1a})}$  keeps its form of the initial condition with renormalized  $g_{12}^{(1)}$ . So the leading order of the vertex function  $G_{12}^{(1_1)}$  can always be written as a commutator of some vertex function  $g_{12}^{(1)}$  in Hilbert space. We furthermore define

$$\tilde{G}_{12}^{(1_{1a})} = \{g_{12}^{(1)}, \cdot\} \quad (11.2.14)$$

which yields the differential equation

$$\Lambda \frac{d\tilde{G}_{12}^{(1_{1a})}}{d\Lambda} = G_{13}^{(1_{1a})} \tilde{G}_{32}^{(1_{1a})} - \tilde{G}_{32}^{(1_{1a})} G_{13}^{(1_{1a})} + \mathcal{O}(J^3). \quad (11.2.15)$$

With these definitions, it was shown in Ref. [Sch09b] that also  $G_{12}^{(1_2)}$  keeps the form of its initial condition during the RG-flow in leading order

$$G_{12}^{(1_2)} = -\frac{\pi}{2}G_{13}^{(1_{1a})}\tilde{G}_{32}^{(1_{1a})} + \frac{\pi}{2}G_{32}^{(1_{1a})}\tilde{G}_{13}^{(1_{1a})}. \quad (11.2.16)$$

In the same sense, we can check if  $L_{\Delta}^{(1_2)}$  is given in leading order by its initial condition with renormalized coupling vertices  $G$ . We calculate the difference of  $L_{\Delta}^{(1_2)}$  and the derivative of the initial condition

$$\begin{aligned} & \Lambda \frac{d}{d\Lambda} \left[ L_{\Delta}^{(1_2)} + i\frac{\pi}{2}G_{12}^{(1_{1a})} \left( \mu_{12} - L_{\Delta}^{(0)} \right) \tilde{G}_{21}^{(1_{1a})} \right] \\ &= -i\frac{\pi}{4}G_{12}^{(1_{1a})} \left[ G_{23}^{(1_{1a})}\tilde{G}_{31}^{(1_{1a})} - G_{31}^{(1_{1a})}\tilde{G}_{23}^{(1_{1a})} - \tilde{G}_{23}^{(1_{1a})}G_{31}^{(1_{1a})} + \tilde{G}_{31}^{(1_{1a})}G_{23}^{(1_{1a})} \right] L_{\Delta}^{(0)}. \end{aligned} \quad (11.2.17)$$

For our two-level model under consideration, we insert our Liouville space basis, and it was shown in Ref. [Sch09c] that  $G^{(1_{1a})} \sim \underline{L}^2$ ,  $\tilde{G}^{(1_{1a})} \sim \underline{L}^1 + \underline{L}^3$  and  $L_{\Delta}^{(0)} \sim \underline{L}^2$  in leading order. Due to the algebra defined in appendix B, it is easy to prove that the r.h.s. of eq. (11.2.17) vanishes in  $\mathcal{O}(J^3)$ , so also  $L_{\Delta}^{(1_2)}$  is exactly the same as its initial condition with renormalized vertices up to higher orders, meaning it coincides with the PMS-solution. The same statement holds for  $\Sigma_{\Delta}^{\gamma(1_2)}$  as the difference between its flow equation in RTRG and the derivative of the initial condition

$$\begin{aligned} & \Lambda \frac{d}{d\Lambda} \left[ \Sigma_{\Delta}^{\gamma(1_2)} + i\frac{\pi}{2}I_{12}^{\gamma(1_{1a})} \left( \mu_{12} - L_{\Delta}^{(0)} \right) \tilde{G}_{21}^{(1_{1a})} \right] \\ &= -i\frac{\pi}{4}I_{12}^{\gamma(1_{1a})} \left[ G_{23}^{(1_{1a})}\tilde{G}_{31}^{(1_{1a})} - G_{31}^{(1_{1a})}\tilde{G}_{23}^{(1_{1a})} - \tilde{G}_{23}^{(1_{1a})}G_{31}^{(1_{1a})} + \tilde{G}_{31}^{(1_{1a})}G_{23}^{(1_{1a})} \right] L_{\Delta}^{(0)}, \end{aligned} \quad (11.2.18)$$

also vanishes due to the Liouville space algebra and  $I^{\gamma(1_{1a})} \sim \underline{L}^1 + \underline{L}^3$ .

The results for the Liouvillian and the current kernel in the regime  $\Lambda < \Lambda_c$  are already equivalent between RTRG and PMS as only the lowest order of the effective two-point vertex (which is similar) evaluated at  $\Lambda = \Lambda_c$  enters into the equation (10.8.20). To conclude, the RG-flow of  $L_{\Delta}^{(1)}$  produces an effective magnetic field, which is not captured in the PMS-approach. Beside this, all other contributions to the Liouvillian and the current kernel are the same to  $\mathcal{O}(J^2)$ , so a PMS-approach with some empirical magnetic field is sufficient to determine the low-energy behavior of the Anderson impurity model with ferromagnetic leads in the Coulomb blockade regime. It has to be mentioned that this statement holds only for our two-level QD, as we need the special Liouville space algebra for this model to show that the  $(1_2)$  parts keep their initial form. A short discussion for more than two levels will be done in section 12.5.





# Chapter 12

## Results

In this chapter, we will present the results for the stationary dot density matrix and the stationary current for the Anderson impurity model with ferromagnetic leads in the Coulomb blockade regime derived in chapter 9. As shown in the previous chapter, it is sufficient to solve the PMS-flow-equations (10.10.2) and (10.10.3) in the regime  $\Lambda > \Lambda_c$  and insert those results into the solution for  $L_\Delta$  and  $\Sigma_\Delta^\gamma$  below  $\Lambda_c$  (10.8.20) with  $L_\Delta^{(1)c}$  containing an effective magnetic field given by  $L_\Delta^{(11)c}$  and  $L_\Delta^{(12)c} = -i\frac{\pi}{2}G_{12}^{(11)c}(\mu_{12} - L_\Delta^{(0)})\tilde{G}_{21}^{(11)c}$ .  $\Sigma_\Delta^\gamma$  can again be calculated analogously by replacing the first vertex with the current vertex. The stationary dot density matrix can then be calculated from eq. (10.2.15) and the current is given by eq. (10.3.11).

To perform those steps, we show that the generic Anderson impurity model with ferromagnetic leads can be rotated to the anisotropic Kondo model with an additional spin-density interaction for the calculation of the reference solution. With this solution known from previous works [Sch09c] we can calculate the leading order correction to the effective magnetic field. Furthermore, also the magnetization and the current are presented for the generic model and we will discuss those for the special case of two reservoirs and the system being in the scaling limit in detail.

### 12.1 Singular Value Decomposition

The reference solutions in the regime  $\Lambda > \Lambda_c$  were defined by setting all physical energy scales like  $E$ ,  $\mu$  and  $h$  equal to zero. Therefore, the reservoirs are all equivalent with respect to their chemical potentials and we could rotate the system in the reservoir space so that the dot couples only to one effective reservoir. This is achieved by a singular value decomposition (SVD) of the hopping matrix  $t_{\alpha\sigma,\sigma'} = (t^\alpha)_{\sigma\sigma'}$  containing all hopping matrices of the various reservoirs, which are defined in eq. (9.1.55). The

SVD reads

$$\underline{\underline{t}} = \underline{\underline{V}} \underline{\underline{\tilde{t}}} \underline{\underline{W}}^\dagger, \quad (12.1.1)$$

where  $\underline{\underline{V}}$  and  $\underline{\underline{W}}$  are unitary transformation matrices in reservoir and dot space, respectively, and  $\underline{\underline{\tilde{t}}}_{\alpha\sigma,\sigma'} = \delta_{\alpha 1} \delta_{\sigma\sigma'} \lambda_\sigma$  is the diagonal coupling matrix between the dot and the remaining reservoir. The hopping matrix elements can be chosen as  $\lambda_\uparrow \geq \lambda_\downarrow > 0$ , where we excluded the exotic case  $\lambda_\downarrow = 0$  meaning that one level completely decouples so that the stationary values would crucially depend on the initial conditions of the system. We can omit the matrix  $\underline{\underline{W}}$  by an appropriate rotation of the dot space leading to the tunneling matrices  $\underline{\underline{t}}^\alpha = \underline{\underline{V}}^\alpha \underline{\underline{\lambda}}$ . Furthermore, for the RG-calculations the matrix  $\underline{\underline{V}}$  can also be omitted, such that we have to consider a QD coupled to one effective reservoir via the tunneling matrix elements  $\lambda_\sigma$ . This equilibrium system has also been studied in Ref. [Kas07] and the  $2 \times 2$  exchange coupling matrix defined in eq. (9.2.52) can be written as

$$\underline{\underline{\vec{J}}} = \frac{2}{D} \underline{\underline{\lambda}} \underline{\underline{\vec{\sigma}}} \underline{\underline{\lambda}} \quad (12.1.2)$$

and be parametrized by the couplings  $J_z = (\lambda_\uparrow^2 + \lambda_\downarrow^2)/D$  and  $J_\perp = 2\lambda_\uparrow\lambda_\downarrow/D$  via

$$\underline{\underline{J}}^{x/y} = J_\perp \underline{\underline{\sigma}}^{x/y}, \quad \underline{\underline{J}}^z = c \underline{\underline{1}} + J_z \underline{\underline{\sigma}}^z, \quad (12.1.3)$$

with  $c^2 = J_z^2 - J_\perp^2$  and  $J_z \geq J_\perp > 0$ . This is the antiferromagnetic anisotropic Kondo model, which was treated in Ref. [Sch09c], with an additional spin-density interaction proportional to the anisotropy parameter  $c$ . The PMS-flow equation (10.10.2) can be rewritten for this parametrization to

$$\Lambda \frac{d}{d\Lambda} J_z = -2J_\perp^2, \quad (12.1.4)$$

$$\Lambda \frac{d}{d\Lambda} J_\perp = -2J_z J_\perp, \quad (12.1.5)$$

which solution was found to be

$$J_z = c \frac{1 + \left(\frac{T_K}{\Lambda}\right)^{4c}}{1 - \left(\frac{T_K}{\Lambda}\right)^{4c}}, \quad (12.1.6)$$

$$J_\perp = 2c \frac{\left(\frac{T_K}{\Lambda}\right)^{2c}}{1 - \left(\frac{T_K}{\Lambda}\right)^{4c}}, \quad (12.1.7)$$

with the two invariants given by

$$c^2 = J_z^2 - J_\perp^2, \quad (12.1.8)$$

$$T_K = \Lambda \left( \frac{J_z - c}{J_z + c} \right)^{\frac{1}{4c}}. \quad (12.1.9)$$

Hence, the exchange couplings of the anisotropic Kondo model are increased during the flow towards the well-known isotropic fixed point

$$J_z = J_\perp = \frac{1}{2 \ln \frac{\Lambda}{T_K}}, \quad (12.1.10)$$

which is reached in the **scaling limit** defined by  $J_z|_{\Lambda_0}, J_\perp|_{\Lambda_0} \rightarrow 0$  and  $\Lambda_0 \rightarrow \infty$  such that  $J_z/J_\perp|_{\Lambda_0} = \text{const}$  and  $T_K = \text{const}$ . We can evaluate all expressions at each step of the RG-flow and find at  $\Lambda = \Lambda_c$  the effective hybridization matrix

$$\underline{\underline{\Gamma}}^\alpha = 2\pi \underline{\underline{\lambda}} \underline{\underline{V}}^{\alpha,\dagger} \underline{\underline{V}}^\alpha \underline{\underline{\lambda}}, \quad (12.1.11)$$

with

$$\underline{\underline{\lambda}}^2 = \frac{\Lambda_c}{2} (J_z \underline{\underline{1}} + c \underline{\underline{\sigma}}^z). \quad (12.1.12)$$

The matrices  $\underline{\underline{V}}^\alpha$  follow from the first two columns of the matrix  $\underline{\underline{V}}$  defined by the SVD of  $\underline{\underline{t}}$  and do not flow under the RG-treatment. From the properties of the SVD follows that  $\underline{\underline{V}}$  is unitary, and we get the property

$$\sum_\alpha \underline{\underline{V}}^{\alpha,\dagger} \underline{\underline{V}}^\alpha = \underline{\underline{1}}. \quad (12.1.13)$$

In a next step, we decompose the hybridization matrix into the basis given by the unity and the Pauli matrices

$$\underline{\underline{\Gamma}}^\alpha = \frac{1}{2} \Gamma \underline{\underline{x}}_\alpha \quad (12.1.14)$$

with  $\underline{\underline{x}}_\alpha = x_\alpha \underline{\underline{1}} + \vec{d}_\alpha \cdot \underline{\underline{\sigma}}$ ,  $\sum_\alpha x_\alpha = 1$ ,  $|\vec{d}_\alpha| = x_\alpha p_\alpha$  and  $0 \leq x_\alpha, p_\alpha \leq 1$ . Here,  $x_\alpha, p_\alpha$  and  $\vec{d}_\alpha$  are the parameters of the effective model with ferromagnetic leads. By using the property (12.1.13) we obtain

$$\Gamma = 2\pi \Lambda_c J_z, \quad d = |\vec{d}| = \frac{c}{J_z}, \quad \vec{d} = \sum_\alpha \vec{d}_\alpha = d \vec{e}_z, \quad (12.1.15)$$

which shows that by omitting the matrix  $\underline{W}$  of the SVD of  $\underline{t}$  we have rotated the dot space such that the vector  $\vec{d}$  points in  $z$ -direction. Furthermore, the system tends to minimize the vector  $\vec{d}$  during the RG-flow. Additionally, the vanishing  $\vec{d}$  in the scaling limit explains why the Kondo effect appears generically in the equilibrium case, as all reservoirs can be taken together such that the spin polarization vanishes, which is in agreement with Refs. [Kas07, Mar03a, Mar03b, Sin07]. However, in the nonequilibrium case the reservoirs cannot be taken together generically, so the fixed point model is not the Kondo model with unpolarized leads but a spin-1/2 coupled to several leads with individual spin vectors  $\vec{d}_\alpha$ .

Comparing the equations (12.1.11) and (12.1.14) the matrix  $\underline{x}_\alpha$  can be defined by

$$\underline{x}_\alpha = x_\alpha \underline{\mathbb{1}} + \vec{d}_\alpha \cdot \underline{\vec{\sigma}} = \left( \underline{\mathbb{1}} + \frac{c}{J_z} \underline{\sigma}^z \right)^{1/2} \underline{V}^{\alpha,\dagger} \underline{V}^\alpha \left( \underline{\mathbb{1}} + \frac{c}{J_z} \underline{\sigma}^z \right)^{1/2}. \quad (12.1.16)$$

So from the SVD of the exchange matrix  $\underline{t}$  of the original model one determines the rotation matrix  $\underline{V}$  and the coupling parameters  $\lambda_\sigma$  and this equation provides now the algorithm to calculate the parameters of the effective model with ferromagnetic leads. It is important to notice that the individual parameters  $x_\alpha$  and  $\vec{d}_\alpha$  for all reservoirs have to be determined to discuss the nonequilibrium properties of the system even in the scaling limit, which is in contrast to the equilibrium situation discussed in Ref. [Kas07]. The Kondo model with unpolarized leads is only realized in the scaling limit when the initial spin vectors have all been equal  $\vec{d}_\alpha^{(0)} = \vec{d}^{(0)}$  (and  $p_\alpha = p \neq 1$ ). Starting with slight differences in the initial polarizations  $p_\alpha$ , one reaches a fixed point with  $p_\alpha \ll 1$  such that the Kondo model with unpolarized leads might still be a good approximation, but a small angle between the  $\vec{d}_\alpha^{(0)}$  would lead to a rotation of the spin orientations with finite polarizations. So the Kondo model with unpolarized leads is a rather artificial situation, such that we can assume that the physical properties of the generic Anderson impurity model with ferromagnetic leads even in the scaling limit show new generic behavior.

Defining an effective tunneling matrix and the effective exchange coupling matrix describing the model in the Coulomb blockade regime (see eq. (9.2.52))

$$\underline{\Gamma}^\alpha = 2\pi \underline{t}^{\alpha,\dagger} \underline{t}^\alpha, \quad (12.1.17)$$

$$\underline{t}^\alpha = \sqrt{\frac{\Gamma}{4\pi}} \sqrt{\underline{x}_\alpha} = \sqrt{\frac{\Lambda_c J_z}{2}} \sqrt{\underline{x}_\alpha}, \quad (12.1.18)$$

$$\underline{J}^{\alpha\alpha'} = \frac{2}{\Lambda_c} \underline{t}^\alpha \underline{\vec{\sigma}} \underline{t}^{\alpha',\dagger} = J_z \sqrt{\underline{x}_\alpha} \underline{\vec{\sigma}} \sqrt{\underline{x}_{\alpha'}}, \quad (12.1.19)$$

the in the following occurring vertices are given by

$$G_{12} = \vec{J}_{12} \cdot (\underline{L}_+ + \underline{L}_-) = -2\vec{J}_{12} \cdot \underline{L}^2, \quad (12.1.20)$$

$$\tilde{G}_{12} = \vec{J}_{12} \cdot (\underline{L}_+ - \underline{L}_-) = \vec{J}_{12} \cdot (\underline{L}^1 + \underline{L}^3), \quad (12.1.21)$$

$$I_{12}^\gamma = c_{\alpha\alpha'}^\gamma \tilde{G}_{12}, \quad (12.1.22)$$

where we omit the superscript  $(1_{1a})$  for the reference solution from now on.

## 12.2 Determination of the Effective Magnetic Field

First, we investigate the leading order correction to the bare magnetic field after the Schrieffer-Wolff transformation (9.2.49). Therefore, we have to solve the leading order differential equation of  $L_\Delta^{(1_1)}$  (11.1.21)

$$\Lambda \frac{\partial}{\partial \Lambda} L_\Delta^{(1_1)} = \mu_{12} G_{12}^{(1_{1a})} G_{21}^{(1_{1a})} - G_{12}^{(1_{1a})} L_\Delta^{(0)} G_{21}^{(1_{1a})} + \mathcal{O}(J^3). \quad (12.2.1)$$

As an intermediate step, we find

$$\text{Tr}_\sigma \underline{J}^{\alpha\alpha',i} \underline{J}^{\alpha'\alpha,j} = 2J_z^2 \left[ \delta_{ij} \left( x_\alpha x_{\alpha'} - \vec{d}_\alpha \cdot \vec{d}_{\alpha'} \right) + i\epsilon_{ijk} \left( d_\alpha^k - d_{\alpha'}^k \right) + d_\alpha^i d_{\alpha'}^j + d_\alpha^j d_{\alpha'}^i \right] \quad (12.2.2)$$

where we did not sum over  $\alpha$  and  $\alpha'$ . With a straightforward calculation by using the equation (10.10.1) it is easy to prove that the term  $\sim \mu$  on the r.h.s. of eq. (12.2.1) can be integrated and reformulated in Hilbert-space leading exactly to the term  $\sim \mu$  on the r.h.s. of (9.2.49) with renormalized  $g$ . The term  $\sim L_\Delta^{(0)}$  on the r.h.s. of eq. (12.2.1) can also be integrated and leads to a total effective Hamiltonian  $\tilde{H}_{\text{eff}}^1$

$$\tilde{H}_{\text{eff}} = h_0(1 - J_z)S_z - 2J_z d^i d^z h S_i + 4c^2 d^i d^z h \ln \frac{D}{\Lambda_c} S_i + \sum_\alpha \mu_\alpha \text{Tr}_\sigma \underline{g}^{\alpha\alpha}. \quad (12.2.3)$$

So, also the correction term to the bare magnetic field in eq. (9.2.49) is reproduced and the additional corrections in eq. (12.2.3) vanish in the scaling limit. To sum up, the RTRG calculation of the effective magnetic field reproduces the bare one with effective vertices in leading order in the scaling limit, only away from this limit one gets an extra contribution. All in all, we have shown that the results for the Anderson impurity model with ferromagnetic leads in the Coulomb blockade regime can be computed by a

<sup>1</sup>In the flow equations always the combination  $Z' L_\Delta$  occurs (see eq. (10.7.5)) such that the effective magnetic field is also determined by  $Z' L_\Delta$  and not by  $L_\Delta$  itself. This effect is already included in  $\tilde{H}_{\text{eff}}$  and changes the sign of the correction to the bare magnetic field from  $h_0(1 + J_z)S_z$  to  $h_0(1 - J_z)S_z$ .

perturbative expansion of the Liouvillian where the vertices and the bare magnetic field have to be renormalized via the PMS-equations, when one considers the scaling limit. Away from it, the perturbative treatment is still valid, but the effective magnetic field has either to be calculated within the RTRG-approach or it has to be determined empirically. From now on, the magnetic field  $h$  will always denote the total one including the external and the exchange field.

### 12.3 Magnetization and Current for the Generic Case

In second order perturbation theory, the Liouvillian and the current kernel follow from eq. (10.8.20) without a specification of the basis

$$L_{\Delta} = L_{\Delta}^{(0)} + G_{12} \left[ -i \frac{\pi}{2} (\mu_{12} - L_{\Delta}^{(0)}) \tilde{G}_{21} + H (\mu_{12} - L_{\Delta}^{(0)}) G_{21} \right], \quad (12.3.1)$$

$$\Sigma_{\Delta}^{\gamma} = I_{12}^{\gamma} \left[ -i \frac{\pi}{2} (\mu_{12} - L_{\Delta}^{(0)}) \tilde{G}_{21} + H (\mu_{12} - L_{\Delta}^{(0)}) G_{21} \right], \quad (12.3.2)$$

with the vertices given by eqs. (12.1.20 - 12.1.22) and

$$L_{\Delta}^{(0)} = -2\vec{h} \cdot \underline{L}^2, \quad H(x) = x \ln \frac{-ix}{\Lambda_c} = -i \frac{\pi}{2} |x| + x \ln \left| \frac{x}{\Lambda_c} \right| \approx -i \frac{\pi}{2} |x|, \quad (12.3.3)$$

as the logarithmic real part of the function  $H(x)$  leads to a weak renormalization of the level splitting and thus changes the results only to higher orders so that we can omit it in the following. Inserting the definitions results in

$$L_{\Delta} = L_{\Delta}^{(0)} + i\pi \left( \text{Tr}_{\sigma} J^{\alpha\alpha',i} \underline{J}^{\alpha'\alpha,j} \right) L_2^i \times \left[ \left( \mu_{\alpha\alpha'} + 2\vec{h} \cdot \underline{L}_2 \right) \left( L_1^j + L_3^j \right) - 2 \left| \mu_{\alpha\alpha'} + 2\vec{h} \cdot \underline{L}_2 \right| L_2^j \right], \quad (12.3.4)$$

$$\Sigma_{\Delta}^{\gamma} = -i \frac{\pi}{2} c_{\alpha\alpha'}^{\gamma} \left( \text{Tr}_{\sigma} J^{\alpha\alpha',i} \underline{J}^{\alpha'\alpha,j} \right) \left( L_1^i + L_3^i \right) \times \left[ \left( \mu_{\alpha\alpha'} + 2\vec{h} \cdot \underline{L}_2 \right) \left( L_1^j + L_3^j \right) - 2 \left| \mu_{\alpha\alpha'} + 2\vec{h} \cdot \underline{L}_2 \right| L_2^j \right]. \quad (12.3.5)$$

Here, one can insert the  $4 \times 4$ -matrices of the Liouville algebra defined in Appendix B.2 and perform the multiplications by using the decomposition of the absolute value of  $\left| \mu_{\alpha\alpha'} + 2\vec{h} \cdot \underline{L}_2 \right|$  given in Appendix B.3. In matrix form we represent the Liouvillian by choosing the order of the basis elements

$$|\uparrow\uparrow\rangle, \quad |\downarrow\downarrow\rangle, \quad |\uparrow\downarrow\rangle, \quad |\downarrow\uparrow\rangle, \quad (12.3.6)$$

and obtain after a lengthy algebra

$$L_{\Delta} = \begin{pmatrix} A & B \\ C & D \end{pmatrix}, \quad (12.3.7)$$

$$A = -i\gamma_1(\mathbb{1} - \sigma_x) - i\gamma_2(\sigma_z + i\sigma_y), \quad (12.3.8)$$

$$B = -\left(\frac{h_x}{2} + \gamma_3\right)(\mathbb{1} - \sigma_x) - i\left(\frac{h_y}{2} - \gamma_4\right)(\sigma_z + i\sigma_y), \quad (12.3.9)$$

$$C = -\left(\frac{h_x}{2} - \gamma_3\right)(\mathbb{1} - \sigma_x) + i\left(\frac{h_y}{2} + \gamma_4\right)(\sigma_z - i\sigma_y) - i\gamma_5(\mathbb{1} + \sigma_x) - \gamma_6(\sigma_z + i\sigma_y), \quad (12.3.10)$$

$$D = h_z\sigma_z - i\gamma_7\mathbb{1} + i\gamma_8\sigma_x + i\gamma_9\sigma_y. \quad (12.3.11)$$

The parameters read

$$\begin{aligned} \gamma_1/(\pi J_z^2) = & x_{\alpha}x_{\alpha'}|\mu_{\alpha\alpha'}| + \frac{1}{4}x_{\alpha}x_{\alpha'}(1 + \phi_z\phi_z)(|\mu_{\alpha\alpha'} + h| + |\mu_{\alpha\alpha'} - h| - 2|\mu_{\alpha\alpha'}|) \\ & - \phi_zx_{\alpha'}d_{\alpha}^z(|\mu_{\alpha\alpha'} + h| - |\mu_{\alpha\alpha'} - h|) \\ & - \frac{1}{2}\vec{d}_{\alpha} \cdot \vec{d}_{\alpha'}(|\mu_{\alpha\alpha'} + h| + |\mu_{\alpha\alpha'} - h|) \\ & + \frac{1}{4}(d_{\alpha}^x d_{\alpha'}^x + d_{\alpha}^y d_{\alpha'}^y)(|\mu_{\alpha\alpha'} + h| + |\mu_{\alpha\alpha'} - h| + 2|\mu_{\alpha\alpha'}|) \\ & + \frac{1}{4}[2\vec{d}_{\alpha} \cdot \vec{\phi}(d_{\alpha'}^x\phi^x + d_{\alpha'}^y\phi^y) + (\epsilon_{xij}\epsilon_{xkl} + \epsilon_{yij}\epsilon_{ykl})d_{\alpha}^i\phi^j d_{\alpha'}^k\phi^l] \\ & \times (|\mu_{\alpha\alpha'} + h| + |\mu_{\alpha\alpha'} - h| - 2|\mu_{\alpha\alpha'}|), \end{aligned} \quad (12.3.12)$$

$$\gamma_2/(\pi J_z^2) = x_{\alpha}x_{\alpha'}h_z - 2x_{\alpha'}d_{\alpha}^z\mu_{\alpha\alpha'} - \vec{d}_{\alpha} \cdot \vec{h} d_{\alpha'}^z, \quad (12.3.13)$$

$$\begin{aligned} \gamma_3/(\pi J_z^2) = & -\frac{1}{4}x_{\alpha}x_{\alpha'}\phi_y\phi_z(|\mu_{\alpha\alpha'} + h| + |\mu_{\alpha\alpha'} - h| - 2|\mu_{\alpha\alpha'}|) \\ & + \frac{1}{2}(\phi_yx_{\alpha'}d_{\alpha}^z + \phi_zx_{\alpha'}d_{\alpha}^y)(|\mu_{\alpha\alpha'} + h| - |\mu_{\alpha\alpha'} - h|) \\ & + \frac{1}{4}d_{\alpha}^y d_{\alpha'}^z(|\mu_{\alpha\alpha'} + h| + |\mu_{\alpha\alpha'} - h| + 2|\mu_{\alpha\alpha'}|) \\ & + \frac{1}{4}[\vec{d}_{\alpha} \cdot \vec{\phi}(d_{\alpha'}^y\phi^z + d_{\alpha'}^z\phi^y) + \epsilon_{yij}\epsilon_{zkl}d_{\alpha}^i\phi^j d_{\alpha'}^k\phi^l] \\ & \times (|\mu_{\alpha\alpha'} + h| + |\mu_{\alpha\alpha'} - h| - 2|\mu_{\alpha\alpha'}|), \end{aligned} \quad (12.3.14)$$

$$(12.3.15)$$

$$\begin{aligned}
\gamma_4/(\pi J_z^2) &= -\frac{1}{4}x_\alpha x_{\alpha'} \phi_x \phi_z (|\mu_{\alpha\alpha'} + h| + |\mu_{\alpha\alpha'} - h| - 2|\mu_{\alpha\alpha'}|) \\
&\quad + \frac{1}{2}(\phi_x x_{\alpha'} d_\alpha^z + \phi_z x_{\alpha'} d_\alpha^x)(|\mu_{\alpha\alpha'} + h| - |\mu_{\alpha\alpha'} - h|) \\
&\quad + \frac{1}{4}d_\alpha^x d_{\alpha'}^z (|\mu_{\alpha\alpha'} + h| + |\mu_{\alpha\alpha'} - h| + 2|\mu_{\alpha\alpha'}|) \\
&\quad + \frac{1}{4}[\vec{d}_\alpha \cdot \vec{\phi}(d_{\alpha'}^x \phi^z + d_{\alpha'}^z \phi^x) + \epsilon_{xij} \epsilon_{zkl} d_\alpha^i \phi^j d_{\alpha'}^k \phi^l] \\
&\quad \times (|\mu_{\alpha\alpha'} + h| + |\mu_{\alpha\alpha'} - h| - 2|\mu_{\alpha\alpha'}|), \tag{12.3.16}
\end{aligned}$$

$$\gamma_5/(\pi J_z^2) = x_\alpha x_{\alpha'} h_x - 2x_{\alpha'} d_\alpha^x \mu_{\alpha\alpha'} - \vec{d}_\alpha \cdot \vec{h} d_{\alpha'}^x, \tag{12.3.17}$$

$$\gamma_6/(\pi J_z^2) = x_\alpha x_{\alpha'} h_y - 2x_{\alpha'} d_\alpha^y \mu_{\alpha\alpha'} - \vec{d}_\alpha \cdot \vec{h} d_{\alpha'}^y, \tag{12.3.18}$$

$$\begin{aligned}
\gamma_7/(\pi J_z^2) &= 2x_\alpha x_{\alpha'} |\mu_{\alpha\alpha'}| - \frac{1}{4}x_\alpha x_{\alpha'} (\phi_z \phi_z - 3) (|\mu_{\alpha\alpha'} + h| + |\mu_{\alpha\alpha'} - h| - 2|\mu_{\alpha\alpha'}|) \\
&\quad - (\phi_x x_{\alpha'} d_\alpha^x + \phi_y x_{\alpha'} d_\alpha^y)(|\mu_{\alpha\alpha'} + h| - |\mu_{\alpha\alpha'} - h|) \\
&\quad - \vec{d}_\alpha \cdot \vec{d}_{\alpha'} (|\mu_{\alpha\alpha'} + h| + |\mu_{\alpha\alpha'} - h|) \\
&\quad + \frac{1}{4}(d_\alpha^x d_{\alpha'}^x + d_\alpha^y d_{\alpha'}^y + 2d_\alpha^z d_{\alpha'}^z)(|\mu_{\alpha\alpha'} + h| + |\mu_{\alpha\alpha'} - h| + 2|\mu_{\alpha\alpha'}|) \\
&\quad + \frac{1}{4}[2\vec{d}_\alpha \cdot \vec{\phi}(d_{\alpha'}^x \phi^x + d_{\alpha'}^y \phi^y + 2d_{\alpha'}^z \phi^z) \\
&\quad \quad + (\epsilon_{xij} \epsilon_{xkl} + \epsilon_{yij} \epsilon_{ykl} + 2\epsilon_{zij} \epsilon_{zkl}) d_\alpha^i \phi^j d_{\alpha'}^k \phi^l] \\
&\quad \times (|\mu_{\alpha\alpha'} + h| + |\mu_{\alpha\alpha'} - h| - 2|\mu_{\alpha\alpha'}|), \tag{12.3.19}
\end{aligned}$$

$$\begin{aligned}
\gamma_8/(\pi J_z^2) &= -\frac{1}{4}x_\alpha x_{\alpha'} (\phi_x \phi_x - \phi_y \phi_y) (|\mu_{\alpha\alpha'} + h| + |\mu_{\alpha\alpha'} - h| - 2|\mu_{\alpha\alpha'}|) \\
&\quad + (\phi_x x_{\alpha'} d_\alpha^x - \phi_y x_{\alpha'} d_\alpha^y)(|\mu_{\alpha\alpha'} + h| - |\mu_{\alpha\alpha'} - h|) \\
&\quad + \frac{1}{4}(d_\alpha^x d_{\alpha'}^x - d_\alpha^y d_{\alpha'}^y)(|\mu_{\alpha\alpha'} + h| + |\mu_{\alpha\alpha'} - h| + 2|\mu_{\alpha\alpha'}|) \\
&\quad + \frac{1}{4}[2\vec{d}_\alpha \cdot \vec{\phi}(d_{\alpha'}^x \phi^x - d_{\alpha'}^y \phi^y) + (\epsilon_{xij} \epsilon_{xkl} - \epsilon_{yij} \epsilon_{ykl}) d_\alpha^i \phi^j d_{\alpha'}^k \phi^l] \\
&\quad \times (|\mu_{\alpha\alpha'} + h| + |\mu_{\alpha\alpha'} - h| - 2|\mu_{\alpha\alpha'}|), \tag{12.3.20}
\end{aligned}$$

$$\begin{aligned}
\gamma_9/(\pi J_z^2) &= -\frac{1}{2}x_\alpha x_{\alpha'} \phi_x \phi_y (|\mu_{\alpha\alpha'} + h| + |\mu_{\alpha\alpha'} - h| - 2|\mu_{\alpha\alpha'}|) \\
&\quad + (\phi_x x_{\alpha'} d_\alpha^y + \phi_y x_{\alpha'} d_\alpha^x)(|\mu_{\alpha\alpha'} + h| - |\mu_{\alpha\alpha'} - h|) \\
&\quad + \frac{1}{2}d_\alpha^x d_{\alpha'}^y (|\mu_{\alpha\alpha'} + h| + |\mu_{\alpha\alpha'} - h| + 2|\mu_{\alpha\alpha'}|) \\
&\quad + \frac{1}{2}[\vec{d}_\alpha \cdot \vec{\phi}(d_{\alpha'}^x \phi^y + d_{\alpha'}^y \phi^x) + \epsilon_{xij} \epsilon_{ykl} d_\alpha^i \phi^j d_{\alpha'}^k \phi^l] \\
&\quad \times (|\mu_{\alpha\alpha'} + h| + |\mu_{\alpha\alpha'} - h| - 2|\mu_{\alpha\alpha'}|), \tag{12.3.21}
\end{aligned}$$

where all contain an implicit sum over  $\alpha$  and  $\alpha'$  and we defined  $\phi_i = h_i/h$ ,  $h = |\vec{h}|$ .



From this, we can calculate a reduced Liouvillian to determine the diagonal part of the dot density matrix via eq. (10.2.15)

$$L_{\text{red}} \begin{pmatrix} \rho_{\uparrow\uparrow} \\ \rho_{\downarrow\downarrow} \end{pmatrix} = 0, \quad L_{\text{red}} = A - B \frac{1}{D} C = i \begin{pmatrix} -\Gamma_{\downarrow\rightarrow\uparrow} & \Gamma_{\uparrow\rightarrow\downarrow} \\ \Gamma_{\downarrow\rightarrow\uparrow} & -\Gamma_{\uparrow\rightarrow\downarrow} \end{pmatrix}, \quad (12.3.22)$$

with

$$\begin{aligned} \Gamma_{\uparrow\rightarrow\downarrow} = & (\gamma_1 - \gamma_2) + 2 (h_z^2 + \gamma_7^2 - \gamma_8^2 - \gamma_9^2)^{-1} \\ & \times \left[ \left( \frac{h_x}{2} + \gamma_3 \right) \left( -\gamma_6\gamma_7 - h_z\gamma_5 + \gamma_6\gamma_8 - \gamma_5\gamma_9 + \frac{h_x}{2}\gamma_7 - \gamma_3\gamma_7 \right. \right. \\ & \quad \left. \left. - \frac{h_y}{2}h_z - h_z\gamma_4 - \frac{h_x}{2}\gamma_8 + \gamma_3\gamma_8 - \frac{h_y}{2}\gamma_9 - \gamma_4\gamma_9 \right) \right. \\ & \left. + \left( \frac{h_y}{2} - \gamma_4 \right) \left( \gamma_5\gamma_7 - h_z\gamma_6 + \gamma_5\gamma_8 + \gamma_6\gamma_9 + \frac{h_y}{2}\gamma_7 + \gamma_4\gamma_7 \right. \right. \\ & \quad \left. \left. + \frac{h_x}{2}h_z - h_z\gamma_3 + \frac{h_y}{2}\gamma_8 + \gamma_4\gamma_8 - \frac{h_x}{2}\gamma_9 + \gamma_3\gamma_9 \right) \right], \quad (12.3.23) \end{aligned}$$

$$\begin{aligned} \Gamma_{\downarrow\rightarrow\uparrow} = & (\gamma_1 + \gamma_2) + 2 (h_z^2 + \gamma_7^2 - \gamma_8^2 - \gamma_9^2)^{-1} \\ & \times \left[ \left( \frac{h_x}{2} + \gamma_3 \right) \left( \gamma_6\gamma_7 + h_z\gamma_5 - \gamma_6\gamma_8 + \gamma_5\gamma_9 + \frac{h_x}{2}\gamma_7 - \gamma_3\gamma_7 \right. \right. \\ & \quad \left. \left. - \frac{h_y}{2}h_z - h_z\gamma_4 - \frac{h_x}{2}\gamma_8 + \gamma_3\gamma_8 - \frac{h_y}{2}\gamma_9 - \gamma_4\gamma_9 \right) \right. \\ & \left. + \left( \frac{h_y}{2} - \gamma_4 \right) \left( -\gamma_5\gamma_7 + h_z\gamma_6 - \gamma_5\gamma_8 - \gamma_6\gamma_9 + \frac{h_y}{2}\gamma_7 + \gamma_4\gamma_7 \right. \right. \\ & \quad \left. \left. + \frac{h_x}{2}h_z - h_z\gamma_3 + \frac{h_y}{2}\gamma_8 + \gamma_4\gamma_8 - \frac{h_x}{2}\gamma_9 + \gamma_3\gamma_9 \right) \right], \quad (12.3.24) \end{aligned}$$

$$\begin{aligned} \Gamma = & \Gamma_{\uparrow\rightarrow\downarrow} + \Gamma_{\downarrow\rightarrow\uparrow} \\ = & 2\gamma_1 + 4 (h_z^2 + \gamma_7^2 - \gamma_8^2 - \gamma_9^2)^{-1} \\ & \times \left[ \left( \frac{h_x}{2} + \gamma_3 \right) \left( \frac{h_x}{2}\gamma_7 - \gamma_3\gamma_7 - \frac{h_y}{2}h_z - h_z\gamma_4 - \frac{h_x}{2}\gamma_8 + \gamma_3\gamma_8 - \frac{h_y}{2}\gamma_9 - \gamma_4\gamma_9 \right) \right. \\ & \left. + \left( \frac{h_y}{2} - \gamma_4 \right) \left( \frac{h_y}{2}\gamma_7 + \gamma_4\gamma_7 + \frac{h_x}{2}h_z - h_z\gamma_3 + \frac{h_y}{2}\gamma_8 + \gamma_4\gamma_8 - \frac{h_x}{2}\gamma_9 + \gamma_3\gamma_9 \right) \right], \quad (12.3.25) \end{aligned}$$

$$\begin{aligned} \Gamma_{\Delta} = & \Gamma_{\uparrow\rightarrow\downarrow} - \Gamma_{\downarrow\rightarrow\uparrow} \\ = & -2\gamma_2 + 4 (h_z^2 + \gamma_7^2 - \gamma_8^2 - \gamma_9^2)^{-1} \\ & \times \left[ \left( \frac{h_x}{2} + \gamma_3 \right) \left( -\gamma_6\gamma_7 - h_z\gamma_5 + \gamma_6\gamma_8 - \gamma_5\gamma_9 \right) \right. \\ & \left. + \left( \frac{h_y}{2} - \gamma_4 \right) \left( \gamma_5\gamma_7 - h_z\gamma_6 + \gamma_5\gamma_8 + \gamma_6\gamma_9 \right) \right], \quad (12.3.26) \end{aligned}$$

we get

$$\rho_{\uparrow\uparrow} = \frac{\Gamma_{\uparrow\rightarrow\downarrow}}{\Gamma}, \quad (12.3.27)$$

$$\rho_{\downarrow\downarrow} = \frac{\Gamma_{\downarrow\rightarrow\uparrow}}{\Gamma}. \quad (12.3.28)$$

The non-diagonal parts of the dot density matrix can be calculated by

$$\begin{pmatrix} \rho_{\uparrow\downarrow} \\ \rho_{\downarrow\uparrow} \end{pmatrix} = -\frac{1}{D} C \begin{pmatrix} \rho_{\uparrow\uparrow} \\ \rho_{\downarrow\downarrow} \end{pmatrix}, \quad (12.3.29)$$

and read

$$\begin{aligned} \rho_{\uparrow\downarrow} &= (h_z^2 + \gamma_7^2 - \gamma_8^2 - \gamma_9^2)^{-1} \\ &\times \left[ -\gamma_5\gamma_7 + h_z\gamma_6 - \gamma_5\gamma_8 - \gamma_6\gamma_9 + i\gamma_6\gamma_7 + ih_z\gamma_5 - i\gamma_6\gamma_8 + i\gamma_5\gamma_9 \right. \\ &\quad + \frac{\Gamma\Delta}{\Gamma} \left( i\frac{h_x}{2}\gamma_7 - i\gamma_3\gamma_7 - i\frac{h_y}{2}h_z - ih_z\gamma_4 - i\frac{h_x}{2}\gamma_8 + i\gamma_3\gamma_8 - i\frac{h_y}{2}\gamma_9 - i\gamma_4\gamma_9 \right. \\ &\quad \left. \left. + \frac{1}{2}h_y\gamma_7 + \gamma_4\gamma_7 + \frac{h_x}{2}h_z - h_z\gamma_3 + \frac{h_y}{2}\gamma_8 + \gamma_4\gamma_8 - \frac{h_x}{2}\gamma_9 + \gamma_3\gamma_9 \right) \right]. \end{aligned} \quad (12.3.30)$$

From these results for the stationary density matrix, we can determine the magnetization

$$M_x = \text{Re}(\rho_{\uparrow\downarrow}), \quad M_y = -\text{Im}(\rho_{\uparrow\downarrow}), \quad M_z = \frac{1}{2}(\rho_{\uparrow\uparrow} - \rho_{\downarrow\downarrow}), \quad (12.3.31)$$

and derive

$$\begin{aligned} M_z &= \left\{ -\gamma_2 (h_z^2 + \gamma_7^2 - \gamma_8^2 - \gamma_9^2) + 2 \left[ \left( \frac{h_x}{2} + \gamma_3 \right) (-\gamma_6\gamma_7 - h_z\gamma_5 + \gamma_6\gamma_8 - \gamma_5\gamma_9) \right. \right. \\ &\quad \left. \left. + \left( \frac{h_y}{2} - \gamma_4 \right) (\gamma_5\gamma_7 - h_z\gamma_6 + \gamma_5\gamma_8 + \gamma_6\gamma_9) \right] \right\} \\ &\times \left\{ 2\gamma_1 (h_z^2 + \gamma_7^2 - \gamma_8^2 - \gamma_9^2) \right. \\ &\quad + 4 \left[ \left( \frac{h_x}{2} + \gamma_3 \right) \left( \frac{h_x}{2}\gamma_7 - \gamma_3\gamma_7 - \frac{h_y}{2}h_z - h_z\gamma_4 - \frac{h_x}{2}\gamma_8 + \gamma_3\gamma_8 - \frac{h_y}{2}\gamma_9 - \gamma_4\gamma_9 \right) \right. \\ &\quad \left. \left. + \left( \frac{h_y}{2} - \gamma_4 \right) \left( \frac{h_y}{2}\gamma_7 + \gamma_4\gamma_7 + \frac{h_x}{2}h_z - h_z\gamma_3 + \frac{h_y}{2}\gamma_8 + \gamma_4\gamma_8 - \frac{h_x}{2}\gamma_9 + \gamma_3\gamma_9 \right) \right] \right\}^{-1}, \end{aligned} \quad (12.3.32)$$

$$M_x = (h_z^2 + \gamma_7^2 - \gamma_8^2 - \gamma_9^2)^{-1} \times \left[ -\gamma_5\gamma_7 + h_z\gamma_6 - \gamma_5\gamma_8 - \gamma_6\gamma_9 \right. \\ \left. + 2M_z \left( \frac{h_y}{2}\gamma_7 + \gamma_4\gamma_7 + \frac{h_x}{2}h_z - h_z\gamma_3 + \frac{h_y}{2}\gamma_8 + \gamma_4\gamma_8 - \frac{h_x}{2}\gamma_9 + \gamma_3\gamma_9 \right) \right], \quad (12.3.33)$$

$$M_y = (h_z^2 + \gamma_7^2 - \gamma_8^2 - \gamma_9^2)^{-1} \times \left[ -\gamma_6\gamma_7 - h_z\gamma_5 + \gamma_6\gamma_8 - \gamma_5\gamma_9 \right. \\ \left. + 2M_z \left( -\frac{h_x}{2}\gamma_7 + \gamma_3\gamma_7 + \frac{h_y}{2}h_z + h_z\gamma_4 + \frac{h_x}{2}\gamma_8 - \gamma_3\gamma_8 + \frac{h_y}{2}\gamma_9 + \gamma_4\gamma_9 \right) \right]. \quad (12.3.34)$$

The current follows from eq. (10.3.11) and reads

$$I^\gamma = -\pi c_{\alpha\alpha'}^\gamma J_z^2 \left\{ 3x_\alpha x_{\alpha'} \mu_{\alpha\alpha'} + 2x_\alpha x_{\alpha'} (|\mu_{\alpha\alpha'} + h| - |\mu_{\alpha\alpha'} - h|) \vec{\phi} \cdot \vec{M} \right. \\ - 4x_{\alpha'} \vec{d}_\alpha \cdot \vec{h} - 8|\mu_{\alpha\alpha'}| x_{\alpha'} \vec{d}_\alpha \cdot \vec{M} \\ - 2(|\mu_{\alpha\alpha'} + h| + |\mu_{\alpha\alpha'} - h| - 2|\mu_{\alpha\alpha'}|) x_{\alpha'} \vec{d}_\alpha \cdot (\vec{M} + \vec{\phi}(\vec{\phi} \cdot \vec{M})) \\ \left. - \mu_{\alpha\alpha'} \vec{d}_\alpha \cdot \vec{d}_{\alpha'} - 2(|\mu_{\alpha\alpha'} + h| - |\mu_{\alpha\alpha'} - h|) \vec{d}_\alpha \cdot \vec{\phi} \vec{d}_{\alpha'} \cdot \vec{M} \right\}, \quad (12.3.35)$$

where the sums over  $\alpha$  and  $\alpha'$  still have to be performed.

**Golden-Rule Regime** The golden-rule regime is defined by  $h \gg \gamma \sim J_{z,\perp}^2 \Lambda_c$ . In this regime, the result for the magnetization simplifies significantly and reads

$$\vec{M} = M \vec{\phi} \\ = \vec{\phi} \left\{ -h \left[ 1 - (\vec{d} \cdot \vec{\phi})^2 \right] + 2\vec{\mu} \cdot \vec{\phi} \right\} \\ \times \left\{ (x_\alpha x_{\alpha'} - \vec{d}_\alpha \cdot \vec{\phi} \vec{d}_{\alpha'} \cdot \vec{\phi}) (|\mu_{\alpha\alpha'} + h| + |\mu_{\alpha\alpha'} - h|) \right. \\ \left. + 2x_\alpha \vec{d}_{\alpha'} \cdot \vec{\phi} (|\mu_{\alpha\alpha'} + h| - |\mu_{\alpha\alpha'} - h|) \right\}^{-1}, \quad (12.3.36)$$

where we defined the vector  $\vec{\mu} = \sum_\alpha (\mu_\alpha - \bar{\mu}) \vec{d}_\alpha$  with  $\bar{\mu} = \sum_\alpha x_\alpha \mu_\alpha$ . This magnetization is zero for a magnetic field pointing to the surface of an ellipsoid, which can be fully characterized by the vectors  $\vec{d}$  and  $\vec{\mu}$  and the stretching factor of the ellipsoid in the direction of  $\vec{d}$  given by

$$s = \frac{1}{\sqrt{1-d^2}} = \frac{1}{\sqrt{1-c^2/J_z^2}} = \frac{J_z}{J_\perp} \geq 1. \quad (12.3.37)$$

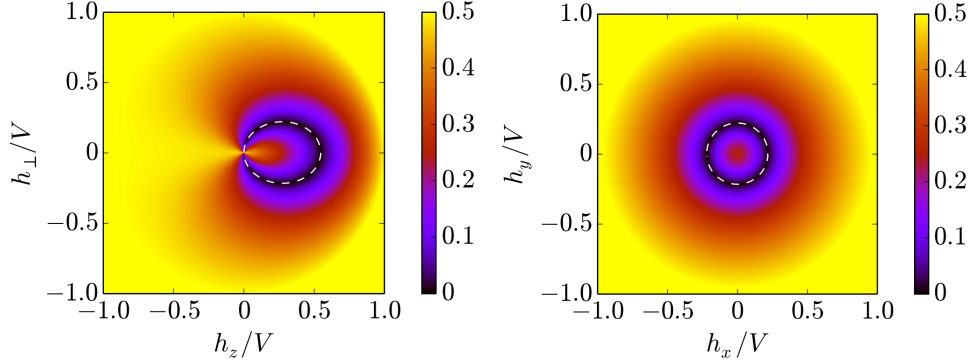


**Figure 12.1:** (Left) Dot magnetization  $M$  as function of  $h_z$  and  $h_\perp$  coupled to two reservoirs for model 1 of table (12.1). The dashed white line indicates the ellipsoid which describes the minimum of  $M$ . The region at  $h \approx V$  has to be taken with care in both plots as logarithmic enhancements have been neglected in our calculation. (Right) Dot magnetization  $M$  as function of  $h_x$  and  $h_y$  with the same parameters as before and  $h_z = s^2 \mu_z$ . The rotational invariance is only given because of the special choice of the parameters.

This ellipsoid is rotationally invariant around  $\vec{d}$  and reads

$$(h_\perp - \mu_\perp)^2 + \left( \frac{h_\parallel - s^2 \mu_\parallel}{s} \right)^2 = \mu_\perp^2 + s^2 \mu_\parallel^2, \quad (12.3.38)$$

where we decomposed the vectors  $\vec{h}$  and  $\vec{\mu}$  into their components parallel and perpendicular to  $\vec{d}$ . This is the **main result** of this part of the thesis and provides a *smoking gun* for experiments to determine the distance to the scaling limit via the stretching factor  $s$ , which becomes  $s = 1$  in this limit turning the ellipsoid into a sphere. We note further that outside the ellipsoid the magnetization is antiparallel to  $\vec{h}$ , whereas it is parallel inside. Additionally, the rotational invariance around the vector  $\vec{d}$  is only valid for the root of the magnetization and not the full magnetization itself, as therefore all the individual scalar products  $\vec{d}_\alpha \cdot \vec{h}$  appear.

To visualize this ellipsoid we want to maximize the stretching factor and the ellipsoid itself. As the stretching factor rises with increasing  $d = |\sum_\alpha \vec{d}_\alpha|$  and the ellipsoid becomes larger for larger  $|\vec{\mu}| = |\sum_\alpha (\mu_\alpha - \bar{\mu}) \vec{d}_\alpha|$ , a compromise has to be found. Just maximizing  $d$  would lead to a nearly vanishing  $|\vec{\mu}|$  and vice versa. In Fig. 12.1 we present the magnetization for two reservoirs coupled to the QD with the parameters given in table 12.1 (Model 1). The dashed white line indicates where  $M$  is minimal. Of course, for this specific choice the rotational symmetry in the  $xy$ -plane is valid not only for the ellipsoid describing the minimal magnetization but for the complete magnetization itself. Another example is shown in Fig. 12.2, where three reservoirs are coupled to

$i$	Model 1		Model 2		
	1	2	1	2	3
$x_i$	0.50	0.50	0.25	0.40	0.35
$p_i$	0.95	0.25	0.80	0.70	0.90
$\Theta_i$	0	$\pi$	$\frac{\pi}{6}$	$\frac{\pi}{3}$	$\text{asin} \frac{0.14\sqrt{3}-0.1}{0.315}$
$\phi_i$	0	0	0	$\pi$	0
$\mu_i$	0.50	-0.50	0.25	0.35	-0.60
$J_z$	0.01		0.01		

**Table 12.1:** Effective model parameters for model 1 and 2 discussed in this section.  $\Theta_i$  and  $\phi_i$  are the azimuth and the polar angle of the normalized spin polarization axis  $\hat{d}_i$ .

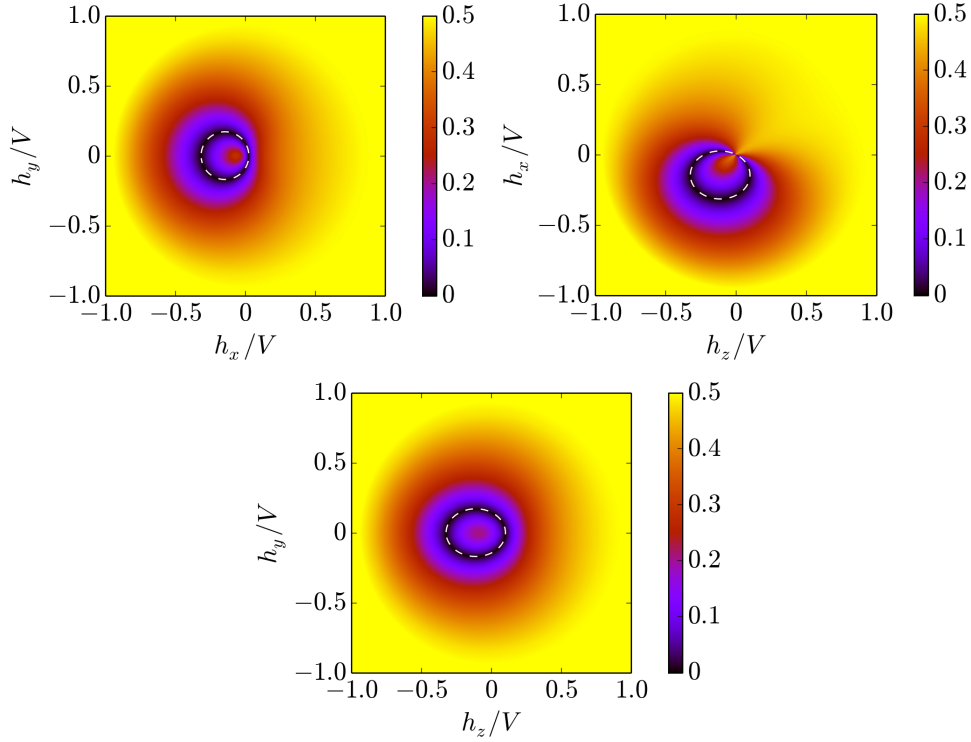


**Figure 12.2:** Dot magnetization  $M$  as function of  $h_x$ ,  $h_y$  and  $h_z$ , respectively. The third, not varied part of the magnetic field is chosen as  $h_i = \mu_i$ . We defined  $V = \max(\mu_i) - \min(\mu_j)$ . The dot is coupled to three reservoirs [Model 2 of table (12.1)]. The dashed white line indicates the ellipsoid which describes the minimum of  $M$ . The region at  $h \approx V$  has to be taken with care in all plots as logarithmic enhancements have been neglected in our calculation. Here, the broken rotational invariance for the magnetization becomes obvious.

the QD (Model 2 of table 12.1). Here, also the broken rotational invariance for the magnetization is seen (except for the ellipsoid).

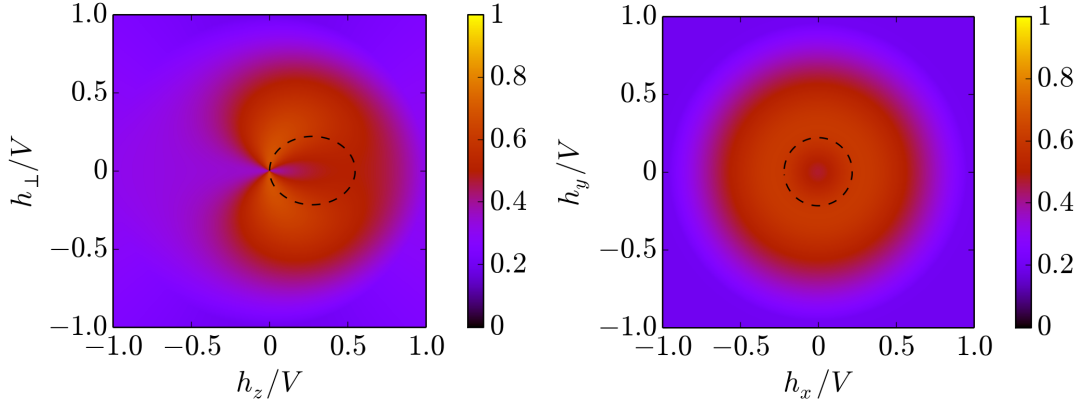


**Figure 12.3:** (Left) Current  $I^1$  from the first lead to the QD in terms of  $\pi J_z^2 V$  as function of  $h_z$  and  $h_\perp$ . The reservoirs are coupled with the coupling parameters given in table (12.1) (Model 1). The dashed line represents the minimum of the magnetization. (Lower right) Current  $I^1$  in terms of  $\pi J_z^2 V$  as function of  $h_x$  and  $h_y$ .

All the previously mentioned features are an important difference to the Kondo model with unpolarized leads, for which  $\vec{d} = \vec{\mu} = 0$  such that the magnetization only vanishes at  $\vec{h} = 0$ .

Finally, the current in the golden-rule regime reads

$$\begin{aligned}
 I^\gamma = -\pi c_{\alpha\alpha'}^\gamma J_z^2 \left\{ \mu_{\alpha\alpha'} (3x_\alpha x_{\alpha'} - \vec{d}_\alpha \cdot \vec{d}_{\alpha'}) \right. \\
 + 2M(|\mu_{\alpha\alpha'} + h| - |\mu_{\alpha\alpha'} - h|)(x_\alpha x_{\alpha'} - \vec{d}_\alpha \cdot \vec{\phi} \vec{d}_{\alpha'} \cdot \vec{\phi}) \\
 \left. + 4x_\alpha \vec{d}_{\alpha'} \cdot \vec{\phi} [h + M(|\mu_{\alpha\alpha'} + h| + |\mu_{\alpha\alpha'} - h|)] \right\}. \quad (12.3.39)
 \end{aligned}$$

The current of model 1 is shown in Fig. 12.3 but does not have such obvious features as the magnetization.

In the next section we will specify the previous results for the case of two reservoirs in the scaling limit and will also investigate the quantum interference regime  $h \lesssim \gamma$ .

## 12.4 Solution for Two Reservoirs in the Scaling Limit

In the case of two reservoirs, labeled by the indices  $\alpha = L/R$  and in the scaling limit ( $J_z = J$ ,  $c/J_z = 0$ ), eq. (12.1.15) leads to

$$\vec{d}_L = -\vec{d}_R, \quad x_{LP} = x_{RP}, \quad (12.4.1)$$

where we choose  $\vec{d}_L$  to point in the  $z$ -direction. For this special case not only the surface of vanishing magnetization but the complete magnetization itself is rotational invariant around the spin polarization axis given by  $\vec{e}_z$ . The bias voltage is given by  $V = \mu_L - \mu_R$  and we choose the magnetic field to be in the  $xz$ -plane breaking the rotational invariance. The rates (12.3.12 - 12.3.21) simplify to

$$\begin{aligned} \frac{\gamma_1}{\pi J^2} &= \frac{1}{2}h(1 + 2x_L x_R - 2x_L x_R p_L p_R)(1 + \phi_z)^2 + V x_L x_R (1 + p_L p_R)(1 - \phi_z^2) \\ &\quad + (|V + h| - |V - h|)x_L p_L \phi_z + \frac{1}{2}(|V + h| + |V - h|)x_L x_R (1 + p_L p_R)(1 + \phi_z^2), \end{aligned} \quad (12.4.2)$$

$$\frac{\gamma_2}{\pi J^2} = h\phi_z - 2V x_L p_L, \quad (12.4.3)$$

$$\frac{\gamma_3}{\pi J^2} = 0, \quad (12.4.4)$$

$$\begin{aligned} \frac{\gamma_4}{\pi J^2} &= -\frac{1}{2}h(1 + 2x_L x_R + 2x_L x_R p_L p_R)\phi_x \phi_z + \frac{1}{2}(|V + h| - |V - h|)x_L p_L \phi_x \\ &\quad - \frac{1}{2}(|V + h| + |V - h| - 2V)x_L x_R (1 + p_L p_R)\phi_x \phi_z, \end{aligned} \quad (12.4.5)$$

$$\frac{\gamma_5}{\pi J^2} = h\phi_x, \quad (12.4.6)$$

$$\frac{\gamma_6}{\pi J^2} = 0, \quad (12.4.7)$$

$$\begin{aligned} \frac{\gamma_7}{\pi J^2} &= -\frac{1}{2}h(1 + 2x_L x_R)(\phi_z^2 - 3) - \frac{1}{2}h x_L x_R p_L p_R (1 - 3\phi_z) \\ &\quad + V x_L x_R [7 + 3p_L p_R (1 + \phi_z^2)] \\ &\quad - \frac{1}{2}(|V + h| + |V - h|)x_L x_R [3 - \phi_z^2 - p_L p_R (1 - 3\phi_z^2)], \end{aligned} \quad (12.4.8)$$

$$\begin{aligned} \frac{\gamma_8}{\pi J^2} &= -\frac{1}{2}h(1 + 2x_L x_R - 2x_L x_R p_L p_R)\phi_x^2 \\ &\quad - \frac{1}{2}(|V + h| + |V - h| - 2V)x_L x_R (1 - p_L p_R)\phi_x^2, \end{aligned} \quad (12.4.9)$$

$$\frac{\gamma_9}{\pi J^2} = 0. \quad (12.4.10)$$

The magnetizations read

$$M_x = (h_z^2 + \gamma_7^2 - \gamma_8^2)^{-1} \left[ M_z h_x h_z + (2M_z \gamma_4 - \gamma_5)(\gamma_7 + \gamma_8) \right], \quad (12.4.11)$$

$$M_y = (h_z^2 + \gamma_7^2 - \gamma_8^2)^{-1} \left[ M_z h_x (\gamma_8 - \gamma_7) + 2M_z h_z \gamma_4 - \gamma_5 h_z \right], \quad (12.4.12)$$

$$\begin{aligned} M_z &= \left[ -\gamma_2 (h_z^2 + \gamma_7^2 - \gamma_8^2) - h_x h_z \gamma_5 - \gamma_4 \gamma_5 (\gamma_7 + \gamma_8) \right] \\ &\quad \times \left[ 2\gamma_1 (h_z^2 + \gamma_7^2 - \gamma_8^2) + h_x^2 (\gamma_7 - \gamma_8) - 4h_x h_z \gamma_4 - \gamma_4^2 (\gamma_7 + \gamma_8) \right]^{-1}, \end{aligned} \quad (12.4.13)$$

and the current

$$I_{h=0}^\gamma/\kappa = \frac{1}{4}(3 + p_L p_R) - (p_L + p_R)M_0, \quad (12.4.14)$$

$$\begin{aligned} I_{V>h}^\gamma/\kappa &= \frac{1}{4}(3 + p_L p_R) - (p_L + p_R)M_z + \frac{h_x}{V}M_x + \frac{h_z}{V}(1 + p_L p_R)M_z - \frac{1}{2}\frac{h_z}{V}(p_L + p_R) \\ &= I_{h=0}^\gamma/\kappa + \frac{\vec{h}_\perp}{V}\vec{M}_\perp + (1 + p_L p_R)(M_z - M_0) \left( \frac{h_z}{V} - 2M_0 \right), \end{aligned} \quad (12.4.15)$$

$$\begin{aligned} I_{V<h}^\gamma/\kappa &= \frac{1}{4}(3 + p_L p_R) - (p_L + p_R)M_z + \phi_x M_x + \phi_z(1 + p_L p_R)M_z - \frac{1}{2}\frac{h_z}{V}(p_L + p_R) \\ &\quad - \frac{1}{2}(h - V)[\phi_x \phi_z M_x + M_z(1 + \phi_z^2)](p_L + p_R) \\ &= I_{V>h}^\gamma/\kappa - \frac{1}{2}(h - V)[\phi_z \vec{\phi}_\perp \cdot \vec{M}_\perp + M_z(1 + \phi_z^2)](p_L + p_R), \end{aligned} \quad (12.4.16)$$

where we defined the Korringa rate  $\kappa = 4x_L x_R \pi J^2 V$  and the magnetization

$$M_0 = M_{h=0} = \frac{1}{2} \frac{p_L + p_R}{1 + p_L p_R}. \quad (12.4.17)$$

**Golden-Rule Regime** In the regime  $h_z \gg \kappa$  or  $h_x \sim \mathcal{O}(V)$  or  $h_x \ll \kappa$  we obtain the golden-rule result

$$\vec{M} \approx \vec{\phi} \frac{x_L p_L V \phi_z - \frac{1}{2}h}{2x_L x_R V(1 + p_L p_R \phi_z^2) + h - 2x_L x_R h(1 + p_L \phi_z)(1 + p_R \phi_z)}, \quad (12.4.18)$$

where we can read off that the minimum of the magnetization is now given by a sphere centered around  $h_z = x_L p_L V$ ,  $h_\perp = 0$  with a radius of  $x_L p_L V$ . It is easy to prove that this sphere will always lie inside the region  $h < V$  as  $2x_L p_L = 2x_L x_R(p_L + p_R) \leq \frac{1}{2}(p_L + p_R) \leq 1$ . For  $h \geq V$  we get  $\vec{M} = -\frac{1}{2}\vec{\phi}$  which follows directly from energy conservation as only the low-lying energy-level of the QD can be occupied. The global direction of the magnetization can also be understood easily in this case. The majority of the spins of the left lead are  $\uparrow$  as  $\vec{d}_L$  is chosen to point in the  $z$ -direction. Applying a small transverse magnetic field  $h_\perp$  and a not too large longitudinal one  $h_z$ , the upper dot-level consists mainly of the spin- $\uparrow$ -state such that it will be occupied due to the coupling to the reservoir with  $\mu_L = \frac{V}{2}$ . This higher energy-level of the dot has nearly no transition amplitude to the right reservoir with  $\mu_R = -\frac{V}{2}$  as this contains mostly  $\downarrow$ -spins. Hence, the magnetization is parallel to the external field. Increasing the transverse magnetic field yields an increased transition rate between the two dot levels until they are equally occupied, defining the minimum of the magnetization. Further increasing this field up to  $h_\perp \sim \mathcal{O}(V)$  reduces the available phase space for transitions from the lower to the upper dot level such that the population of the lower level rises



and the magnetization becomes antiparallel to the external field. For the case  $h_z < 0$  this discussion becomes more trivial as the lower energy level of the dot has always a higher occupation and the magnetization does not change its direction with respect to the magnetic field.

From eq. (12.4.18) we can determine the magnetization at the special point  $h_x = 0$  leading to

$$M_x = M_y = 0, \quad (12.4.19)$$

$$M_z = \frac{x_L p_L V - \frac{1}{2} h \operatorname{sign}(h_z)}{h + 2x_L x_R (1 + p_L p_R)(V - h) - 2x_L p_L h \operatorname{sign}(h_z)}, \quad (12.4.20)$$

giving rise to a characteristic jump of the first derivative at  $h_z = 0$

$$\frac{\partial M}{\partial h_z} \Big|_{h_z=0^+, h_x=0} - \frac{\partial M}{\partial h_z} \Big|_{h_z=0^-, h_x=0} = \frac{(1 + p_L)(1 + p_R)}{(1 - p_L)(1 - p_R)} \cdot \frac{1 - 2x_L p_L}{1 + 2x_L p_L}. \quad (12.4.21)$$

This jump can be used in experiments to determine the strength of the external magnetic field such that it compensates the exchange field generated by the ferromagnetic leads so that the total magnetic field vanishes  $h = 0$ . Furthermore, also the  $z$ -axis can be determined in this way.

The current in this regime can be evaluated by inserting eq. (12.4.18) into eqs. (12.4.15) and (12.4.16) but does not simplify significantly. The maximum of the current for fixed  $h_z$  as function of  $h_\perp$  is roughly at the same order as the minimum of the magnetization due to enhanced inelastic processes, which increase the current. However, this maximum is rather broad so it cannot be used to determine the model parameters. Instead, we can evaluate eq. (12.4.16) at  $h = V$  leading to

$$I_{h=V}^L / \kappa = \frac{1}{4} \left[ 1 - p_L p_R \left( 2 \frac{h_z^2}{V^2} - 1 \right) \right], \quad (12.4.22)$$

which yields

$$I_{h_z=0, h_\perp=V}^L / \kappa = \frac{1}{4} (1 + p_L p_R), \quad (12.4.23)$$

$$I_{h_z=V, h_\perp=0}^L / \kappa = \frac{1}{4} (1 - p_L p_R). \quad (12.4.24)$$

Using eq. (12.4.14), we can calculate  $p_L$ ,  $p_R$  and  $J$  and with  $x_L + x_R = 1$ ,  $x_L p_L = x_R p_R$  follow  $x_L$  and  $x_R$ .

The results for the magnetization and the current in the golden-rule regime are shown in the main part of Fig. 12.4 for  $x_L = x_R = 0.5$ ,  $p_L = p_R = 0.75$ ,  $J = 0.01/\sqrt{\pi}$ .

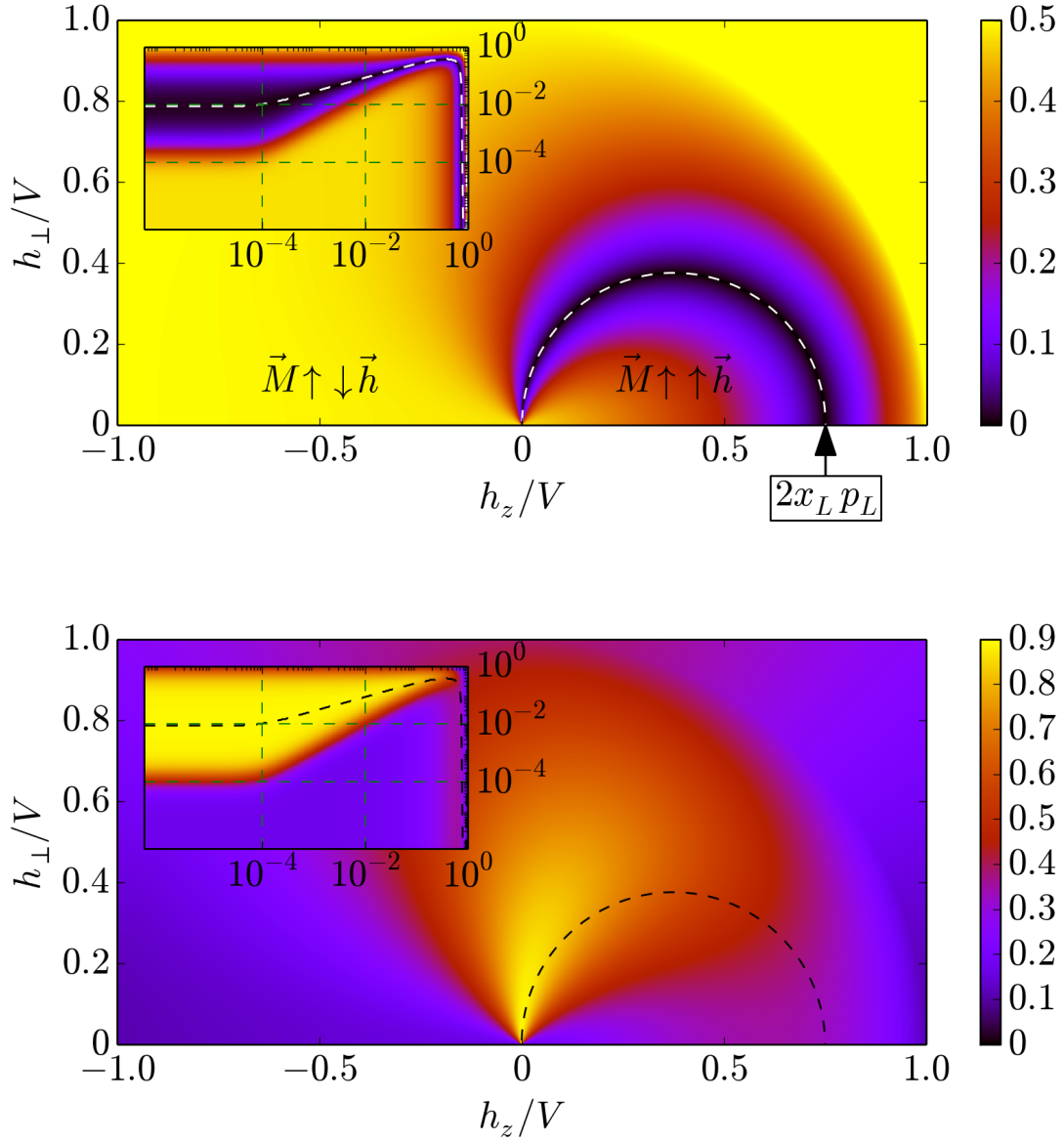


**Figure 12.4:** (Upper) Dot magnetization  $M$  as function of  $h_z$  and  $h_\perp$  coupled to two reservoirs in the scaling limit with  $x_L = x_R = 0.5$ ,  $p_L = p_R = 0.75$ ,  $\mu_L = -\mu_R = 0.5$  and  $J = 0.01/\sqrt{\pi}$ . The dashed white line indicates the circle with radius  $x_L p_L$  which describes the minimum of  $M$ . Inset: The same plot on a logarithmic scale for  $h_z > 0$ . The region at  $h \approx V$  has to be taken with care in all plots as logarithmic enhancements have been neglected in our calculation. (Lower) The current  $I^L/\kappa$  in units of the Korringa rate  $\kappa = 10^{-4}V$ . The black line corresponds to the white one of the left plot.

**Quantum-Interference Regime** The golden-rule theory from the previous paragraph breaks down for small magnetic fields  $h_z \lesssim \kappa$  and  $J^2V \lesssim h_x \lesssim JV$  as quantum interference processes become important. Here, a finite magnetization in  $y$ -direction arises. For  $h_z \sim \kappa$ ,  $h_x \ll V$  we obtain

$$M_x \approx \frac{1}{2} \frac{h_z}{h_x} x^2 \frac{p_L + p_R - \frac{h_x^2}{2x_L x_R h_z V}}{1 + p_L p_R + x^2}, \quad (12.4.25)$$

$$M_y \approx \frac{1}{2} \frac{\kappa}{h_x} x^2 \frac{p_L + p_R}{1 + p_L p_R + x^2}, \quad (12.4.26)$$

$$M_z \approx \frac{1}{2} \frac{p_L + p_R - \frac{h_z x^2}{2x_L x_R V}}{1 + p_L p_R + x^2}, \quad (12.4.27)$$

with  $x = h_x / \sqrt{h_z^2 + \kappa^2}$ . These results hold also for  $h_z \ll \kappa$  and  $h_x \ll V$  except for  $h_z \ll \kappa$  and  $h_x \lesssim \kappa$  where  $M_x$  changes to

$$M_x \approx \frac{1}{4x_L x_R} \frac{h_x}{V} \left( \frac{p_L p_R}{1 + p_L p_R + x^2} - 1 \right). \quad (12.4.28)$$

However, as  $h_x \lesssim \kappa \sim J^2$ , also  $M_x \lesssim J^2$  such that it can be neglected. All in all, we get for  $h_z \lesssim \kappa \lesssim h_x \ll V$  the total magnetization

$$M \approx \sqrt{\pi^2 J^4 x^2 + M_z^2 (1 + x^2)}, \quad (12.4.29)$$

$$M_z \approx \frac{1}{2} \frac{p_L + p_R - \frac{h_z x^2}{2x_L x_R V}}{1 + p_L p_R + x^2} = \frac{1}{2} \frac{p_L + p_R - 2\pi J^2 x^2 h_z / \kappa}{1 + p_L p_R + x^2}. \quad (12.4.30)$$

It is important to note that due to the quantum-interference processes the position of the minimum of the magnetization saturates at  $h_\perp \sim \mathcal{O}(JV)$  and by a further reduction of  $h_\perp$  the magnetization increases again (see inset of Fig. 12.4).

To calculate the current in this regime, we can neglect all terms proportional to  $h$  in eq. (12.4.15) yielding

$$(I_{V>h}^\gamma - I_{h=0}^\gamma) / \kappa \approx -(p_L + p_R)(M_z - M_0). \quad (12.4.31)$$

Inserting the magnetization (12.4.30) the term proportional to  $h_z x^2 / V$  in the numerator can be neglected as it only becomes important for  $x^2 \sim V / h_z \gtrsim 1 / J^2$  where the magnetization itself becomes of  $\mathcal{O}(J^2)$  such that it will be neglected anyhow. Therefore, for  $h_z \lesssim \kappa$  and  $J^2V \lesssim h_x \lesssim JV$  we get the result

$$(I_{V>h}^\gamma - I_{h=0}^\gamma) / \kappa \approx \frac{(p_L + p_R) M_0 x^2}{1 + p_L p_R + x^2}. \quad (12.4.32)$$

## 12.5 Problems for more than 2 Dot-Levels

In section 10.7 we derived the initial conditions for the Liouvillian and the current kernel of a generic QD. Their form is independent of the number of dot levels and contains a nonuniversal term proportional to the high-energy cutoff function  $D$ . For a two-level QD it is easy to prove that this term vanishes exactly. The form of the initial conditions of the vertices [eqs. (11.1.11) and (11.1.12)] is conserved during the RG-flow. The nonuniversal term in the initial condition of  $L$  is proportional to  $G_{12}\tilde{G}_{2\bar{1}}$  which can be evaluated

$$\begin{aligned}
G_{12}\tilde{G}_{2\bar{1}} &= 2G_{12}\tilde{G}_{21} = -4J_{12}^i L_i^2 J_{21}^j (L_j^1 + L_j^3) \\
&= 2i\epsilon_{ijk} J_{12}^i J_{21}^j L_k^3 \\
&= 2i\epsilon_{ijk} J_{12}^j J_{21}^i L_k^3 \\
&= 0,
\end{aligned} \tag{12.5.1}$$

where we exchanged  $1 \leftrightarrow 2$  in the thirdline. Therefore, for a two-level QD the initial conditions are independent of the precise choice of the cutoff function. For more than two levels, this statement does not hold any longer. Generically, we find [Sch11a]

$$\begin{aligned}
\left(G_{12}\tilde{G}_{2\bar{1}}\right)_{s_1 s_2, s_3 s_4} &= 2 \left[ (g_{12})_{s_1 s'} (g_{21})_{s' s_3} \delta_{s_2 s_4} + (g_{12})_{s_1 s_3} (g_{21})_{s_4 s_2} \right. \\
&\quad \left. - (g_{12})_{s_4 s_2} (g_{21})_{s_1 s_3} - (g_{12})_{s' s_2} (g_{21})_{s_4 s'} \delta_{s_1 s_3} \right],
\end{aligned} \tag{12.5.2}$$

where  $s_i$  is an index in the Hilbert dot-space and with eq. (9.2.47)

$$g_{12} = -\frac{1}{D} \sum_{ll'} t_l^1 t_{l'}^{2*} [c_l, c_{l'}^\dagger]. \tag{12.5.3}$$

This yields

$$\begin{aligned}
\left(G_{12}\tilde{G}_{2\bar{1}}\right)_{s_1 s_2, s_3 s_4} &= 8 \left[ \delta_{s_2 s_4} \left( t_{s_3}^1 t_{s_1}^{1*} \sum_l |t_l^2|^2 - t_{s_3}^1 t_{s_1}^{2*} \sum_l t_l^2 t_l^{1*} \right) \right. \\
&\quad \left. - \delta_{s_1 s_3} \left( t_{s_2}^1 t_{s_4}^{1*} \sum_l |t_l^2|^2 - t_{s_2}^1 t_{s_4}^{2*} \sum_l t_l^2 t_l^{1*} \right) \right].
\end{aligned} \tag{12.5.4}$$

Defining the matrix

$$\gamma_{ij} = \sum_1 t_i^1 t_j^{1*} = \gamma_{ji}^*, \quad (12.5.5)$$

$$\gamma_i = \gamma_{ii} = \gamma_i^* \quad (12.5.6)$$

the conditions that the initial conditions of the Liouvillian do not depend on the cutoff function  $D$ , meaning that the term  $G_{12}\tilde{G}_{\bar{2}\bar{1}}$  vanishes, can be written as

$$\gamma_{ij} \sum_k \gamma_k = \sum_k \gamma_{ik} \gamma_{kj} \quad \text{for } i \neq j, \quad (12.5.7)$$

$$(\gamma_i - \gamma_j) \sum_k \gamma_k = \sum_k \gamma_{ik} \gamma_{ki} - \sum_k \gamma_{jk} \gamma_{kj}. \quad (12.5.8)$$

In matrix notation, these read

$$\gamma_{ij} \text{Tr} \gamma = (\gamma^2)_{ij} \quad \text{for } i \neq j, \quad (12.5.9)$$

$$(\gamma_i - \gamma_j) \text{Tr} \gamma = (\gamma^2)_{ii} - (\gamma^2)_{jj}. \quad (12.5.10)$$

Introducing the matrix  $M_{ij} = \gamma_{ij}/\text{Tr} \gamma$ , this matrix has to fulfill

$$\text{Tr} M = 1, \quad (12.5.11)$$

$$M = M^\dagger, \quad (12.5.12)$$

$$M_{ii} > 0, \quad (12.5.13)$$

$$M_{ij} = (M^2)_{ij} \quad \text{for } i \neq j, \quad (12.5.14)$$

$$M_{ii} - (M^2)_{ii} = M_{jj} - (M^2)_{jj} \equiv C \quad \text{independent of } i, j. \quad (12.5.15)$$

A self-adjoint matrix can always be diagonalized. Choosing one eigenvector  $\underline{x}$  with eigenvalue  $\lambda$  we find

$$M_{ii} x_i + \sum_{j \neq i} M_{ij} x_j = \lambda x_i, \quad (12.5.16)$$

$$(M^2)_{ii} x_i + \sum_{j \neq i} (M^2)_{ij} x_j = \lambda^2 x_j. \quad (12.5.17)$$

Taking the difference of these equations and inserting the conditions (12.5.14) and (12.5.15) leads to

$$C = \lambda - \lambda^2 \quad \Rightarrow \quad \lambda = \lambda_{\pm} = \frac{1}{2}(1 \pm \sqrt{1 - 4C}), \quad (12.5.18)$$

where we choose the root  $\sqrt{1-4C} > 0$ . So, the matrix  $M$  can only have the two eigenvalues  $\lambda_{\pm}$ , which occur  $n_{\pm}$  times with  $n_+ + n_- = n$ , where  $n$  is the number of dot-levels. From eq. (12.5.11) we get the condition

$$n_+\lambda_+ + n_-\lambda_- = 1 \quad \Rightarrow \quad \lambda_+ = \frac{1-n_-}{n_+-n_-} = \frac{1}{2}(1 + \sqrt{1-4C}), \quad (12.5.19)$$

such that

$$C = \frac{(n_+-1)(1-n_-)}{(n_+-n_-)^2}. \quad (12.5.20)$$

As we have chosen  $\sqrt{1-4C} > 0$ , only the solutions with  $n_- > n_+$  are allowed. Otherwise, one would get an inconsistency as for  $n_+ \geq n_-$  we find  $\lambda_+ \leq \frac{1}{n} \leq \frac{1}{2}$ .

For  $n_+ = 0$  we get  $\lambda_- = \frac{1}{n}$  and  $M_{ij} = \frac{1}{n}\delta_{ij}$  so that the vectors  $\underline{t}_i$  in reservoir space must be orthogonal to each other.

For  $n_+ = 1$  we find  $C = 0$  such that  $\lambda_+ = 1$  and  $\lambda_- = 0$ . Therefore, we get the solution

$$M_{ij} = (x_+)_i(x_+)_j^*, \quad \sum_i |(x_+)_i|^2 = 1, \quad (12.5.21)$$

where  $\underline{x}_+$  is the eigenvector corresponding to  $\lambda_+$ . To fulfill this condition, the tunneling matrix has to decompose into a part for the reservoir and one for the dot-level  $t_i^1 = a_1 b_i$ . If the QD consists of three or four levels, no additional solutions are possible. To sum up, only for very special points in parameter-space the initial conditions of the Liouvillian and the current kernel do not depend on the high-energy cutoff function. Generically, for three or more levels the precise form of the bandwidth in the reservoirs has to be taken into account and the results are no longer universal.

Additionally, also the proofs that the  $(1_2)$  parts of the Liouvillian and the current kernel are equivalent to their initial conditions with renormalized couplings (11.2.17, 11.2.18) are based on the superoperator-algebra for the two-level QD and therefore this statement could become invalid for more than two levels.

# Chapter 13

## Conclusion and Outlook

### 13.1 Conclusion

In this part of the thesis, we discussed a generic QD coupled to an arbitrary number of noninteracting reservoirs. At first, we were able to show that for the calculation of physical observables local to the dot, namely the dot density matrix and the current, only the hybridization matrix  $\underline{\Gamma}_\alpha$  and not the reservoir density of states and the hopping matrix themselves are important. Thus, we could shift parts of the hopping matrix in the reservoir density of states or vice versa. Therefore, a generic two-level QD can be mapped to the Anderson impurity model with ferromagnetic leads which are characterized by their spin polarizations  $\vec{d}_\alpha$ . Being interested in the Coulomb blockade regime, we performed a standard Schrieffer-Wolff transformation such that the multiple- and the unoccupied dot states are projected out resulting in an effective dot Hamiltonian and an effective dot-reservoir interaction.

Afterwards, we presented the technical details to tackle this model with the RTRG. Starting with the von-Neumann equation, we rephrased the problem in Liouville space and showed that the stationary dot density matrix is given as the eigenvector to the eigenvalue zero of an effective Liouvillian. A perturbative expansion of this Liouvillian in the dot-reservoir interaction leads to logarithmic divergent frequency integrals, such that a RG-treatment becomes necessary. Therefore, we introduced the E-Flow scheme of the RTRG. It relies on the basic idea that the Laplace-variable  $E$  occurs always in combination with the frequencies, such that a second derivative of the Liouvillian with respect to  $E$  can solve the divergency problems of the frequency integrations. We derived the corresponding flow-equations for the Liouvillian and the effective vertex and performed the frequency integrals within those. For those quantities, we considered the weak-coupling regime and solved the flow-equations in the high- and the low-energy regime separately. To compute the stationary current the current kernel is

treated analogously.

In a next step, we compared those solutions with a PMS-approach and find that for a two-level QD the results coincide up to an effective magnetic field, which is only generated in the RTRG-calculations.

Furthermore, we were able to show analytically that for this two-level QD the flow-equations in the high-energy regime agreed with those of the anisotropic Kondo model, whose solutions are known. We clarified that the Kondo model with unpolarized leads is only realized if all spin polarizations of the different reservoirs are equal  $\vec{d}_\alpha = 1/Z_{\text{res}}\vec{d}$ , such that this is generically not the correct fixed point. Exploiting the solution of the anisotropic Kondo model, we could calculate the effective magnetic field generated by the RTRG, the stationary magnetization of the dot and the current. The minimum of the magnetization as a function of the magnetic field in various directions is given by an ellipsoid, which is stretched in the direction of  $\vec{d} = \sum_\alpha \vec{d}_\alpha$ , and the stretching factor relates with the distance of the scaling limit of the model.

Afterwards, we described this results for the special case of two reservoirs coupled to the QD in the scaling limit. The equations for the magnetization and the current simplifies significantly, such that we could present detailed results not only in the golden-rule regime  $h \gg J_z^2 \Lambda_c$  but also in the quantum-interference regime  $h \lesssim J_z^2 \Lambda_c$ . Additionally, we discussed the current for special values of the magnetic field from which one can determine the effective model parameters  $\vec{d}_\alpha$  in experiments.

Last but not least, we also considered the case of more than two dot-levels, where problems of nonuniversal terms generated by the Schrieffer-Wolff transformation arises. Furthermore, it is not clear whether the RTRG- and PMS-results for the Liouvillian and the current still coincide.

## 13.2 Outlook

Here, we will present some open questions arising from this thesis, which could pose avenues of future research.

As mentioned before, the Schrieffer-Wolff transformation of a generic  $Z$ -level QD leads to nonuniversal terms proportional to the high-energy cutoff function  $D$ , which dominates the physics. Therefore, the proceeding presented in this thesis is no longer useful. Probably, for more than two dot-levels, one needs to incorporate the charge fluctuations of the original model and cannot integrate them out in an universal way. C. Lindner follows this line currently.

In this thesis, we considered the weak-coupling regime, meaning that at least one physical scale like the magnetic field or the voltage is much larger than the Kondo temper-



ature, such that the renormalized dot-reservoir couplings stay small until the RG-flow is cut by this scale. It would be of strong interest to extend this to the strong coupling regime and calculate the universal properties of the model. This could perhaps be done in a more refined version of the E-Flow scheme of the RTRG, which was successfully applied to the isotropic Kondo model [Ple12, Rei14]. Also the Keldysh effective action theory seems promising [Smi13a]. Other possible candidates are the density-matrix renormalization group [Sch11b] and QMC [Gul11, Coh13] which could analyze the strong-coupling regime numerically exact and not only perturbatively, but both have their individual problems which have to be solved first. Furthermore, the FRG could tackle this regime from a contrary ansatz, as it is exact in  $\Gamma$ , but perturbatively in the Coulomb interaction  $U$  on the dot.

Finally, we want to emphasize an additional aspect, namely the time-evolution. Here, we focused on the stationary magnetization and current through the dot, but as quantum quenches become more and more of physical interest theoretical and in experiments [Han07, Kin06], also the time evolution into this stationary state is important. The previously mentioned methods could also be useful for this problem. Calculating the transient time-regime within the RTRG should be a straightforward extension of this work. While we only solved the flow-equations for the Laplace-variable  $E = 0$ , one needs to solve them in the complete Laplace-space to determine the time-evolution, which has at least been done for the Kondo model [Rei14]. The FRG has been extended to the transient-time regime by Kennes *et al.* [Ken12] and can again be used as a complementary ansatz.



# Appendix



## Appendix A

# Flow Equations for the Vertices of the Spin-FRG

The final flow equations for  $\Sigma$  and  $\Gamma$ , which are solved numerically, are derived by inserting the parametrizations eq. (5.5.6) and eq. (5.5.7) into the generic flow equations eq. (5.5.2) and eq. (5.5.3). Defining the function

$$P^\Lambda(\omega_1, \omega_2) = \frac{\delta(|\omega_1| - \Lambda)\Theta(|\omega_2| - \Lambda)}{(\omega_1 + i\Sigma^\Lambda(\omega_1))(\omega_2 + i\Sigma^\Lambda(\omega_2))} + i \left( \frac{d}{d\Lambda} \Sigma^\Lambda(\omega_1) \right) \frac{\Theta(|\omega_1| - \Lambda)\Theta(|\omega_2| - \Lambda)}{(\omega_1 + i\Sigma^\Lambda(\omega_1))^2(\omega_2 + i\Sigma^\Lambda(\omega_2))}$$

and using the symmetry relations with respect to the the frequencies  $s$ ,  $t$  and  $u$ , the flow equations read

$$i \frac{d}{d\Lambda} \Sigma^\Lambda(\omega) = \left\{ -2 \sum_j \left[ \Gamma_{d|\vec{i}-\vec{j}|_1}^\Lambda(\omega + \Lambda, 0, \omega - \Lambda) - \Gamma_{d|\vec{i}-\vec{j}|_1}^\Lambda(\omega - \Lambda, 0, \omega + \Lambda) \right] + \Gamma_{z0}^\Lambda(\omega + \Lambda, \omega - \Lambda, 0) - \Gamma_{z0}^\Lambda(\omega - \Lambda, \omega + \Lambda, 0) + 2 \left[ \Gamma_{xy0}^\Lambda(\omega + \Lambda, \omega - \Lambda, 0) - \Gamma_{xy0}^\Lambda(\omega - \Lambda, \omega + \Lambda, 0) \right] + \Gamma_{d0}^\Lambda(\omega + \Lambda, \omega - \Lambda, 0) - \Gamma_{d0}^\Lambda(\omega - \Lambda, \omega + \Lambda, 0) \right\} \frac{1}{2\pi(\Lambda + i\Sigma(\Lambda))},$$

$$\begin{aligned}
 \frac{d}{d\Lambda} \Gamma_{z|\vec{i}-\vec{j}|_1}^\Lambda(s, t, u) = & \frac{1}{2\pi} \int_{-\infty}^{\infty} d\omega' \left\{ \right. \\
 & \left[ -2\Gamma_{xy|\vec{i}-\vec{j}|_1}^\Lambda(s, -\omega_{2'} - \omega', \omega_{1'} + \omega') \Gamma_{xy|\vec{i}-\vec{j}|_1}^\Lambda(s, \omega_2 + \omega', \omega_1 + \omega') \right. \\
 & + \Gamma_{z|\vec{i}-\vec{j}|_1}^\Lambda(s, -\omega_{2'} - \omega', \omega_{1'} + \omega') \Gamma_{d|\vec{i}-\vec{j}|_1}^\Lambda(s, \omega_2 + \omega', \omega_1 + \omega') \\
 & \left. + \Gamma_{d|\vec{i}-\vec{j}|_1}^\Lambda(s, -\omega_{2'} - \omega', \omega_{1'} + \omega') \Gamma_{z|\vec{i}-\vec{j}|_1}^\Lambda(s, \omega_2 + \omega', \omega_1 + \omega') \right] \\
 & \times \left[ P^\Lambda(\omega', \omega' + s) + P^\Lambda(\omega' + s, \omega') \right] \\
 & + \left[ 2 \sum_{\vec{k}} \Gamma_{z|\vec{i}-\vec{k}|_1}^\Lambda(\omega_{1'} + \omega', t, \omega_1 - \omega') \Gamma_{z|\vec{k}-\vec{j}|_1}^\Lambda(\omega_2 + \omega', t, -\omega_{2'} + \omega') \right. \\
 & - \Gamma_{z|\vec{i}-\vec{j}|_1}^\Lambda(\omega_{1'} + \omega', t, \omega_1 - \omega') \Gamma_{z0}^\Lambda(\omega_2 + \omega', -\omega_{2'} + \omega', t) \\
 & + 2\Gamma_{z|\vec{i}-\vec{j}|_1}^\Lambda(\omega_{1'} + \omega', t, \omega_1 - \omega') \Gamma_{xy0}^\Lambda(\omega_2 + \omega', -\omega_{2'} + \omega', t) \\
 & - \Gamma_{z|\vec{i}-\vec{j}|_1}^\Lambda(\omega_{1'} + \omega', t, \omega_1 - \omega') \Gamma_{d0}^\Lambda(\omega_2 + \omega', -\omega_{2'} + \omega', t) \\
 & - \Gamma_{z0}^\Lambda(\omega_{1'} + \omega', \omega_1 - \omega', t) \Gamma_{z|\vec{i}-\vec{j}|_1}^\Lambda(\omega_2 + \omega', t, -\omega_{2'} + \omega') \\
 & + 2\Gamma_{xy0}^\Lambda(\omega_{1'} + \omega', \omega_1 - \omega', t) \Gamma_{z|\vec{i}-\vec{j}|_1}^\Lambda(\omega_2 + \omega', t, -\omega_{2'} + \omega') \\
 & \left. - \Gamma_{d0}^\Lambda(\omega_{1'} + \omega', \omega_1 - \omega', t) \Gamma_{z|\vec{i}-\vec{j}|_1}^\Lambda(\omega_2 + \omega', t, -\omega_{2'} + \omega') \right] \\
 & \times \left[ P^\Lambda(\omega', \omega' + t) + P^\Lambda(\omega' + t, \omega') \right] \\
 & - \left[ 2\Gamma_{xy|\vec{i}-\vec{j}|_1}^\Lambda(\omega_{2'} - \omega', -\omega_1 - \omega', u) \Gamma_{xy|\vec{i}-\vec{j}|_1}^\Lambda(\omega_2 - \omega', \omega_{1'} + \omega', u) \right. \\
 & + \Gamma_{z|\vec{i}-\vec{j}|_1}^\Lambda(\omega_{2'} - \omega', -\omega_1 - \omega', u) \Gamma_{d|\vec{i}-\vec{j}|_1}^\Lambda(\omega_2 - \omega', \omega_{1'} + \omega', u) \\
 & \left. + \Gamma_{d|\vec{i}-\vec{j}|_1}^\Lambda(\omega_{2'} - \omega', -\omega_1 - \omega', u) \Gamma_{z|\vec{i}-\vec{j}|_1}^\Lambda(\omega_2 - \omega', \omega_{1'} + \omega', u) \right] \\
 & \left. \times \left[ P^\Lambda(\omega', \omega' + u) + P^\Lambda(\omega' + u, \omega') \right] \right\},
 \end{aligned}$$

$$\begin{aligned}
\frac{d}{d\Lambda} \Gamma_{xy|\vec{i}-\vec{j}|_1}^\Lambda(s, t, u) &= \frac{1}{2\pi} \int_{-\infty}^{\infty} d\omega' \left\{ \right. \\
&\left[ -\Gamma_{z|\vec{i}-\vec{j}|_1}^\Lambda(s, -\omega_{2'} - \omega', \omega_{1'} + \omega') \Gamma_{xy|\vec{i}-\vec{j}|_1}^\Lambda(s, \omega_2 + \omega', \omega_1 + \omega') \right. \\
&\quad - \Gamma_{xy|\vec{i}-\vec{j}|_1}^\Lambda(s, -\omega_{2'} - \omega', \omega_{1'} + \omega') \Gamma_{z|\vec{i}-\vec{j}|_1}^\Lambda(s, \omega_2 + \omega', \omega_1 + \omega') \\
&\quad + \Gamma_{xy|\vec{i}-\vec{j}|_1}^\Lambda(s, -\omega_{2'} - \omega', \omega_{1'} + \omega') \Gamma_{d|\vec{i}-\vec{j}|_1}^\Lambda(s, \omega_2 + \omega', \omega_1 + \omega') \\
&\quad \left. + \Gamma_{d|\vec{i}-\vec{j}|_1}^\Lambda(s, -\omega_{2'} - \omega', \omega_{1'} + \omega') \Gamma_{xy|\vec{i}-\vec{j}|_1}^\Lambda(s, \omega_2 + \omega', \omega_1 + \omega') \right] \\
&\times \left[ P^\Lambda(\omega', \omega' + s) + P^\Lambda(\omega' + s, \omega') \right] \\
&+ \left[ 2 \sum_{\vec{k}} \Gamma_{xy|\vec{i}-\vec{k}|_1}^\Lambda(\omega_{1'} + \omega', t, \omega_1 - \omega') \Gamma_{xy|\vec{k}-\vec{j}|_1}^\Lambda(\omega_2 + \omega', t, -\omega_{2'} + \omega') \right. \\
&\quad + \Gamma_{xy|\vec{i}-\vec{j}|_1}^\Lambda(\omega_{1'} + \omega', t, \omega_1 - \omega') \Gamma_{z0}^\Lambda(\omega_2 + \omega', -\omega_{2'} + \omega', t) \\
&\quad - \Gamma_{xy|\vec{i}-\vec{j}|_1}^\Lambda(\omega_{1'} + \omega', t, \omega_1 - \omega') \Gamma_{d0}^\Lambda(\omega_2 + \omega', -\omega_{2'} + \omega', t) \\
&\quad + \Gamma_{z0}^\Lambda(\omega_{1'} + \omega', \omega_1 - \omega', t) \Gamma_{xy|\vec{i}-\vec{j}|_1}^\Lambda(\omega_2 + \omega', t, -\omega_{2'} + \omega') \\
&\quad \left. - \Gamma_{d0}^\Lambda(\omega_{1'} + \omega', \omega_1 - \omega', t) \Gamma_{xy|\vec{i}-\vec{j}|_1}^\Lambda(\omega_2 + \omega', t, -\omega_{2'} + \omega') \right] \\
&\times \left[ P^\Lambda(\omega', \omega' + t) + P^\Lambda(\omega' + t, \omega') \right] \\
&- \left[ \Gamma_{z|\vec{i}-\vec{j}|_1}^\Lambda(\omega_{2'} - \omega', -\omega_1 - \omega', u) \Gamma_{xy|\vec{i}-\vec{j}|_1}^\Lambda(\omega_2 - \omega', \omega_{1'} + \omega', u) \right. \\
&\quad + \Gamma_{xy|\vec{i}-\vec{j}|_1}^\Lambda(\omega_{2'} - \omega', -\omega_1 - \omega', u) \Gamma_{z|\vec{i}-\vec{j}|_1}^\Lambda(\omega_2 - \omega', \omega_{1'} + \omega', u) \\
&\quad + \Gamma_{xy|\vec{i}-\vec{j}|_1}^\Lambda(\omega_{2'} - \omega', -\omega_1 - \omega', u) \Gamma_{d|\vec{i}-\vec{j}|_1}^\Lambda(\omega_2 - \omega', \omega_{1'} + \omega', u) \\
&\quad \left. + \Gamma_{d|\vec{i}-\vec{j}|_1}^\Lambda(\omega_{2'} - \omega', -\omega_1 - \omega', u) \Gamma_{xy|\vec{i}-\vec{j}|_1}^\Lambda(\omega_2 - \omega', \omega_{1'} + \omega', u) \right] \\
&\times \left. \left[ P^\Lambda(\omega', \omega' + u) + P^\Lambda(\omega' + u, \omega') \right] \right\},
\end{aligned}$$

$$\begin{aligned}
 \frac{d}{d\Lambda} \Gamma_{d|\vec{i}-\vec{j}|_1}^\Lambda(s, t, u) = & \frac{1}{2\pi} \int_{-\infty}^{\infty} d\omega' \left\{ \right. \\
 & \left[ 2\Gamma_{xy|\vec{i}-\vec{j}|_1}^\Lambda(s, -\omega_{2'} - \omega', \omega_{1'} + \omega') \Gamma_{xy|\vec{i}-\vec{j}|_1}^\Lambda(s, \omega_2 + \omega', \omega_1 + \omega') \right. \\
 & + \Gamma_{z|\vec{i}-\vec{j}|_1}^\Lambda(s, -\omega_{2'} - \omega', \omega_{1'} + \omega') \Gamma_{z|\vec{i}-\vec{j}|_1}^\Lambda(s, \omega_2 + \omega', \omega_1 + \omega') \\
 & \left. + \Gamma_{d|\vec{i}-\vec{j}|_1}^\Lambda(s, -\omega_{2'} - \omega', \omega_{1'} + \omega') \Gamma_{d|\vec{i}-\vec{j}|_1}^\Lambda(s, \omega_2 + \omega', \omega_1 + \omega') \right] \\
 & \times \left[ P^\Lambda(\omega', \omega' + s) + P^\Lambda(\omega' + s, \omega') \right] \\
 & + \left[ 2 \sum_{\vec{k}} \Gamma_{d|\vec{i}-\vec{k}|_1}^\Lambda(\omega_{1'} + \omega', t, \omega_1 - \omega') \Gamma_{d|\vec{k}-\vec{j}|_1}^\Lambda(\omega_2 + \omega', t, -\omega_{2'} + \omega') \right. \\
 & - \Gamma_{d|\vec{i}-\vec{j}|_1}^\Lambda(\omega_{1'} + \omega', t, \omega_1 - \omega') \Gamma_{z0}^\Lambda(\omega_2 + \omega', -\omega_{2'} + \omega', t) \\
 & - 2\Gamma_{d|\vec{i}-\vec{j}|_1}^\Lambda(\omega_{1'} + \omega', t, \omega_1 - \omega') \Gamma_{xy0}^\Lambda(\omega_2 + \omega', -\omega_{2'} + \omega', t) \\
 & - \Gamma_{d|\vec{i}-\vec{j}|_1}^\Lambda(\omega_{1'} + \omega', t, \omega_1 - \omega') \Gamma_{d0}^\Lambda(\omega_2 + \omega', -\omega_{2'} + \omega', t) \\
 & - \Gamma_{z0}^\Lambda(\omega_{1'} + \omega', \omega_1 - \omega', t) \Gamma_{d|\vec{i}-\vec{j}|_1}^\Lambda(\omega_2 + \omega', t, -\omega_{2'} + \omega') \\
 & - 2\Gamma_{xy0}^\Lambda(\omega_{1'} + \omega', \omega_1 - \omega', t) \Gamma_{d|\vec{i}-\vec{j}|_1}^\Lambda(\omega_2 + \omega', t, -\omega_{2'} + \omega') \\
 & \left. - \Gamma_{d0}^\Lambda(\omega_{1'} + \omega', \omega_1 - \omega', t) \Gamma_{d|\vec{i}-\vec{j}|_1}^\Lambda(\omega_2 + \omega', t, -\omega_{2'} + \omega') \right] \\
 & \times \left[ P^\Lambda(\omega', \omega' + t) + P^\Lambda(\omega' + t, \omega') \right] \\
 & - \left[ 2\Gamma_{xy|\vec{i}-\vec{j}|_1}^\Lambda(\omega_{2'} - \omega', -\omega_1 - \omega', u) \Gamma_{xy|\vec{i}-\vec{j}|_1}^\Lambda(\omega_2 - \omega', \omega_{1'} + \omega', u) \right. \\
 & + \Gamma_{z|\vec{i}-\vec{j}|_1}^\Lambda(\omega_{2'} - \omega', -\omega_1 - \omega', u) \Gamma_{z|\vec{i}-\vec{j}|_1}^\Lambda(\omega_2 - \omega', \omega_{1'} + \omega', u) \\
 & \left. + \Gamma_{d|\vec{i}-\vec{j}|_1}^\Lambda(\omega_{2'} - \omega', -\omega_1 - \omega', u) \Gamma_{d|\vec{i}-\vec{j}|_1}^\Lambda(\omega_2 - \omega', \omega_{1'} + \omega', u) \right] \\
 & \left. \times \left[ P^\Lambda(\omega', \omega' + u) + P^\Lambda(\omega' + u, \omega') \right] \right\}.
 \end{aligned}$$

For completeness, the initial conditions are again mentioned

$$\begin{aligned}
 \Sigma^{\Lambda=\infty}(\omega) &= 0, \\
 \Gamma_{z|\vec{i}-\vec{j}|_1}^{\Lambda=\infty}(s, t, u) &= \frac{\Delta}{4} J_{|\vec{i}-\vec{j}|_1}, \\
 \Gamma_{xy|\vec{i}-\vec{j}|_1}^{\Lambda=\infty}(s, t, u) &= \frac{1}{4} J_{|\vec{i}-\vec{j}|_1}, \\
 \Gamma_{d|\vec{i}-\vec{j}|_1}^{\Lambda=\infty}(s, t, u) &= 0.
 \end{aligned}$$



## Appendix B

# Liouville Algebra and Useful Relations

### B.1 Superoperator Basis for the 2-Level Quantum Dot

The local Hamiltonian of the 2-level QD described in chapter (9) is given by a product of an effective magnetic field times a spin-1/2-operator (see eq. (9.2.43)). Thus, the basis of the dot Liouville space is spanned by the superoperators  $\underline{L}^+$  and  $\underline{L}^-$  with

$$\underline{L}^+ b = \underline{S} b, \quad \underline{L}^- b = -b \underline{S}, \quad (\text{B.1.1})$$

according to the left and right acting spin-operator  $\underline{S}$  on some arbitrary operator  $b$ . Furthermore, we define the scalar basis superoperators

$$L^a = \frac{3}{4} \mathbb{1} + \underline{L}^+ \cdot \underline{L}^-, \quad (\text{B.1.2})$$

$$L^b = \frac{1}{4} \mathbb{1} - \underline{L}^+ \cdot \underline{L}^-, \quad (\text{B.1.3})$$

the vector basis superoperators

$$\underline{L}^1 = \frac{1}{2} (\underline{L}^+ - \underline{L}^- - 2i \underline{L}^+ \times \underline{L}^-), \quad (\text{B.1.4})$$

$$\underline{L}^2 = -\frac{1}{2} (\underline{L}^+ + \underline{L}^-), \quad (\text{B.1.5})$$

$$\underline{L}^3 = \frac{1}{2} (\underline{L}^+ - \underline{L}^- + 2i \underline{L}^+ \times \underline{L}^-), \quad (\text{B.1.6})$$

and the symmetric tensor superoperator

$$T^{ij} = L_i^3 L_j^1 + L_j^3 L_i^1 - 2\delta_{ij} L^a. \quad (\text{B.1.7})$$

With the additional relation  $\sum_i T^{ii} = -4L^a$ , we have a complete basis set of superoperators for the four dimensional Liouville space.

The bare dot Liouvillian after the Schrieffer-Wolff transformation can be deduced from eq. (9.2.43) and is given in this basis by

$$L_D^{(0)} = -2\vec{h}_{\text{eff}} \cdot \underline{L}^2 \quad (\text{B.1.8})$$

## B.2 Superoperator Algebra

All products of  $L^{a,b}$  and components of  $\underline{L}^{1,2,3}$  are summarized in the following table, where the row and the column correspond to the first and second factor of the product, respectively:

	$L^a$	$L^b$	$L_j^1$	$L_j^2$	$L_j^3$	
$L^a$	$L^a$	0	0	$L_j^2$	$L_j^3$	
$L^b$	0	$L^b$	$L_j^1$	0	0	
$L_i^1$	$L_i^1$	0	0	$-\frac{i}{2}\epsilon_{ijk}L_k^1$	$\delta_{ij}L^b$	
$L_i^2$	$L_i^2$	0	0	$-\frac{i}{4}\epsilon_{ijk}L_k^2 - \frac{1}{8}T^{ij}$	$-\frac{i}{2}\epsilon_{ijk}L_k^3$	
$L_i^3$	0	$L_i^3$	$-i\epsilon_{ijk}L_k^2 + \frac{1}{2}T^{ij} + \delta_{ij}L^a$	0	0	(B.2.1)

Multiplying the superoperator  $T^{ij}$  with another superoperator from the right yields

$$T^{ij}L^a = T^{ij}, \quad (\text{B.2.2})$$

$$T^{ij}L^b = 0, \quad (\text{B.2.3})$$

$$T^{ij}L_k^1 = 0, \quad (\text{B.2.4})$$

$$T^{ij}L_k^2 = -\delta_{ij}L_k^2 - \frac{1}{2}\delta_{ik}L_j^2 - \frac{1}{2}\delta_{jk}L_i^2 - \frac{i}{4}(\epsilon_{jkm}T^{im} + \epsilon_{ikm}T^{jm}), \quad (\text{B.2.5})$$

$$T^{ij}L_k^3 = \delta_{jk}L_i^3 + \delta_{ik}L_j^3 - 2\delta_{ij}L_k^3, \quad (\text{B.2.6})$$

and multiplying  $T^{ij}$  with another superoperator from the left yields

$$L^aT^{ij} = T^{ij}, \quad (\text{B.2.7})$$

$$L^bT^{ij} = 0, \quad (\text{B.2.8})$$

$$L_i^1T^{jk} = \delta_{ij}L_k^1 + \delta_{ik}L_j^1 - 2\delta_{jk}L_i^1, \quad (\text{B.2.9})$$

$$L_i^2T^{jk} = -\delta_{jk}L_i^2 - \frac{1}{2}\delta_{ik}L_j^2 - \frac{1}{2}\delta_{ij}L_k^2 - \frac{i}{4}(\epsilon_{ijm}T^{mk} + \epsilon_{ikm}T^{mj}), \quad (\text{B.2.10})$$

$$L_i^3T^{jk} = 0. \quad (\text{B.2.11})$$

The product of two components  $T^{ij}$  and  $T^{jk}$  reads

$$\begin{aligned} T^{ij}T^{kl} &= -i(\delta_{jk}\epsilon_{ilm} + \delta_{jl}\epsilon_{ikm} + \delta_{ik}\epsilon_{jlm} + \delta_{il}\epsilon_{jkm})L_m^2 \\ &+ \left( \frac{1}{2}\delta_{jk}T^{il} + \frac{1}{2}\delta_{jl}T^{ik} + \frac{1}{2}\delta_{ik}T^{jl} + \frac{1}{2}\delta_{il}T^{jk} - 2\delta_{ij}T^{kl} - 2\delta_{kl}T^{ij} \right) \\ &+ 2(\delta_{jk}\delta_{il} + \delta_{ik}\delta_{jl} - 2\delta_{ij}\delta_{kl})L^a. \end{aligned} \quad (\text{B.2.12})$$

### B.3 Spectral Decomposition of the Bare Liouvillian

The bare Liouvillian is given by

$$L_{\Delta}^{(0)} = -2\vec{h} \cdot \underline{L}^2, \quad (\text{B.3.1})$$

with some effective magnetic field  $\vec{h} = h\vec{\phi}$ . The eigenvalues read

$$\lambda_{1,2} = 0, \quad (\text{B.3.2})$$

$$\lambda_3 = h, \quad (\text{B.3.3})$$

$$\lambda_4 = -h, \quad (\text{B.3.4})$$

with the projection operators

$$P_1 = L^b, \quad (\text{B.3.5})$$

$$P_2 = L^a + \frac{1}{2}\phi_i\phi_jT^{ij}, \quad (\text{B.3.6})$$

$$P_{3,4} = \mp \phi_iL_i^2 - \frac{1}{4}\phi_i\phi_jT^{ij}. \quad (\text{B.3.7})$$

With this decomposition, we can rewrite any function  $f$  as

$$\begin{aligned} f(\mu_{\alpha\alpha'} - L_{\Delta}^{(0)}) &= f(\mu_{\alpha\alpha'})1 \\ &+ [f(\mu_{\alpha\alpha'} + h) - f(\mu_{\alpha\alpha'} - h)]\phi_iL_i^2 \\ &- \frac{1}{4}[f(\mu_{\alpha\alpha'} + h) + f(\mu_{\alpha\alpha'} - h) - 2f(\mu_{\alpha\alpha'})]\phi_i\phi_jT^{ij} \end{aligned} \quad (\text{B.3.8})$$

which is helpful to perform the superoperator products in eqs. (12.3.4) and (12.3.5).

## B.4 Useful Relations

In this part of the appendix, we mention some useful relations for the vertices and the Liouvillian, which has been proven, e.g., in Ref. [Rei09]. For any superoperator  $A$ , we first define the  $c$ -transform

$$(A^c)_{ss',\bar{s}\bar{s}'} = A_{s's,\bar{s}'\bar{s}}^*. \quad (\text{B.4.1})$$

The list of the relations is then given by

$$G_{11'}(E) = -G_{1'1}(E), \quad (\text{B.4.2})$$

$$I_{11'}^\gamma(E) = -I_{1'1}^\gamma(E), \quad (\text{B.4.3})$$

$$\text{Tr}_D \{L_D^{\text{eff}}(E)b\} = 0, \quad (\text{B.4.4})$$

$$\text{Tr}_D \{G_{11'}b\} = 0, \quad (\text{B.4.5})$$

$$[L_D^{\text{eff}}(E)]^c = -L_D^{\text{eff}}(-E^*), \quad (\text{B.4.6})$$

$$[\Sigma^\gamma(E)]^c = -\Sigma^\gamma(-E^*), \quad (\text{B.4.7})$$

$$[G_{11'}(E)]^c = -G_{\bar{1}'\bar{1}}(-E^*), \quad (\text{B.4.8})$$

$$[I_{11'}^\gamma(E)]^c = -I_{\bar{1}'\bar{1}}^\gamma(-E^*), \quad (\text{B.4.9})$$

with

$$1 \equiv \eta\alpha\sigma\omega, \quad 1' \equiv \eta'\alpha'\sigma'\omega' \quad (\text{B.4.10})$$

which are preserved under the RG-flow.

# Supplements



# Bibliography

- [Abr65] A. Abrisokov. *Electron scattering on magnetic impurities in metals and anomalous resistivity effects*. Physics, **2** 5 (1965).
- [Ale05] F. Alet, S. Wessel and M. Troyer. *Generalized directed loop method for quantum monte carlo simulations*. Phys. Rev. E, **71** 036706 (2005).
- [And52] P. W. Anderson. *An approximate quantum theory of the antiferromagnetic ground state*. Phys. Rev., **86** 694 (1952).
- [And70] P. W. Anderson. *A poor man's derivation of scaling laws for the kondo problem*. Journal of Physics C: Solid State Physics, **3** 2436 (1970).
- [And04] S. Andergassen, T. Enss, V. Meden, W. Metzner, U. Schollwöck and K. Schönhammer. *Functional renormalization group for luttinger liquids with impurities*. Phys. Rev. B, **70** 075102 (2004).
- [And10] S. Andergassen, V. Meden, H. Schoeller, J. Splettstoesser and M. R. Wegewijs. *Charge transport through single molecules, quantum dots and quantum wires*. Nanotechnology, **21** 272001 (2010).
- [Ass08] F. Assaad and H. Evertz. *World-line and determinantal quantum monte carlo methods for spins, phonons and electrons*. In H. Fehske, R. Schneider and A. Weiße (eds.), *Computational Many-Particle Physics*, volume 739 of *Lecture Notes in Physics*, 277–356. Springer Berlin Heidelberg (2008).
- [Bal10] L. Balents. *Spin liquids in frustrated magnets*. Nature, **464** 199 (2010).
- [Bed86] J. G. Bednorz and K. A. Müller. *Possible high  $t_c$  superconductivity in the ba-la-cu-o system*. Zeitschrift für Physik B Condensed Matter, **64** 189 (1986).
- [Bet31] H. Bethe. *Zur theorie der metalle*. Zeitschrift für Physik, **71** 205 (1931).
- [Bin81] K. Binder. *Finite size scaling analysis of ising model block distribution functions*. Zeitschrift für Physik B Condensed Matter, **43** 119 (1981).

- [Blo08] I. Bloch, J. Dalibard and W. Zwerger. *Many-body physics with ultracold gases*. Rev. Mod. Phys., **80** 885 (2008).
- [Boe01] D. Boese, W. Hofstetter and H. Schoeller. *Interference and interaction effects in multilevel quantum dots*. Phys. Rev. B, **64** 125309 (2001).
- [Boe02] D. Boese, W. Hofstetter and H. Schoeller. *Interference in interacting quantum dots with spin*. Phys. Rev. B, **66** 125315 (2002).
- [Boh51] D. Bohm and D. Pines. *A collective description of electron interactions. i. magnetic interactions*. Phys. Rev., **82** 625 (1951).
- [Boh53] D. Bohm and D. Pines. *A collective description of electron interactions: Iii. coulomb interactions in a degenerate electron gas*. Phys. Rev., **92** 609 (1953).
- [Bra04] M. Braun, J. König and J. Martinek. *Theory of transport through quantum-dot spin valves in the weak-coupling regime*. Phys. Rev. B, **70** 195345 (2004).
- [Bri05] J. Brinckmann and P. Wölfle. *Description of magnetic short-range order in the 2d heisenberg model: Auxiliary fermions with reduced self-consistency*. Physica B: Condensed Matter, **359–361** 798 (2005). Proceedings of the International Conference on Strongly Correlated Electron Systems.
- [Bru04] H. Bruus and K. Flensberg. *Many-Body Quantum Theory in Condensed Matter Physics*. Oxford Graduate Texts (2004).
- [Chu87] C. W. Chu, P. H. Hor, R. L. Meng, L. Gao, Z. J. Huang and Y. Q. Wang. *Evidence for superconductivity above 40 k in the la-ba-cu-o compound system*. Phys. Rev. Lett., **58** 405 (1987).
- [Coh13] G. Cohen, E. Gull, D. R. Reichman, A. J. Millis and E. Rabani. *Numerically exact long-time magnetization dynamics at the nonequilibrium kondo crossover of the anderson impurity model*. Phys. Rev. B, **87** 195108 (2013).
- [Cos94] T. A. Costi, A. C. Hewson and V. Zlatic. *Transport coefficients of the anderson model via the numerical renormalization group*. Journal of Physics: Condensed Matter, **6** 2519 (1994).
- [Cra04] N. J. Craig, J. M. Taylor, E. A. Lester, C. M. Marcus, M. P. Hanson and A. C. Gossard. *Tunable nonlocal spin control in a coupled-quantum dot system*. Science, **304** 565 (2004).



- 
- [Cro98] S. M. Cronenwett, T. H. Oosterkamp and L. P. Kouwenhoven. *A tunable kondo effect in quantum dots*. Science, **281** 540 (1998).
- [Cuc03] A. Cuccoli, T. Roscilde, V. Tognetti, R. Vaia and P. Verrucchi. *Quantum monte carlo study of  $s = \frac{1}{2}$  weakly anisotropic antiferromagnets on the square lattice*. Phys. Rev. B, **67** 104414 (2003).
- [Dan84] P. Danielewicz. *Quantum theory of nonequilibrium processes*. Ann. Phys. (N.Y.), **152** 239 (1984).
- [Dua03] L.-M. Duan, E. Demler and M. D. Lukin. *Controlling spin exchange interactions of ultracold atoms in optical lattices*. Phys. Rev. Lett., **91** 090402 (2003).
- [Eck10] J. Eckel, F. Heidrich-Meisner, S. G. Jakobs, M. Thorwart, M. Pletyukhov and R. Egger. *Comparative study of theoretical methods for non-equilibrium quantum transport*. New Journal of Physics, **12** 043042 (2010).
- [Ens05] T. Enss. *Renormalization, conservation laws and transport in correlated electron systems*. Ph.D. thesis, Universität Stuttgart (2005).
- [Far04] D. Farnell and R. Bishop. *Quantum Magnetism*. Lecture Notes in Physics Vol. 645. Springer (2004).
- [Fri10] P. Fritsch and S. Kehrein. *Nonequilibrium kondo model with voltage bias in a magnetic field*. Phys. Rev. B, **81** 035113 (2010).
- [GG98a] D. Goldhaber-Gordon, J. Göres, M. A. Kastner, H. Shtrikman, D. Mahalu and U. Meirav. *From the kondo regime to the mixed-valence regime in a single-electron transistor*. Phys. Rev. Lett., **81** 5225 (1998).
- [GG98b] D. Goldhaber-Gordon, H. Shtrikman, D. Mahalu, D. Abusch-Magder, U. Meirav and M. Kastner. *Kondo effect in a single-electron transistor*. Nature, **391** 156 (1998).
- [Gia03] T. Giamarchi. *Quantum Physics in One Dimension*. Oxford University Press (2003).
- [Gl93] S. D. Glazek and K. G. Wilson. *Renormalization of hamiltonians*. Phys. Rev. D, **48** 5863 (1993).
- [Gla88] L. I. Glazman and M. E. Raikh. *Resonant kondo transparency of a barrier with quasilocal impurity states*. Sov. Phys. JETP Lett., **47** 452 (1988).

- [Gla94] S. D. Glazek and K. G. Wilson. *Perturbative renormalization group for hamiltonians*. Phys. Rev. D, **49** 4214 (1994).
- [Gla05] L. I. Glazman and M. Pustilnik. *Nanophysics: Coherence and Transport*. Elsevier (2005).
- [Gul11] E. Gull, A. J. Millis, A. I. Lichtenstein, A. N. Rubtsov, M. Troyer and P. Werner. *Continuous-time monte carlo methods for quantum impurity models*. Rev. Mod. Phys., **83** 349 (2011).
- [Gö11] S. Göttel. *Funktionale Renormierungsgruppe für Spinketten*. Master's thesis, RWTH Aachen (2011).
- [Gö12] S. Göttel, S. Andergassen, C. Honerkamp, D. Schuricht and S. Wessel. *Critical scales in anisotropic spin systems from functional renormalization*. Phys. Rev. B, **85** 214406 (2012).
- [Gö15a] S. Göttel, F. Reininghaus and H. Schoeller. *The generic fixed point model for pseudo-spin-1/2 quantum dots in nonequilibrium: Spin-valve systems with compensating spin polarizations*. (Submitted to Phys. Rev. Lett.) ArXiv e-prints, 1411.4460 (2015).
- [Gö15b] S. Göttel, F. Reininghaus and H. Schoeller. *Nonequilibrium renormalization group for generic pseudo-spin-1/2 quantum dots in the coulomb blockade regime*. in preparation (2015).
- [Hal78] F. D. M. Haldane. *Scaling theory of the asymmetric anderson model*. Phys. Rev. Lett., **40** 416 (1978).
- [Han07] R. Hanson, L. Kouwenhoven, J. Petta, S. Tarucha and L. Vandersypen. *Spins in few-electron quantum dots*. Rev. Mod. Phys., **79** 1217 (2007).
- [Hau08] H. Haug and A.-P. Jauho. *Quantum Kinetics in Transport and Optics of Semiconductors*. Springer (2008).
- [Hei28] W. Heisenberg. *Zur theorie des ferromagnetismus*. Zeitschrift für Physik, **49** 619 (1928).
- [Hew93] A. Hewson. *The Kondo Problem to Heavy Fermions*. Cambridge University Press, Cambridge (1993).
- [Hö12a] C. B. M. Högig and D. Schuricht. *Transport properties of a multichannel kondo dot in a magnetic field*. Phys. Rev. B, **85** 134413 (2012).

- 
- [Hö12b] C. B. M. Hög, D. Schuricht and S. Andergassen. *Renormalization group analysis of a spin-1 kondo dot: Nonequilibrium transport and relaxation dynamics*. Phys. Rev. B, **85** 054418 (2012).
- [Hö14] C. B. M. Hög, C. Mora and D. Schuricht. *Transport properties of fully screened kondo models*. Phys. Rev. B, **89** 165411 (2014).
- [Jak03] S. Jakobs. *Renormierungsgruppen-Methoden für nichtlinearen Transport*. Master's thesis, RWTH Aachen (2003).
- [Jak07] S. G. Jakobs, V. Meden and H. Schoeller. *Nonequilibrium functional renormalization group for interacting quantum systems*. Phys. Rev. Lett., **99** 150603 (2007).
- [Jak10a] S. Jakobs. *Functional renormalization group studies of quantum transport through mesoscopic systems*. Ph.D. thesis, RWTH Aachen (2010).
- [Jak10b] S. G. Jakobs, M. Pletyukhov and H. Schoeller. *Nonequilibrium functional renormalization group with frequency-dependent vertex function: A study of the single-impurity anderson model*. Phys. Rev. B, **81** 195109 (2010).
- [Kar10] C. Karrasch, M. Pletyukhov, L. Borda and V. Meden. *Functional renormalization group study of the interacting resonant level model in and out of equilibrium*. Phys. Rev. B, **81** 125122 (2010).
- [Kas07] V. Kashcheyevs, A. Schiller, A. Aharony and O. Entin-Wohlman. *Unified description of phase lapses, population inversion, and correlation-induced resonances in double quantum dots*. Phys. Rev. B, **75** 115313 (2007).
- [Kas13] O. Kashuba and H. Schoeller. *Transient dynamics of open quantum systems*. Phys. Rev. B, **87** 201402 (2013).
- [Kat04] A. A. Katanin. *Fulfillment of ward identities in the functional renormalization group approach*. Phys. Rev. B, **70** 115109 (2004).
- [Keh05] S. Kehrein. *Scaling and decoherence in the nonequilibrium kondo model*. Phys. Rev. Lett., **95** 056602 (2005).
- [Kel75] L. Keldysh. *Diagram technique for nonequilibrium processes*. Sov. Phys. JETP, **41** 960 (1975).
- [Ken12] D. M. Kennes, S. Jakobs, C. Karrasch and V. Meden. *Renormalization group approach to time-dependent transport through correlated quantum dots*. Phys. Rev. B, **85** 085113 (2012).

- [Ken13] D. M. Kennes, O. Kashuba, M. Pletyukhov, H. Schoeller and V. Meden. *Oscillatory dynamics and non-markovian memory in dissipative quantum systems*. Phys. Rev. Lett., **110** 100405 (2013).
- [Kin06] T. Kinoshita, T. Wenger and D. S. Weiss. *A quantum newton's cradle*. Nature, **440** 900 (2006).
- [Klo13] O. Klochan, A. P. Micolich, A. R. Hamilton, D. Reuter, A. D. Wieck, F. Reininghaus, M. Pletyukhov and H. Schoeller. *Scaling of the kondo zero-bias peak in a hole quantum dot at finite temperatures*. Phys. Rev. B, **87** 201104 (2013).
- [Kor07] T. Korb, F. Reininghaus, H. Schoeller and J. König. *Real-time renormalization group and cutoff scales in nonequilibrium applied to an arbitrary quantum dot in the coulomb blockade regime*. Phys. Rev. B, **76** 165316 (2007).
- [Kre12] A. V. Kretinin, H. Shtrikman and D. Mahalu. *Universal line shape of the kondo zero-bias anomaly in a quantum dot*. Phys. Rev. B, **85** 201301 (2012).
- [Kuk03] A. B. Kuklov and B. V. Svistunov. *Counterflow superfluidity of two-species ultracold atoms in a commensurate optical lattice*. Phys. Rev. Lett., **90** 100401 (2003).
- [Kö03] J. König and J. Martinek. *Interaction-driven spin precession in quantum-dot spin valves*. Phys. Rev. Lett., **90** 166602 (2003).
- [Man91] E. Manousakis. *The spin-1/2 heisenberg antiferromagnet on a square lattice and its application to the cuprous oxides*. Rev. Mod. Phys., **63** 1 (1991).
- [Mar03a] J. Martinek, M. Sindel, L. Borda, J. Barnaś, J. König, G. Schön and J. von Delft. *Kondo effect in the presence of itinerant-electron ferromagnetism studied with the numerical renormalization group method*. Phys. Rev. Lett., **91** 247202 (2003).
- [Mar03b] J. Martinek, Y. Utsumi, H. Imamura, J. Barnaś, S. Maekawa, J. König and G. Schön. *Kondo effect in quantum dots coupled to ferromagnetic leads*. Phys. Rev. Lett., **91** 127203 (2003).
- [Mer66] N. D. Mermin and H. Wagner. *Absence of ferromagnetism or antiferromagnetism in one- or two-dimensional isotropic heisenberg models*. Phys. Rev. Lett., **17** 1133 (1966).
- [Met98] W. Metzner, C. Castellani and C. Di Castro. *Fermi systems with strong forward scattering*. Adv. Phys., **47** 317 (1998).

- 
- [Met12] W. Metzner, M. Salmhofer, C. Honerkamp, V. Meden and K. Schönhammer. *Functional renormalization group approach to correlated fermion systems*. Rev. Mod. Phys., **84** 299 (2012).
- [Mis05] G. Misguich, C. Lhuillier and H. Diep. *Frustrated spin systems*. World Scientific Singapore (2005).
- [Neg88] J. Negele and H. Orland. *Quantum Many-Particle Systems*. Addison-Wesley (1988).
- [Ng88] T. K. Ng and P. A. Lee. *On-site coulomb repulsion and resonant tunneling*. Phys. Rev. Lett., **61** 1768 (1988).
- [Ons44] L. Onsager. *Crystal statistics. i. a two-dimensional model with an order-disorder transition*. Phys. Rev., **65** 117 (1944).
- [Paa10] J. Paaske, A. Andersen and K. Flensberg. *Exchange cotunneling through quantum dots with spin-orbit coupling*. Phys. Rev. B, **82** 081309 (2010).
- [Pet04] J. R. Petta, A. C. Johnson, C. M. Marcus, M. P. Hanson and A. C. Gossard. *Manipulation of a single charge in a double quantum dot*. Phys. Rev. Lett., **93** 186802 (2004).
- [Pet05] J. R. Petta, A. C. Johnson, J. M. Taylor, E. A. Laird, A. Yacoby, M. D. Lukin, C. M. Marcus, M. P. Hanson and A. C. Gossard. *Coherent manipulation of coupled electron spins in semiconductor quantum dots*. Science, **309** 2180 (2005).
- [Pin52] D. Pines and D. Bohm. *A collective description of electron interactions: Ii. collective vs individual particle aspects of the interactions*. Phys. Rev., **85** 338 (1952).
- [Pla12] J. Pla, K. Tan, J. Dehollain, W. Lim, J. Morton, D. Jamieson, A. Dzurak and A. Morello. *A single-atom electron spin qubit in silico*. Nature, **489** 541 (2012).
- [Ple10] M. Pletyukhov, D. Schuricht and H. Schoeller. *Relaxation versus decoherence: Spin and current dynamics in the anisotropic kondo model at finite bias and magnetic field*. Phys. Rev. Lett., **104** 106801 (2010).
- [Ple11] M. Pletyukhov and D. Schuricht. *Nonequilibrium transport through quantum dots with dzyaloshinsky-moriya-kondo interaction*. Phys. Rev. B, **84** 041309 (2011).

- [Ple12] M. Pletyukhov and H. Schoeller. *Nonequilibrium kondo model: Crossover from weak to strong coupling*. Phys. Rev. Lett., **108** 260601 (2012).
- [Pol84] J. Polchinski. *Renormalization and effective lagrangians*. Nuclear Physics B, **231** 269 (1984).
- [Pol87] E. Pollock and D. Ceperley. *Path-integral computation of superfluid densities*. Phys. Rev. B, **36** 8343 (1987).
- [Pop88] V. Popov and S. Fedotov. *The functional-integration method and diagram technique for spin systems*. Sov. Phys. JETP, **67** 535 (1988).
- [Ram86] J. Rammer and H. Smith. *Quantum field-theoretical methods in transport theory of metals*. Rev. Mod. Phys., **58** 323 (1986).
- [Rei09] F. Reininghaus. *Decoherence Effects in Nonequilibrium Transport Through Mesoscopic Systems*. Ph.D. thesis, RWTH Aachen (2009).
- [Rei14] F. Reininghaus, M. Pletyukhov and H. Schoeller. *Kondo model in nonequilibrium: Interplay between voltage, temperature, and crossover from weak to strong coupling*. Phys. Rev. B, **90** 085121 (2014).
- [Reu10] J. Reuther and P. Wölfle.  *$j_1 - j_2$  frustrated two-dimensional heisenberg model: Random phase approximation and functional renormalization group*. Phys. Rev. B, **81** 144410 (2010).
- [Reu11a] J. Reuther. *Frustrated Quantum Heisenberg Antiferromagnets: Functional Renormalization-Group Approach in Auxiliary-Fermion Representation*. Ph.D. thesis, Universität Karlsruhe (2011).
- [Reu11b] J. Reuther, D. A. Abanin and R. Thomale. *Magnetic order and paramagnetic phases in the quantum  $J_1$ - $J_2$ - $J_3$  honeycomb model*. Phys. Rev. B, **84** 014417 (2011).
- [Reu11c] J. Reuther and R. Thomale. *Functional renormalization group for the anisotropic triangular antiferromagnet*. Phys. Rev. B, **83** 024402 (2011).
- [Reu11d] J. Reuther, R. Thomale and S. Trebst. *Finite-temperature phase diagram of the heisenberg-kitaev model*. Phys. Rev. B, **84** 100406 (2011).
- [Reu11e] J. Reuther, P. Wölfle, R. Darradi, W. Brenig, M. Arlego and J. Richter. *Quantum phases of the planar antiferromagnetic  $j_1 - j_2 - j_3$  heisenberg model*. Phys. Rev. B, **83** 064416 (2011).

- 
- [Ros01] A. Rosch, J. Kroha and P. Wölfle. *Kondo effect in quantum dots at high voltage: Universality and scaling*. Phys. Rev. Lett., **87** 156802 (2001).
- [Ros03] A. Rosch, J. Paaske, J. Kroha and P. Wölfle. *Nonequilibrium transport through a kondo dot in a magnetic field: Perturbation theory and poor man's scaling*. Phys. Rev. Lett., **90** 076804 (2003).
- [Sac99] S. Sachdev. *Quantum Phase Transitions*. Cambridge University Press (1999).
- [Sal01] M. Salmhofer and C. Honerkamp. *Fermionic renormalization group flows*. Progress of Theoretical Physics, **105** 1 (2001).
- [San99] A. Sandvik. *Stochastic series expansion method with operator-loop update*. Phys. Rev. B, **59** R14157 (1999).
- [Sch66] J. R. Schrieffer and P. A. Wolff. *Relation between the anderson and kondo hamiltonians*. Phys. Rev., **149** 491 (1966).
- [Sch05] F. Schütz, L. Bartosch and P. Kopietz. *Collective fields in the functional renormalization group for fermions, ward identities, and the exact solution of the tomonaga-luttinger model*. Phys. Rev. B, **72** 035107 (2005).
- [Sch09a] H. Schoeller. *Lecture: Quantum theory of condensed matter 1*. RWTH Aachen (2009).
- [Sch09b] H. Schoeller. *A perturbative nonequilibrium renormalization group method for dissipative quantum mechanics*. The European Physical Journal Special Topics, **168** 179 (2009).
- [Sch09c] H. Schoeller and F. Reininghaus. *Real-time renormalization group in frequency space: A two-loop analysis of the nonequilibrium anisotropic kondo model at finite magnetic field*. Phys. Rev. B, **80** 045117 (2009).
- [Sch11a] H. Schoeller. *Lecture: Quantum statistics in nonequilibrium*. RWTH Aachen (2011).
- [Sch11b] U. Schollwöck. *The density-matrix renormalization group in the age of matrix product states*. Annals of Physics, **326** 96 (2011). January 2011 Special Issue.
- [Sha94] R. Shankar. *Renormalization-group approach to interacting fermions*. Rev. Mod. Phys., **66** 129 (1994).

- [Sim99] F. Simmel, R. H. Blick, J. P. Kotthaus, W. Wegscheider and M. Bichler. *Anomalous kondo effect in a quantum dot at nonzero bias*. Phys. Rev. Lett., **83** 804 (1999).
- [Sin07] M. Sindel, L. Borda, J. Martinek, R. Bulla, J. König, G. Schön, S. Maekawa and J. von Delft. *Kondo quantum dot coupled to ferromagnetic leads: Numerical renormalization group study*. Phys. Rev. B, **76** 045321 (2007).
- [Sin12] Y. Singh, S. Manni, J. Reuther, T. Berlijn, R. Thomale, W. Ku, S. Trebst and P. Gegenwart. *Relevance of the heisenberg-kitaev model for the honeycomb lattice iridates  $A_2\text{IrO}_3$* . Phys. Rev. Lett., **108** 127203 (2012).
- [Smi13a] S. Smirnov and M. Grifoni. *Keldysh effective action theory for universal physics in spin- $\frac{1}{2}$  kondo dots*. Phys. Rev. B, **87** 121302 (2013).
- [Smi13b] S. Smirnov and M. Grifoni. *Nonequilibrium kondo transport through a quantum dot in a magnetic field*. New Journal of Physics, **15** 073047 (2013).
- [Syl02] O. Syljuåsen and A. Sandvik. *Quantum monte carlo with directed loops*. Phys. Rev. E, **66** 046701 (2002).
- [Sä11] K. Sääskilähti. *Application of functional renormalization group on quantum spin chains*. Master's thesis, Aalto University - School of Science, Helsinki (2011).
- [S679] J. Sólyom. *The fermi gas model of one-dimensional conductors*. Advances in Physics, **28** 201 (1979).
- [vdW00] W. G. van der Wiel, S. D. Franceschi, T. Fujisawa, J. M. Elzerman, S. Tarucha and L. P. Kouwenhoven. *The kondo effect in the unitary limit*. Science, **289** 2105 (2000).
- [War50] J. C. Ward. *An identity in quantum electrodynamics*. Phys. Rev., **78** 182 (1950).
- [Weg00] F. Wegner. *Flow equations for hamiltonians*. In B. Kramer (ed.), *Advances in Solid State Physics 40*, volume 40 of *Advances in Solid State Physics*, 133–142. Springer Berlin Heidelberg (2000).
- [Wet93] C. Wetterich. *Exact evolution equation for the effective potential*. Physics Letters B, **301** 90 (1993).



- [Wey07] I. Weymann and J. Barnaś. *Cotunneling through quantum dots coupled to magnetic leads: Zero-bias anomaly for noncollinear magnetic configurations*. Phys. Rev. B, **75** 155308 (2007).
- [Wic50] G. C. Wick. *The evaluation of the collision matrix*. Phys. Rev., **80** 268 (1950).
- [Wil74] K. G. Wilson and J. Kogut. *The renormalization group and the [epsilon] expansion*. Physics Reports, **12** 75 (1974).



# List of Publications

1. S. Göttel, S. Andergassen, C. Honerkamp, D. Schuricht, and S. Wessel  
*'Critical scales in anisotropic spin systems from functional renormalization'*  
Phys. Rev. B **85**, 214406 (2012)
2. S. Göttel, F. Reininghaus, and H. Schoeller  
*'The generic fixed point model for pseudo-spin-1/2 quantum dots in nonequilibrium: Spin-valve systems with compensating spin polarizations'*  
(Submitted to Phys. Rev. Lett.) ArXiv e-prints 1411.4460 (2015)
3. S. Göttel, F. Reininghaus, and H. Schoeller  
*'Nonequilibrium renormalization group for generic pseudo-spin-1/2 quantum dots in the Coulomb blockade regime'*  
in preparation (2015)



# Curriculum Vitae

Stefan Göttel

born on September 12th 1986 in Bochum, Germany

## Academic record:

June 2006	Abitur Theodor-Körner Gymnasium, Bochum, Germany
2006–2009	Bachelor Studies of Physics RWTH Aachen University, Germany
August 2009	Bachelor Thesis Institute for Theory of Statistical Physics, RWTH Aachen University, Germany <i>‘Transport durch Störstellen in Luttingerflüssigkeiten’</i> Advisor: Herbert Schoeller
2009–2011	Master Studies of Physics RWTH Aachen University, Germany
September 2009 – February 2010	Master Studies of Physics ETH Zürich, Switzerland
June 2011	Master Thesis Institute for Theory of Statistical Physics, RWTH Aachen University, Germany <i>‘Funktionale Renormierungsgruppe für Spinketten’</i> Advisor: Sabine Andergassen
2011–2015	Ph.D. Studies Institute for Theory of Statistical Physics, RWTH Aachen University, Germany Advisor: Herbert Schoeller
<b>Awards</b>	Springorum Commemorative Medal, RWTH Aachen University



# Acknowledgment

At first, I would like to thank Herbert Schoeller for giving me the opportunity to do my Ph.D. studies in the fascinating field of quantum many-body physics. I appreciated his continuous willingness to discuss any of my problems with the real-time RG and the various calculations.

Furthermore, I appreciate that Dirk Schuricht agrees to become the co-referee of my thesis. I also want to thank him for fruitful discussions, especially concerning the spin-FRG, and sharing his broad knowledge of low-dimensional spin-systems.

Regarding the first part of this thesis, I am thankful that Sabine Andergassen, Carsten Honerkamp and Stefan Weßel supported my studies not only by providing benchmarking data, but even more from their enlightening insights.

The real-time RG study of quantum dots benefited significantly from the collaboration with Frank Reininghaus. He supported me with programs and data for use and comparison and was open for discussions about the real-time RG.

I want to thank numerous members of the Institute for Theory of Statistical Physics, especially my (former) office colleagues Katharina Eissing and Dante Kennes, for uncountable discussions about physics and mostly non-physics creating a great atmosphere at the institute.

Additionally, I want to mention those, who shared their time with me during my nine years of study and research in Aachen. In particular, thanks to: David Altmann, Jennifer Arif, Sören Boyn, Kristina Broering, Lasse Büsing, Benedikt Dolzer, Katharina Eissing, Andreas Engelhardt, Lisa Glaser, Stephan Grab, Christoph Hörig, Severin Jakobs, Laura Jenniches, Matthias Kaes, Dante Kennes, Moritz Küpper, Tobias van Leeuwen, Mathias Müller, Frank Reininghaus, Kathrin Schönauer, and Victoria Schumann.

Finally, I thank my family and friends for taking care of me while not at work.





# Erklärung

Hiermit erkläre ich eidesstattlich, dass ich die vorliegende Arbeit selbständig verfasst und dabei nur die angegebenen Quellen verwendet habe. Ferner erkläre ich, dass durch die Veröffentlichung der Arbeit keine Urheberrechte verletzt werden und dass ich bisher keine Promotionsanträge gestellt habe.

---

Aachen, den 01.06.2015